Chapter 4: The consequences of framework flexibility on the gas adsorption characteristics of $(Me_2NH_2)[In(ABDC)_2]$

4.1 Abstract

The gas uptake properties of the indium carboxylate MOF $(Me_2NH_2)[In(ABDC)_2]$ are explored in relation to the solvent-dependent breathing behaviour reported in the previous chapters. The adsorption of CO_2 and CH_4 by the framework is shown to vary substantially based on the starting solvent choice, despite complete removal of the solvent from the MOF pores prior to the gas uptake. These effects can be directly related to flexibility of the framework and changes in the accessible pore space, and have been followed using gravimetric and volumetric adsorption isotherms combined with *in situ* crystallographic studies. The framework is further studied using partially desolvated materials, showing that a gate pressure can be introduced into the adsorption profile.

4.2 Introduction

The previous report of $(Me_2NH_2)[In(ABDC)_2]$ showed that framework exhibited a moderately high CO_2 uptake, but almost no CH_4 uptake (reported to be below the detection limit) leading to an extremely high CO_2 *vs* CH_4 selectivity.[1] The original authors attributed the selectivity to a combination of the free amino group, the charged framework and the small pore sizes. The free amino group was deemed "mostly responsible for the high CO_2 uptake" and the low CH_4 uptake was attributed to a molecular sieving effect.[1] This analysis is quite speculative, particularly in the absence of *in situ* studies to provide structural or spectroscopic details. The real-time separation performance was also measured by passing an equimolar mixture of CO_2 and CH_4 down a column packed with the MOF. During the first 100s only CH_4 was recorded exiting the column, after which time the CO_2 started to elute. The relative ratio of the two gases returned to 50/50 after 300s and no subsequent changes were then observed. The results can be attributed to all the CO_2 being taken up by the framework until reaching its saturation point at t = 300s. After the saturation point neither gas was adsorbed and therefore the equimolar mixture passed directly though the column. The adsorption results and the breakthrough plot are shown in Figure 1.

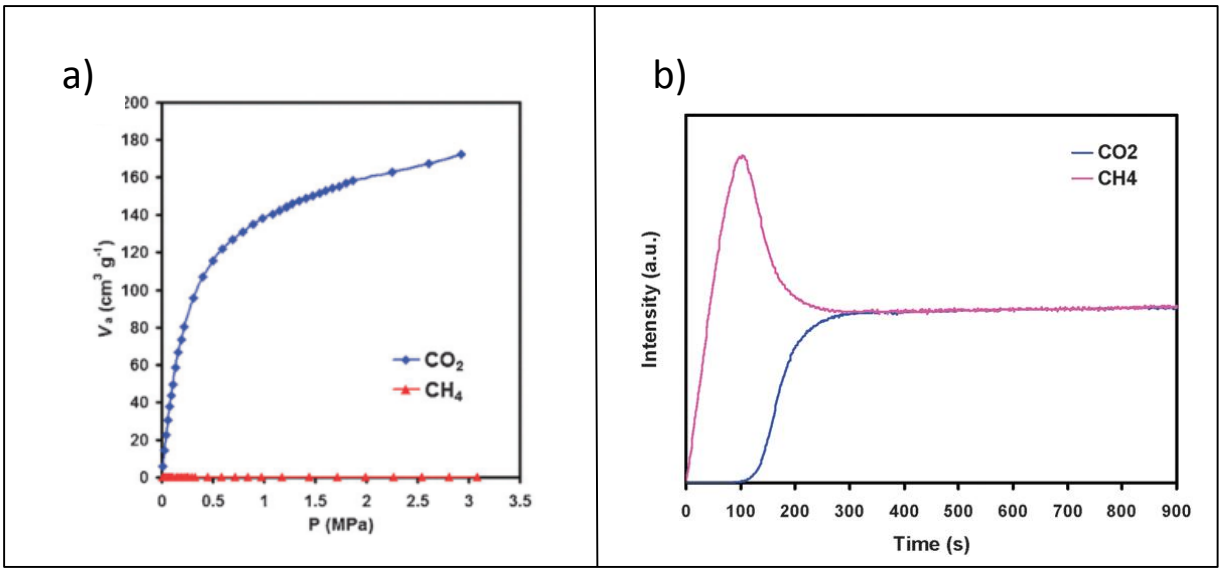

Figure 1 - a) High-pressure volumetric gas adsorption isotherm of $(Me_2NH_2)[In(ABDC)_2]$ for CO_2 and CH_4. b) Breakthrough profile for an equimolar CO_2/CH_4 mixture. Adapted with permission from B. Yuan *et al.* , *Chem. Commun.*, 2012, 48, 1135–1137. Copyright 2012 Royal Society of Chemistry.[1]

The CO_2 and CH_4 isotherms were based on volumetric adsorption measurements for a $CHCl_3$ exchanged MOF after activating at 80 °C under high vacuum.[1] The isotherm can be seen to follow a standard type I behaviour and the authors presented a powder pattern after solvent removal, showing the framework was still in the same open form as the fully solvated structure. This strongly indicated a rigid framework which maintained its structure during gas adsorption. While the work described in the previous two chapters confirms that the framework exists in the open structure after removal of the $CHCl_3$, it also shows that the MOF can actually be incredibly flexible, and the dynamics of the structure vary based on the solvent. This chapter covers the effect this flexibility has on both the gas adsorption profile and the CO_2/CH_4 selectivity, by exploring the gas adsorption in the as-synthesised MOF compared to the $CHCl_3$-exchanged MOF. The continuous flexibility displayed by $(Me_2NH_2)[In(ABDC)_2]$ is rare within the scientific literature and only a limited number of gas adsorption studies have been carried out on the prototypical continuously flexible MOF MIL-88.[2, 3] Very little is therefore currently known about the gas sorption behaviour in these types of materials.

4.3 Experimental

4.3.1 General

Descriptions for the synthesis all compounds used in this chapter can be found in Chapters 2 & 3.

4.3.2 Analysis

Solution-phase ^{1}H NMR spectroscopy (400 MHz, DMSO-d6) was carried out using a Bruker DPX-400 spectrometer. The MOF sample (10 mg) was digested using 50 µL of acid (35% DCl in D_2O) in 1 mL of DMSO-d6, and recorded without neutralising the solution. All the constituent parts were observed to be soluble in the DMSO after the digestion.

Solid-state NMR spectroscopy (500 MHz) was carried out using a Bruker DPX-500 spectrometer equipped with a solid state probe. 50 mg of MOF sample was used. The ^{13}C spectrum was recorded using a CP-MAS program at 10 kHz.

Solid-State IR was recorded using a PerkinElmer Spectrum 100 spectrometer fitted with a universal diamond ATR accessory.

In situ single crystal diffraction studies of the MOF during gas adsorption were carried out at beamline I19[4] Diamond Light Source, using synchrotron radiation(λ = 0.6889(1) Å). The samples were glued to a MiTeGen 100 µm Microloop using araldite adhesive and fixed inside the I19 gas cell constructed from a 1 mm quartz capillary. A full hemisphere of data was collected using three 132 °, and one 180 ° omega scans at 0.4 ° slicing on a Newport diffractometer equipped with a Pilatus 300K detector. Data took 15 min to collect and were processed and corrected for adsorption using Agilent Crysalis Pro software.[5, 6] All crystal structures were solved and refined against F^2 values using the SHELX 2013 suite accessed within the OLEX2 program.[7, 8] Non-disordered, non-hydrogen framework atoms were refined anisotropically, but disordered framework atoms and cations were modelled with isotropic displacement parameters, using a combination of crystallographic restraints and constraints. Hydrogen atoms were placed in calculated positions with idealised geometries and then refined using a riding model with isotropic displacement parameters. Final CIFs were checked using checkCIF/PLATON.[9] PLATON SQUEEZE was used to obtain a residual electron count within the pore, but was not used in the structure refinements.[10]

In situ powder diffraction studies of the MOF during gas adsorption were carried out at beamline I11[11, 12] Diamond Light Source, using synchrotron radiation. Powdered samples were loaded into 0.5 mm or 0.7 mm quartz capillaries and glued into the I11 gas cell using araldite adhesive. Data were

collected using a wide angle (90 °) position sensitive detector (PSD) comprising 18 Mythen-2 modules.[11, 12] A pair of scans related by a 0.25 ° detector offset was collected for each measurement to account for gaps between detector modules. The resulting patterns were summed to give the final pattern for analysis. Indexing, Pawley and Rietveld refinements were carried out using TOPAS version 4.1[13–18] Measures of agreement between the calculated and experimental diffraction data (R_{wp} and R_{wp}') are defined by the equations below.

$$R_{wp} = \sqrt{\frac{\Sigma[w(Y_{\mathrm{obs}} - Y_{\mathrm{calc}})^2]}{\Sigma[wY_{\mathrm{obs}}{}^2]}} \qquad R_{wp}{}' = \sqrt{\frac{\Sigma[w(Y_{\mathrm{obs}} - Y_{\mathrm{calc}})^2]}{\Sigma[w(Y_{\mathrm{obs}} - bkgr)^2]}}$$

Gravimetric adsorption measurements were recorded using an Intelligent Gravimetric Analyser (IGA) model 003 supplied by Hiden Isochema Ltd. The balance and pressure control system of the instrument are fully thermostatted to 0.1 K and the microbalance has a weighing resolution of 0.2 µg. Prior to the measurements the sample was outgassed using conditions specific to each run. During measurements the pressure of the gas was gradually increased over ≈ 15 s avoiding disruption to the micro balance. Pressure control used two pressure transducers with ranges 0 - 0.1 and 0 - 2 MPa, each with an accuracy of 0.02% in the specified range. The pressure was maintained at the set point by active computer control. The mass uptake was measured as a function of time and the approach to equilibrium monitored in real time with a computer algorithm. The maximum time for equilibration of any one pressure point was 6 hours. After equilibration was established the pressure of the gas was increased to the next set value. The sample temperature was constantly monitored and maintained through the experiment using a thermostirrer.

Volumetric nitrogen isotherms were recorded using a Micromeritics ASAP 2420. Prior to the measurements the sample was outgassed using conditions specific to each run. The sample temperature was maintained at 77 K using a cryostat and monitored throughout the duration of the experiment.

4.3.3 Gravimetric gas adsorption measurements for as-synthesised $(Me_2NH_2)[In(ABDC)_2]$

CO_2 uptake on a fully desolvated framework

The gravimetric CO_2 adsorption of as-synthesised $(Me_2NH_2)[In(ABDC)_2]$ was recorded between 0 - 20 bar at both 298K (**G1**) and 258K (**G2**) as detailed in section 4.3.2. The solvent was removed prior to the experiments by heating to 423K (150 °C) under a constant flow of nitrogen. The sample was then cooled to 298K and placed under high vacuum ($\geq 10^{-6}$ mbar). The final masses were stable and the mass loss of **G1** was 24.3%. The isotherms are displayed in Figure 2 and Figure 3. **G1** is shown on absolute pressure scale and **G2** is shown on a relative pressure scale.

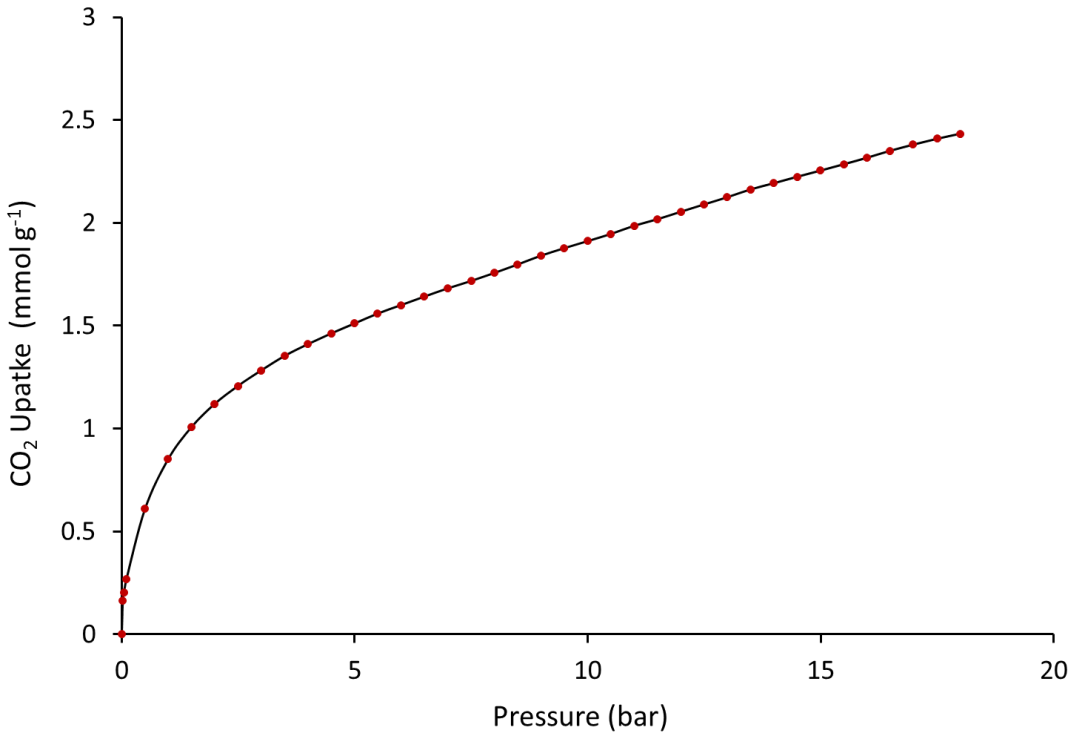

Figure 2 - Gravimetric CO_2 adsorption isotherm for as-synthesied MOF $(Me_2NH_2)[In(ABDC)_2]$ at 298K **G1**

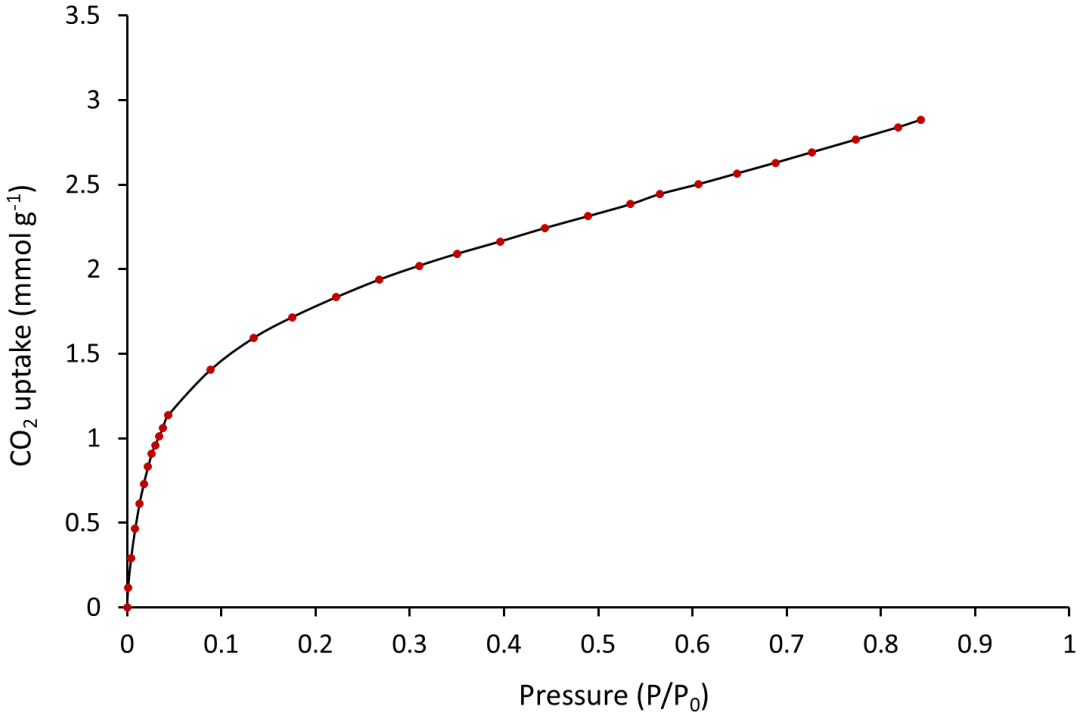

Figure 3 – Gravimetric CO_2 adsorption isotherm for as-synthesied MOF $(Me_2NH_2)[In(ABDC)_2]$ at 258K **G2**

Numerical fitting of CO_2 adsorption data

The isotherm profile of the gravimetric CO_2 uptake (**G1**) in the as-synthesised MOF was fitted to both a Langmuir and a BET model using Equation 1 and Equation 2. A Langmuirian isotherm should show a linear correlation in a plot of P/n_{ads} against P,[19] and a BET isotherm should show a linear correlation in a plot of $P/n_{ads}(P_0-P)$ against P/P_0.[20, 21] The fittings of the isotherm are displayed in Figure 4 and Figure 5, and show a poor fit to the Langmuir model but a good fit to the BET model. A range of $0.05<P/P_0<0.279$ was chosen for the BET fit.

$$\frac{P}{n_{ads}} = \frac{1}{bn_m} + \frac{P}{n_m}$$

Equation 1 - Langmuir isotherm behaviour

$$\frac{P}{n_{ads}(P_o - P)} = \frac{1}{n_m C} + \frac{(C-1)}{n_m C} \cdot \frac{P}{P_o}$$

Equation 2 - BET isotherm behaviour

P = pressure, b and C = constants, n_{ads} = amount adsorbed

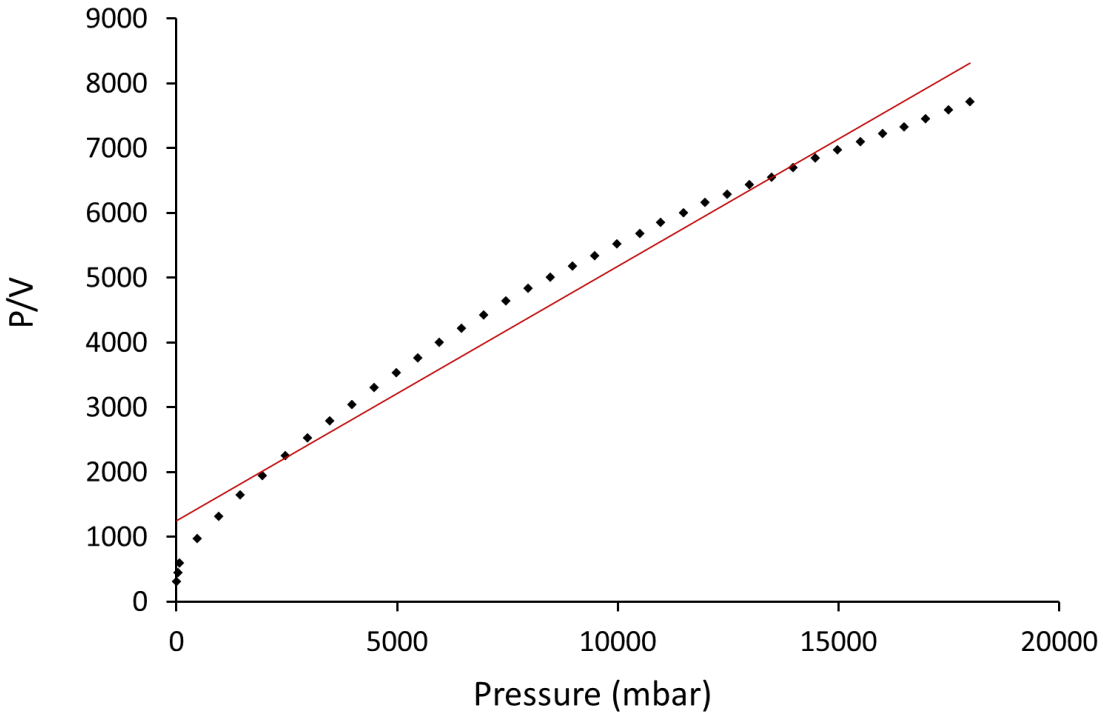

Figure 4 - Fitting of CO_2 uptake isotherm **G1** for the desolvated as-synthesised MOF $(Me_2NH_2)[In(ABDC)_2]$ to a Langmuir adsorption model (red line).

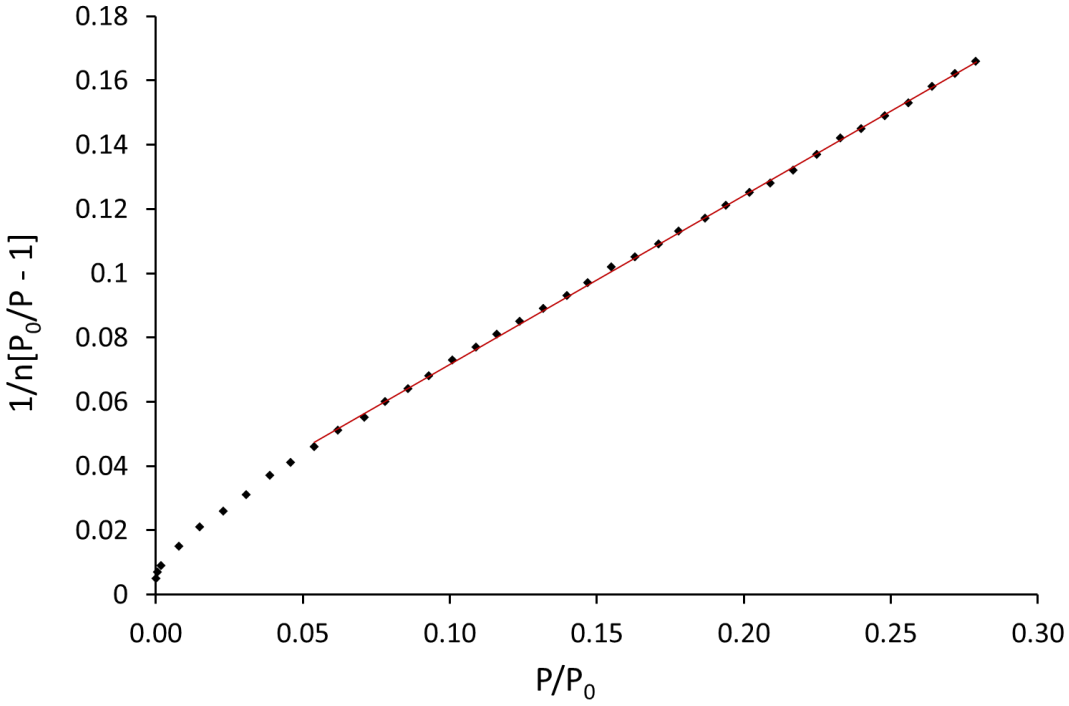

Figure 5 –Fitting of CO_2 uptake isotherm **G1** for the desolvated as-synthesised MOF $(Me_2NH_2)[In(ABDC)_2]$ to a BET adsorption model (red line).

CH_4 uptake on a fully desolvated framework

The gravimetric CH_4 adsorption of as-synthesised $(Me_2NH_2)[In(ABDC)_2]$ was recorded in the range 0 - 5 bar at 298K (**G3**) as detailed in section 4.3.2. The sample, same as used for **G1**, was outgassed prior to measurements placing the sample under high vacuum directly after the CO_2 isotherm **G1**. The isotherm is displayed in Figure 6.

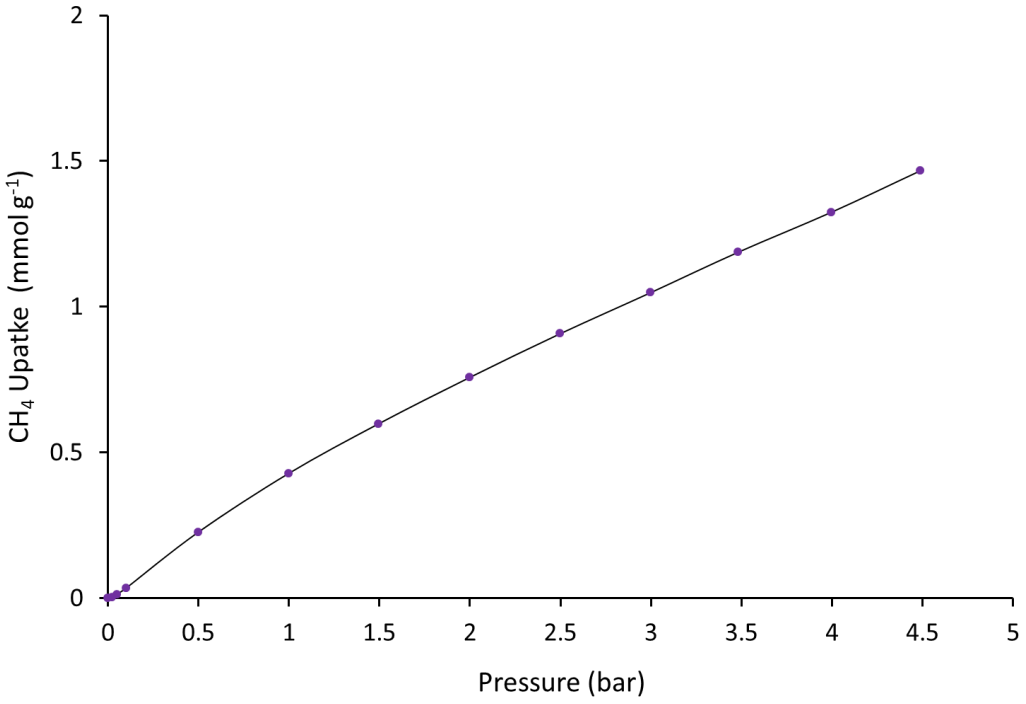

Figure 6 – Gravimetric CH_4 adsorption isotherm **G3** for as-synthesied MOF $(Me_2NH_2)[In(ABDC)_2]$ at 298K

4.3.4 Gravimetric gas adsorption measurements for $CHCl_3$-exchanged $(Me_2NH_2)[In(ABDC)_2]$

CO_2 uptake for the fully desolvated framework

The gravimetric CO_2 adsorption for $CHCl_3$-exchanged $(Me_2NH_2)[In(ABDC)_2]$ was recorded between 0 - 20 bar at 298K (**G4** & **G5**) as detailed in section 4.3.2. The isotherm **G4** was recorded after outgassing the sample at high vacuum ($\geq 10^{-6}$ mbar) and 80 °C. The mass loss was stable and recorded to be 28.0%. The isotherm **G5** was recorded on a separate sample after outgassing by just applying high vacuum. The isotherms are displayed in Figure 7 and Figure 8 shown on absolute pressure scales.

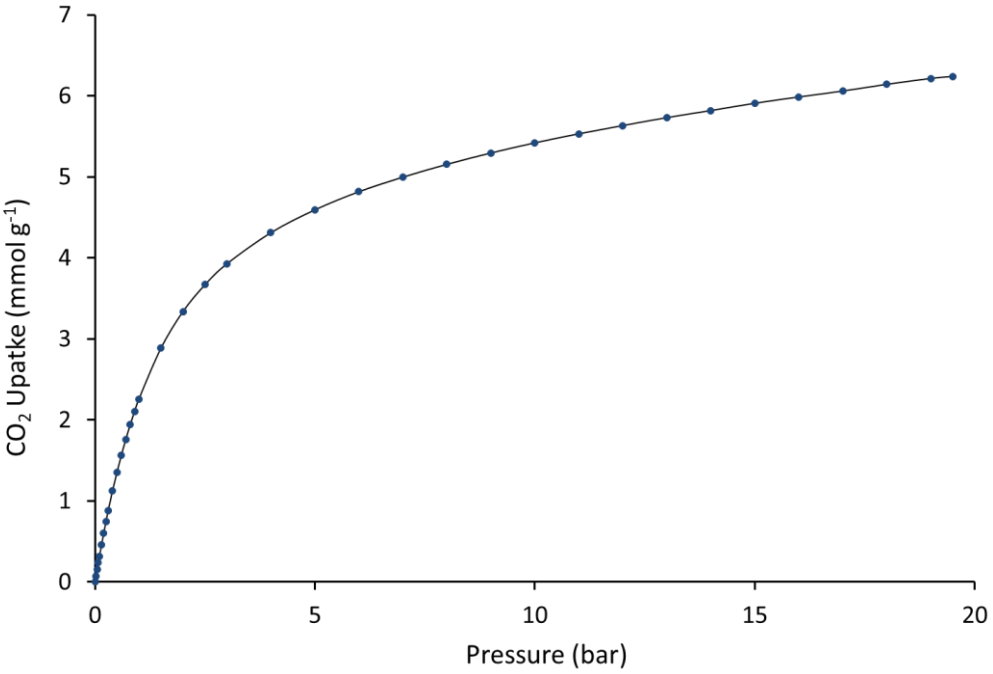

Figure 7 – Gravimetric CO_2 adsorption isotherm **G4** for $CHCl_3$-exchanged MOF $(Me_2NH_2)[In(ABDC)_2]$ at 298K (Sample outgassed under high vacuum at 353 K).

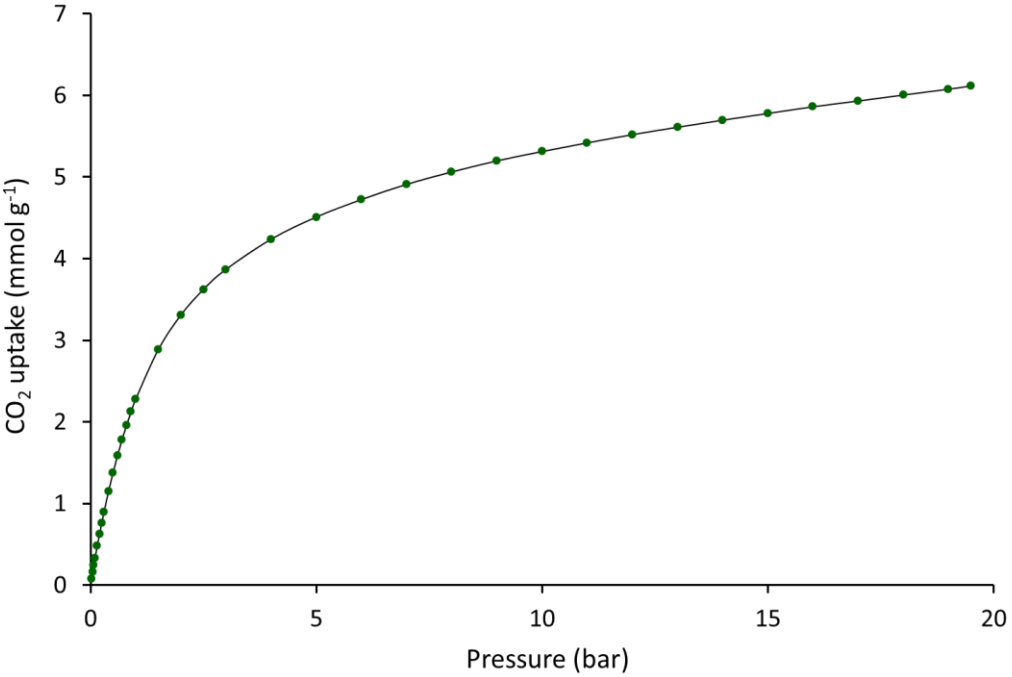

Figure 8 – Gravimetric CO_2 adsorption isotherm **G5** for $CHCl_3$-exchanged MOF $(Me_2NH_2)[In(ABDC)_2]$ at 298 K. (Sample outgassed under high vacuum at 298 K).

Numerical fitting of CO_2 adsorption data

The isotherm profile of the gravimetric CO_2 uptake (**G4**) in the $CHCl_3$ exchanged MOF was fitted to a Langmuir model using Equation 1, as detailed in section 4.3.3.[19] The fitting of the profile is displayed in Figure 9 showing a high linear correlation.

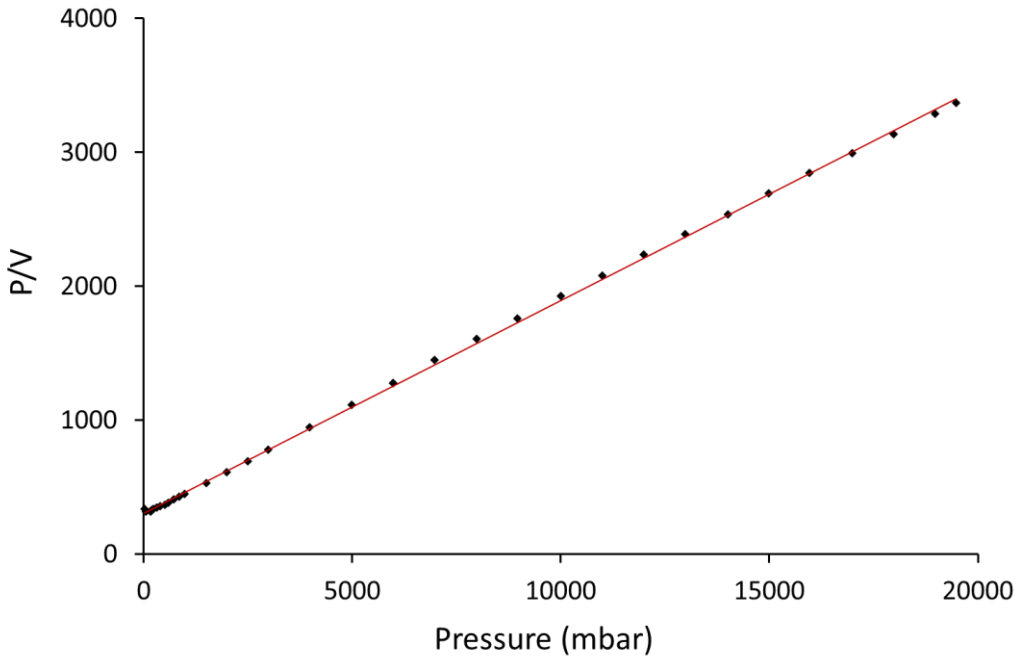

Figure 9 –Fitting of CO_2 uptake isotherm **G4** for the $CHCl_3$-exchanged MOF $(Me_2NH_2)[In(ABDC)_2]$ to a Langmuir adsorption model (red line).

CH_4 uptake on a fully desolvated framework

The gravimetric CH_4 adsorption of $CHCl_3$ exchanged $(Me_2NH_2)[In(ABDC)_2]$ was recorded between 0 - 5 bar at 298K (**G6**) as detailed in section 4.3.2. The sample, same as **G4**, was outgassed prior to measurements by taking the sample of high vacuum directly after the CO_2 isotherm. The isotherm is displayed in Figure 10.

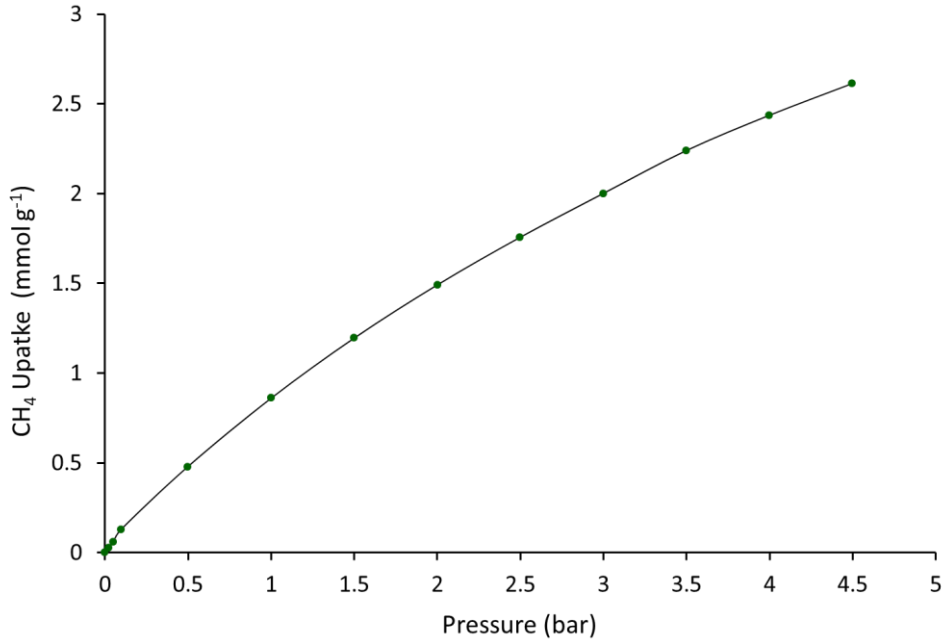

Figure 10 – Gravimetric CH_4 adsorption isotherm **G6** for the $CHCl_3$ exchanged MOF $(Me_2NH_2)[In(ABDC)_2]$

4.3.5 Gravimetric gas adsorption measurements for partially desolvated as-synthesised $(Me_2NH_2)[In(ABDC)_2]$

The gravimetric CO_2 adsorption and desorption of two partially desolvated samples of the as-synthesised $(Me_2NH_2)[In(ABDC)_2]$ were recorded between 0 - 20 bar at 298K (**G7.1** & **G7.2**) as detailed in section 4.3.2. A defined fraction of the solvent mass was removed prior to the experiments by heating to 150 ^oC under a constant flow of nitrogen. The mass losses corresponded to a ≈ 33% solvent loss for **G7.1** and a 66% solvent loss for **G7.2**. Study **G7.2** directly followed at the end of **G7.1** using the same sample after further solvent removal. The isotherms are both displayed in Figure 11 on an absolute pressure scale. A repeat of the adsorption measurement for 33% solvent loss was also recorded at 298K **G8.1** followed by a measurement of the fully desolvated sample **G8.2** Figure 12.

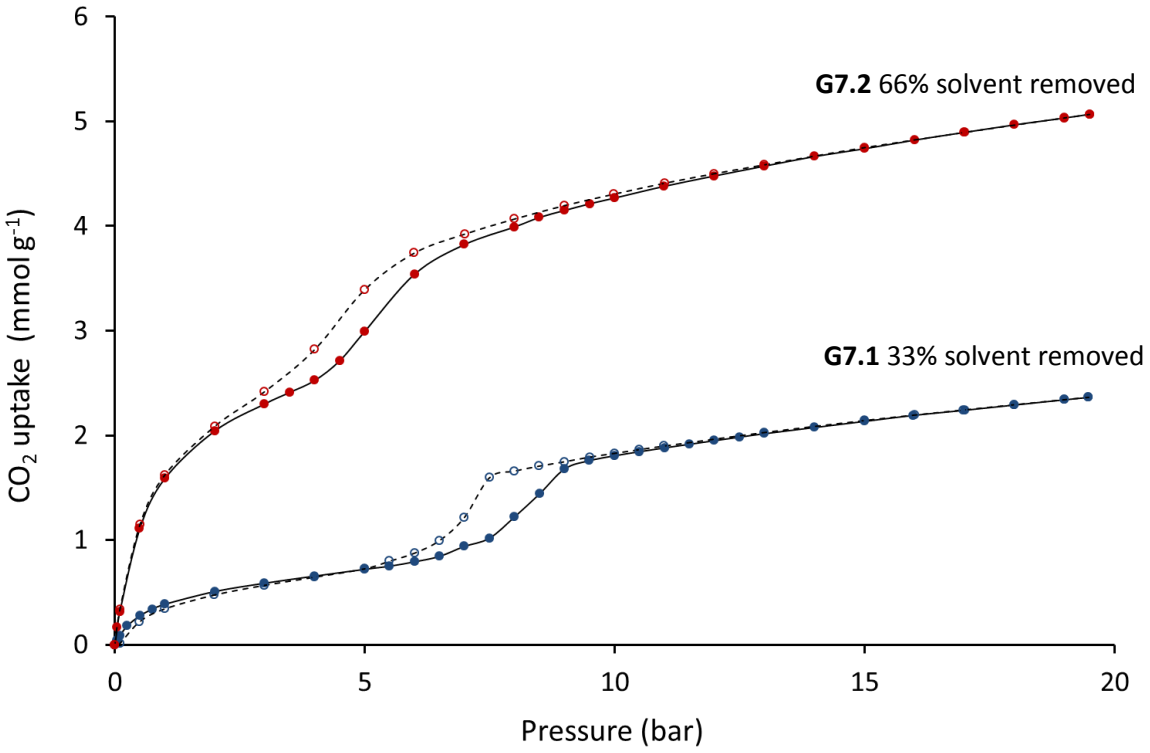

Figure 11 – Gravimetric CO_2 adsorption and desorption isotherms **G7.1** and **G7.2** for partially desolvated as-synthesied MOFs $(Me_2NH_2)[In(ABDC)_2]$. Data were recorded at 298K

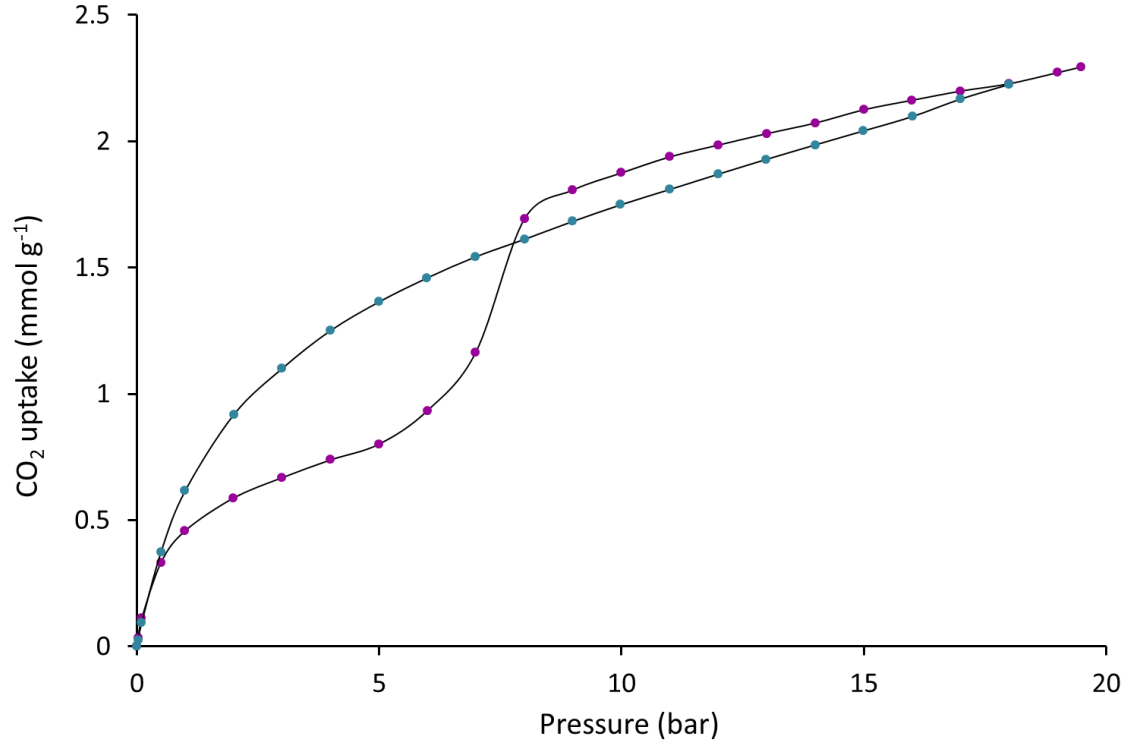

Figure 12 – Gravimetric CO_2 adsorption isotherms **G8.1** and **G8.2**.for as-synthesied MOF $(Me_2NH_2)[In(ABDC)_2]$ after partial and full desolvation, respectively. Data were recorded at 298K

4.3.6 Volumetric nitrogen adsorption at 77K

As-synthesised framework

The accessible surface area of the desolvated as-synthesised framework was calculated to be 2.93 m^2g^{-1} using a volumetric nitrogen isotherm at 77K (**V1**). Prior to the measurements the solvent was removed by heating the sample to 150 °C under a constant flow of nitrogen. The calculated surface area was determined using equation 3. The monolayer capacity (n_m) used for the calculation was obtained from the gradient and intercept of fitting **V1** to a BET model using Equation 2. The nitrogen isotherm is shown in Figure 13.

$$SA = n_m \cdot N_A \cdot A_m$$

Equation 3 - Accessible Surface area during adsorption

n_m = monolayer capacity, N_A = Avogrado's Constant, A_m = cross section area of adsorbate molecule

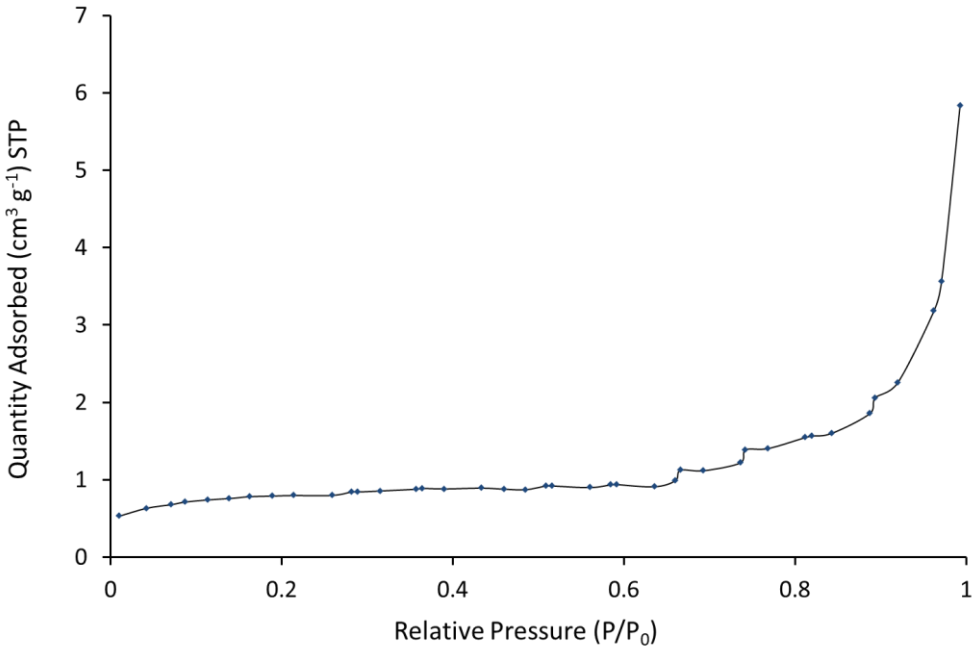

Figure 13 - Volumetric nitrogen isotherm **V1** for as-synthesised MOF $(Me_2NH_2)[In(ABDC)_2]$ at 77K

$CHCl_3$ exchanged framework

The accessible surface area of the desolvated $CHCl_3$-exchnaged framework was calculated to be 544.15 m^2g^{-1} using a volumetric nitrogen isotherm at 77K (**V2**). Prior to the measurements the sample was outgassed at high vacuum (≥10^{-6} mbar) and 80 °C. The calculated surface area was determined using equation 3. The monolayer capacity (n_m) used for the calculation was obtained from the gradient and intercept of fitting **V2** to a Langmuir model using Equation 1. The nitrogen isotherm is shown in Figure 14.

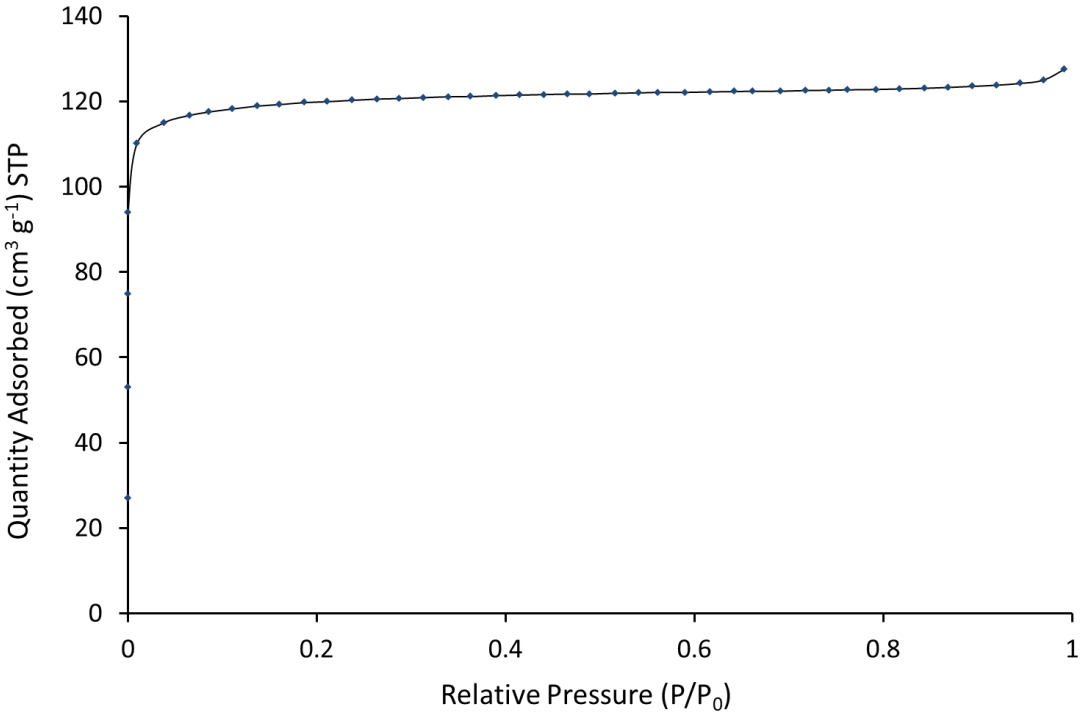

Figure 14 – Volumetric nitrogen isotherm **V2** for $CHCl_3$-exchanged MOF $(Me_2NH_2)[In(ABDC)_2]$ at 77K

4.3.7 *In situ* crystallographic studies of gas sorption in $CHCl_3$-exchanged $(Me_2NH_2)[In(ABDC)_2]$

A powdered sample of $CHCl_3$-exchanged MOF $(Me_2NH_2)[In(ABDC)_2]$ was packed into a 0.5 mm quartz capillary and heated in a temperature-controlled furnace for 2 hours at 100 °C. The capillary was then fixed into the gas cell at the I11 beamline using araldite adhesive. The sample was placed under dynamic vacuum (≈10^{-5} mbar) for 3 hours before collecting a powder pattern on the I11 beamline (**I1.1**), λ = 0.82582(1) Å.[11, 12] The sample was then loaded with 20 bar CO_2 and allowed to equilibrate for 30 mins before collecting another powder pattern (**I1.2**). The powder patterns, both recorded at room temperature, are displayed in Figure 15.

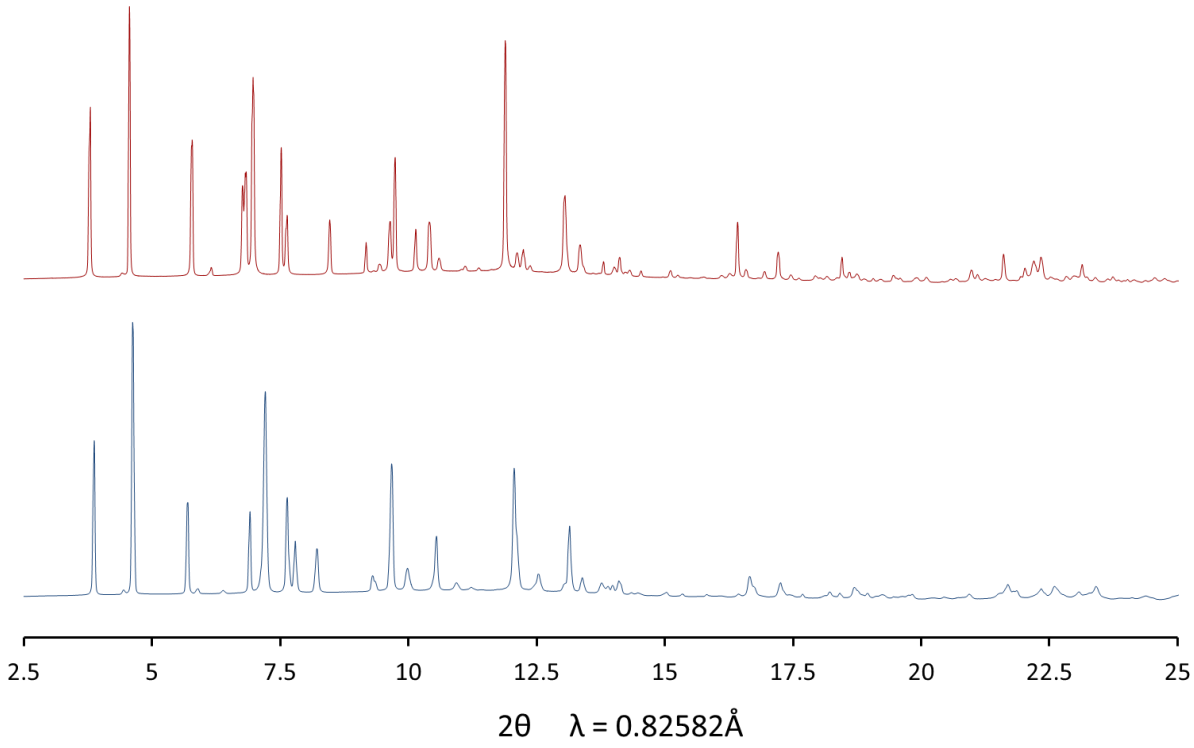

Figure 15 - Powder diffraction patterns obtained under vacuum (blue) and 20 bar CO_2 (red) for desolvated $CHCl_3$-exchanged MOF $(Me_2NH_2)[In(ABDC)_2]$ (**I1.1** & **I1.2**)

The unit cells of the framework in powder patterns **I1** and **I2** were initially determined by analysis of the positions of the first few Bragg reflections and their known Miller indices. These unit cell parameters were used as a starting point for single phase Pawley[15] refinements. The refinement of **I1** employed 1,027 parameters (10 background, 1 zero error, 5 profile, 3 cell and 1,008 reflections), resulting in final indices of fit R_{wp} = 5.959, $R_{wp'}$ = 14.702. The final unit cell parameters were orthorhombic a = 15.0623 (9) Å, b = 26.246 (2) Å, c = 31.931 (2) Å, V = 12623 (1) Å^3. The refinement of **I2** employed 1,075 parameters (10 background, 1 zero error, 5 profile, 3 cell and 1,056 reflections), resulting in final indices of fit R_{wp} = 6.252, $R_{wp'}$ = 16.026. The final unit cell parameters were orthorhombic a = 15.4407 (5) Å, b = 27.7879 (9) Å, c = 30.5431 (9) Å, V = 13104.9 (7) Å^3. The fits are displayed in Figure 16 and Figure 17 respectively.

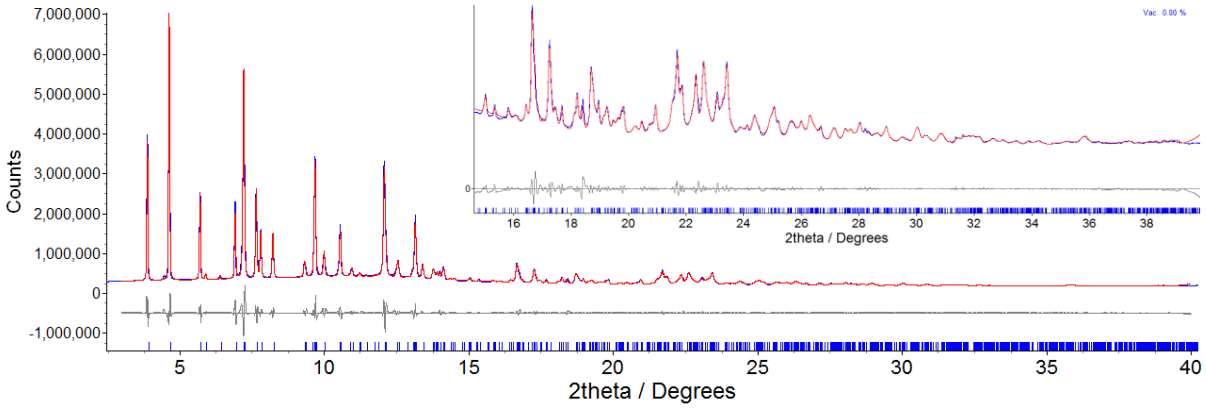

Figure 16 – Observed (blue) and calculated (red) and difference plot [I_{obs} - I_{calc}] (grey) of the Pawley[15] refinement of desolvated $CHCl_3$-exchanged $(Me_2NH_2)[In(ABDC)_2]$ under vacuum (**I1.1**) (2θ range 3.0 – 40.0 °, d_{min} = 1.2Å).

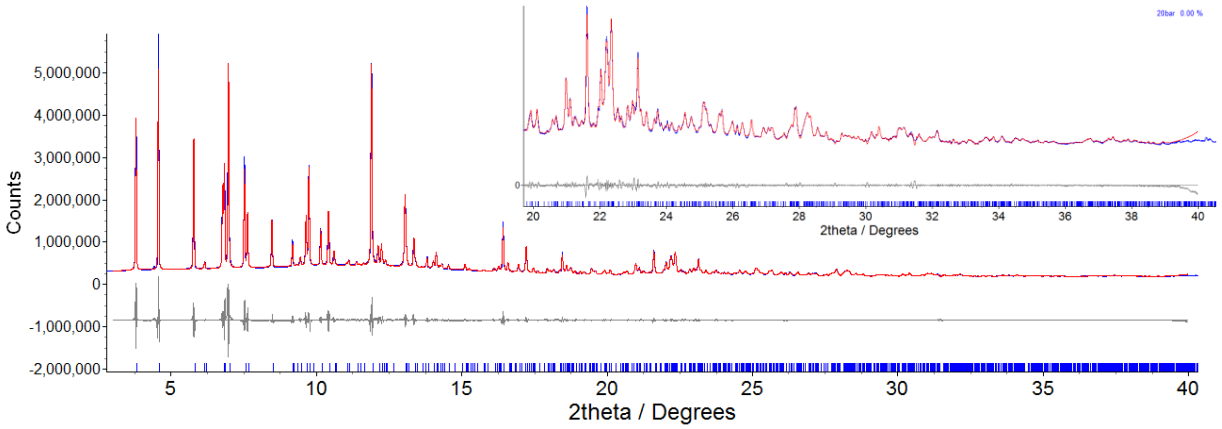

Figure 17 – Observed (blue) and calculated (red) and difference plot [I_{obs} - I_{calc}] (grey) of the Pawley[15] refinement of desolvated $CHCl_3$-exchanged $(Me_2NH_2)[In(ABDC)_2]$ under 20 bar CO_2 (**I1.2**) (2θ range 3.0 – 40.0 °, d_{min} = 1.2Å).

4.3.8 *In situ* crystallographic studies of CO_2 sorption in partially desolvated as-synthesised $(Me_2NH_2)[In(ABDC)_2]$

Single Crystal diffraction experiment 1 (**I2**)

A single crystal of as-synthesised MOF $(Me_2NH_2)[In(ABDC)_2]$ was selected from the DMF mother liquor and mounted in the gas cell at beamline I19 as detailed in section 4.3.2. An initial data collection was recorded at ambient conditions (**I2.1**) followed by heating of the cell to 175 ^oC at 6 ^oC/min using a Cryostream. The sample was held at 175 ^oC for 15 minutes before cooling to RT at 6 ^oC/min and recording a data set under vacuum (**I2.2**). Successive pressures of CO_2 were introduced at 1 bar, 5 bar , 10 bar and 20 bar allowing 30 minutes for equilibration at each pressure before recording diffraction data (**I2.3 - I2.6**). Full crystal structure solutions were achievable for all measurements except **I2.3** and **I2.6**, where the data quality was too low. Unit cell parameters for the 20 bar measurement (**I2.6**) were convincingly determined using all of the reflection collected, but the measurement at 1 bar could not be suitably indexed. Table 1 shows the refined cell parameters during the study and Figure 18 shows the data points in comparison to the known breathing trend. Table 2 shows the refinement parameters for the full structure solutions.

Table 1 - Unit cell parameters determined during crystallographic studies of CO_2 uptake in partially desolvated as-synthesised MOF $(Me_2NH_2)[In(ABDC)_2]$ (**I2**)

Sample Description	Data set Code	*a* (Å)	*b* (Å)	*c* (Å)	*V* (Å^3)
Solvated in Cell	**I2.1**	15.8532(4)	27.8955(7)	30.7522(9)	13599.6(6)
After heat treatment, under vacuum	**I2.2**	15.2129(6)	24.490(2)	33.440(2)	12458.7(16)
1 bar CO_2	**I2.3**	N/A			
5 bar CO_2	**I2.4**	15.4920(5)	26.7238(14)	31.7627(19)	13149.9(11)
10 bar CO_2	**I2.5**	15.5561(5)	27.0768(9)	31.4398(13)	13242.8(8)
20 bar CO_2	**I2.6**	15.615(2)	27.260(8)	31.294(2)	13320(4)

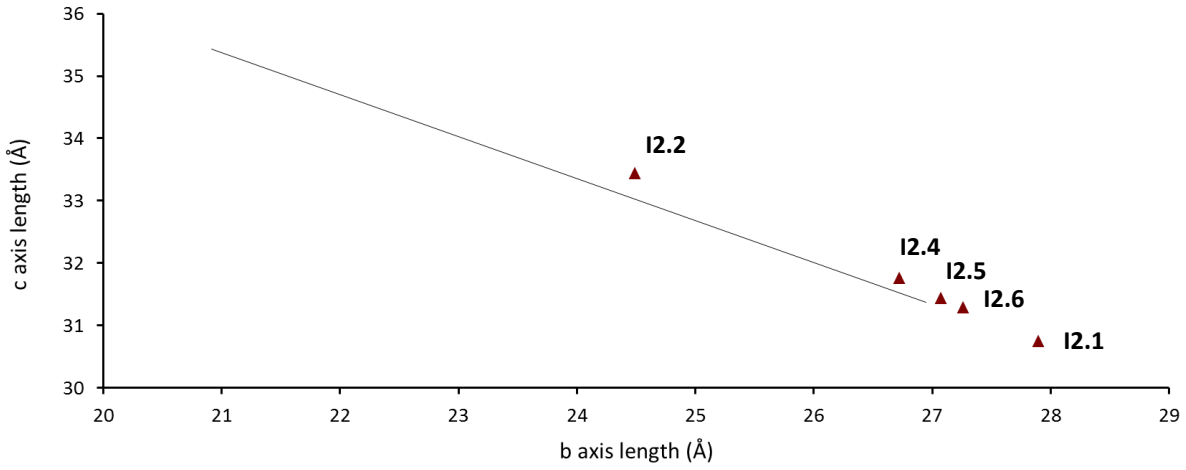

Figure 18 – *b* and *c* axis values for *in situ* single crystal diffraction experiment under CO_2 atmospheres (**I2**) on a partially desolvated as-synthesised $(Me_2NH_2)[In(ABDC)_2]$ in comparison to the trend line from single crystal desolvation studies of as-synthesised $(Me_2NH_2)[In(ABDC)_2]$ (**1-10**)

Table 2 - Data collection, structure solution and refinement parameters for single crystal X-ray structure determinations during *in situ* CO_2 uptake experiments on a partially desolvated as-synthesised MOF $(Me_2NH_2)[In(ABDC)_2]$

	DMF-solvated in gas cell **(I2.1)**	Partially desolvated while in gas cell **(I2.2)**	Partially desolvated and 5 bar CO_2 **(I2.4)**	Partially desolvated and 10 bar CO_2 **(I2.5)**
Crystal Habit	Octahedron	Octahedron	Octahedron	Octahedron
Crystal Colour	Brown	Brown	Brown	Brown
Crystal Size (mm)	0.27 x 0.25 x 0.25	0.27 x 0.25 x 0.25	0.27 x 0.25 x 0.25	0.27 x 0.25 x 0.25
Crystal System	Orthorhombic	Orthorhombic	Orthorhombic	Orthorhombic
Space Group, Z	*Fddd*, 16	*Fddd*, 16	*Fddd*, 16	*Fddd*, 16
a (Å)	15.8532(4)	15.2129(6)	15.4920(5)	15.5561(5)
b (Å)	27.8955(7)	24.490(2)	26.7238(14)	27.0768(9)
c (Å)	30.7522(9)	33.440(2)	31.7627(19)	31.4398(13)
α (°)	90	90	90	90
β (°)	90	90	90	90
γ (°)	90	90	90	90
V (Å^3)	13599.6(6)	12458.7(16)	13149.9(11)	13242.8(8)
Radiation	Sync (λ = 0.6889Å)	Sync (λ = 0.6889Å)	Sync (λ = 0.6889Å)	Sync (λ = 0.6889Å)
Density (g cm^{-3})[b]	1.015	1.108	1.049	1.042
Temperature (K)	298	298	298	298
μ (mm^{-1})[c]	0.667	0.728	0.690	0.685
2θ Range (°)	3.14 to 58.94°	4.68 to 51	3.2 to 51	3.18 to 51
Reflns collected	26679	14389	17415	17985
Independent reflns (R_{int})	5149 (0.0843)	3041 (0.0987)	3270 (0.1249)	3339 (0.1203)
Reflns used in refinement, *n*	5149	3041	3270	3339
L.S. parameters, *p*	121	93	123	124
No. of restraints, *r*	4	4	0	0
Completeness	0.989	0.956	0.972	0.983
$R1(F)$[a] $I > 2\sigma(I)$	0.0820	0.1603	0.1355	0.1140
$wR2(F^2)$[a], all data	0.2535	0.4862	0.4190	0.3780
$S(F^2)$[a], all data	1.105	2.164	1.822	1.658

[a] $R1(F) = \sum(|F_o| - |F_c|)/\sum|F_o|$; $wR2(F^2) = \sqrt{\sum w\left(F_o^2 - F_c^2\right)^2/\sum wF_o^4}$; $S(F^2) = \sqrt{\sum w\left(F_o^2 - F_c^2\right)^2/(n+r-p)}$.

[b] Densities are calculated using only framework atoms and cations, and do not include guest molecules.

[c] Adsorption coefficients are calculated based on the crystallographic model

Single Crystal diffraction experiment 2 (**I3**)

Single crystals of as-synthesised MOF $(Me_2NH_2)[In(ABDC)_2]$ were removed from the DMF mother-liquor, dried in air for 15 minutes, and heated to 150 °C in a temperature-controlled oven. The sample was held at 150 °C for 15 minutes and the removed from the oven while still at 150 °C. A crystal was then chosen and mounted in the gas cell at beamline I19, λ = 0.6889Å, as detailed in section 4.3.2. The sample was placed under vacuum and an initial data collection was recorded (**I3.1**). Successive pressures of CO_2 were then introduced at 1 bar, 5 bar , 10 bar and 20 bar allowing 30 minutes for equilibration at each pressure before recording diffraction data (**I3.2 - I2.5**). Full structure solutions were not achievable but unit cell parameters for these measurements were able to be determined using all of the reflections collected. Table 3 shows the refined unit cell parameters during the study and Figure 19 shows the data points in comparison to the known breathing trend line.

Table 3 - Unit cell parameters determined during crystallographic studies of CO_2 uptake in partially desolvated as-synthesised MOF $(Me_2NH_2)[In(ABDC)_2]$ (**I3**)

Sample Description	Data set Code	*a* (Å)	*b* (Å)	*c* (Å)	*V* (Å^3)
Vacuum after heat treatment	**I3.1**	15.063(2)	22.398(7)	34.740(6)	11720(5)
1 bar CO_2	**I3.2**	15.075(2)	22.600(7)	34.618(6)	11794(6)
5 bar CO_2	**I3.3**	15.085(3)	22.929(6)	34.431(5)	11909(4)
10 bar CO_2	**I3.4**	15.113(3)	23.139(6)	34.253(5)	11978(4)
20 bar CO_2	**I3.5**	15.111(4)	23.406(7)	34.007(6)	12028(5)

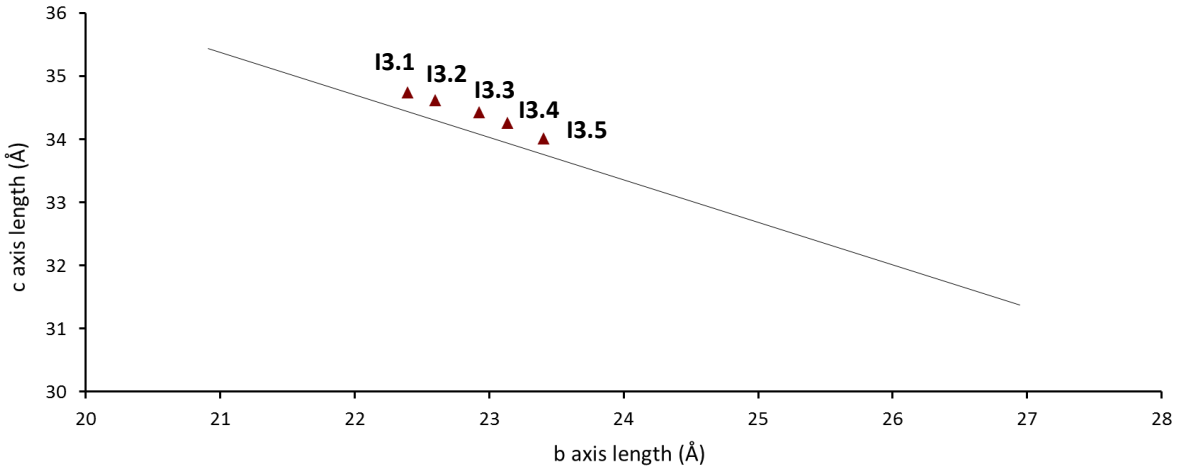

Figure 19 – *b* and *c* axis values for *in situ* single crystal diffraction experiment under CO_2 atmospheres **I3** on a partially desolvated as-synthesised $(Me_2NH_2)[In(ABDC)_2]$ in comparison to the trend line from single crystal desolvation studies of as-synthesised $(Me_2NH_2)[In(ABDC)_2]$ (**1-10**)

Powder diffraction experiment 1 (**I4**)

A powdered sample of as-synthesised MOF $(Me_2NH_2)[In(ABDC)_2]$ was packed into a 0.5 mm quartz capillary and heated in a temperature controlled furnace for 30 mins at 200 ^oC. The capillary was then fixed into the I11 gas cell using araldite adhesive. The sample was placed under dynamic vacuum (≈10^{-5} mbar) for 30 mins before collecting a powder pattern on the I11 beamline (**I4.1**), λ = 0.82562(2) Å.[11, 12] The sample was then loaded with successive pressures of CO_2; 1 bar, 5 bar, 10 bar and 20 bar, and allowed to equilibrate for 30 mins before collected powder patterns (**I4.2 – I4.5**). The powder patterns are displayed in Figure 20, the unit cell values from Pawley refinements are shown in Table 4, and the progression along the known breathing trend line in Figure 21. Two values are displayed for **I4.3** (5 bar CO_2) due to the presence of two major phases. All data was recorded at room temperature.

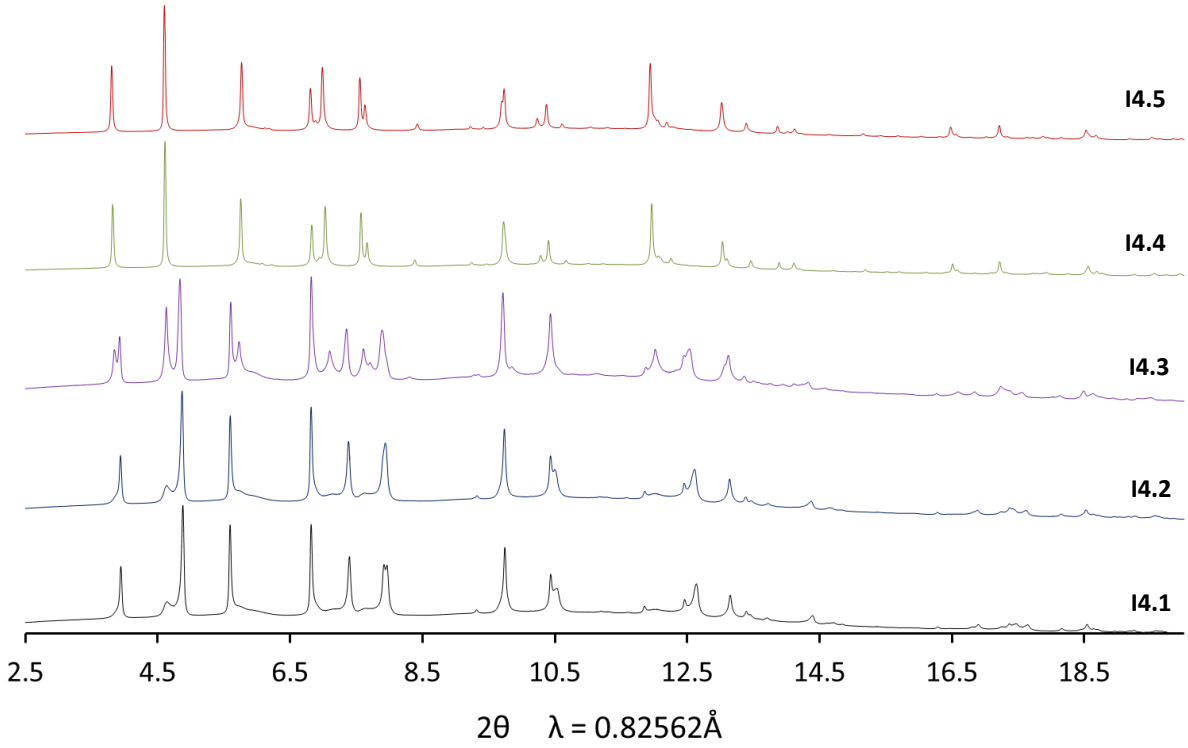

Figure 20 - Powder diffraction patterns obtained during *in situ* crystallographic CO_2 uptake experiment **I4** on a partially desolvated as-synthesised sample of MOF $(Me_2NH_2)[In(ABDC)_2]$

Table 4 - Unit cell parameters determined during crystallographic studies of CO_2 uptake in partially desolvated as-synthesised MOF $(Me_2NH_2)[In(ABDC)_2]$ (**I4**)

Sample Description	Data set Code	*a* (Å)	*b* (Å)	*c* (Å)	*V* (Å^3)
Vacuum after heat treatment	**I4.1**	15.1978(6)	23.623(1)	33.734(2)	12111(1)
1 bar CO_2	**I4.2**	15.2077(6)	23.743(2)	33.659(3)	12154(2)
5 bar CO_2	**I4.3_1**	15.211(1)	24.022(2)	33.453(3)	12223(2)
5 bar CO2 (2nd phase)	**I4.3_2**	15.317(3)	26.723(5)	31.522(5)	12903(3)
10 bar CO_2	**I4.4**	15.4548(4)	27.2005(7)	31.0616(9)	13057.6(6)
20 bar CO_2	**I4.5**	15.5353(3)	27.4235(7)	30.8506(8)	13143.3(6)

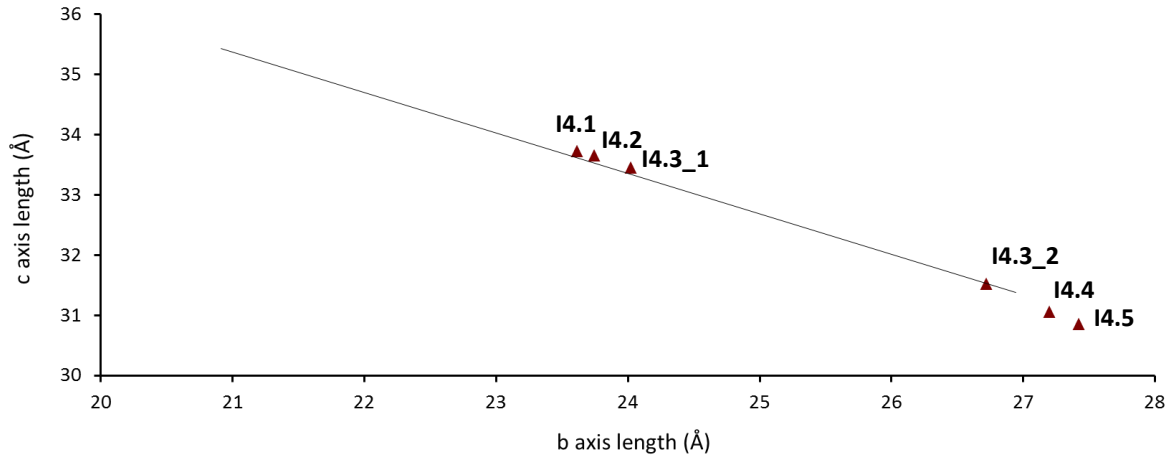

Figure 21 – *b* and *c* axis values for *in situ* powder diffraction experiment under CO_2 atmospheres **I4** on a partially desolvated as-synthesised $(Me_2NH_2)[In(ABDC)_2]$ in comparison to the trend from single crystal desolvation studies of as-synthesised $(Me_2NH_2)[In(ABDC)_2]$ (**1-10**)

The unit cells of the framework were initially determined by analysis of the positions of the first few Bragg reflections and their known Miller indices. These unit cell parameters were used as a starting point for Pawley[15] refinements. Representative fits for vacuum (**I4.1**), 5 bar (**I4.3**) and 20 bar (**I4.5**) are detailed below. Patterns for vacuum, 1 bar and 5 bar were fit using two-phase refinements and 10 bar and 20 bar were fit with single-phase refinements. The minor component in vacuum and 1 bar patterns was fixed using the unit cell values from the refined 5 bar measurement.

The two-phase Pawley refinement of **I4.1** employed 889 parameters (16 background, 1 zero error, 9 profile, 3 cell and 860 reflections), resulting in final indices of fit R_{wp} = 2.583, $R_{wp'}$ = 9.853. The final unit cell parameters of the refined phase were orthorhombic a = 15.1978 (6) Å, b = 23.623 (1) Å, c = 33.734 (2) Å, V = 12111 (1) Å^3. The fit is displayed in Figure 22

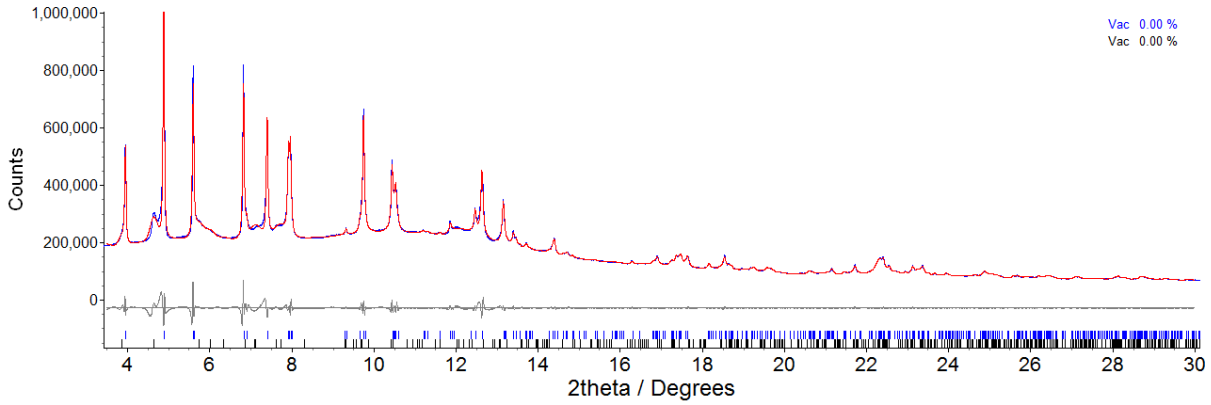

Figure 22 – Observed (blue) and calculated (red) and difference plot [I_{obs} - I_{calc}] (grey) of the Pawley[15] refinement of partially desolvated as-synthesised MOF $(Me_2NH_2)[In(ABDC)_2]$ under vacuum (**I4.1**) (2θ range 3.0 – 30.0 °, d_{min} = 1.6Å).

The two-phase refinement of **I4.3** employed 903 parameters (16 background, 1 zero error, 9 profile, 6 cell and 871 reflections), resulting in final indices of fit R_{wp} = 2.644, $R_{wp'}$ = 11.541. The final unit cell parameters were orthorhombic a = 15.211 (1) Å, b = 24.022 (2) Å, c = 33.453 (3) Å, V = 12223 (2) Å^3, and orthorhombic a = 15.317 (3) Å, b = 26.723 (5) Å, c = 31.522 (5) Å, V = 12903 (3) Å^3. The fit is displayed in Figure 23

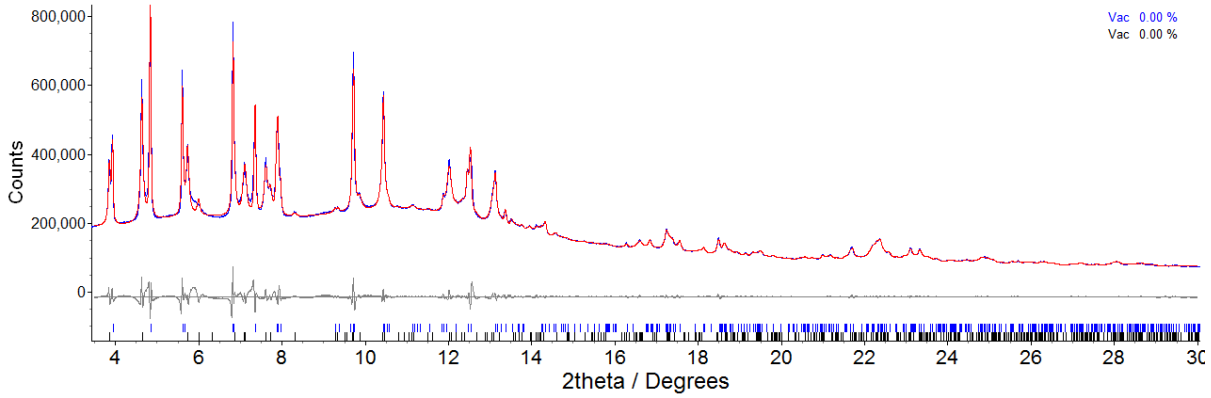

Figure 23 – Observed (blue) and calculated (red) and difference plot [I_{obs} - I_{calc}] (grey) of the Pawley[15] refinement of partially desolvated as-synthesised MOF $(Me_2NH_2)[In(ABDC)_2]$ under 5 bar CO_2 (**I4.3**) (2θ range 3.0 – 30.0 °, d_{min} = 1.6Å).

The single-phase refinement of **I4.5** employed 469 parameters (16 background, 1 zero error, 5 profile, 3 cell and 444 reflections), resulting in final indices of fit R_{wp} = 2.781, $R_{wp'}$ = 11.118. The final unit cell parameters were orthorhombic a = 15.5353 (3) Å, b = 27.4235 (7) Å, c = 30.8506 (8) Å, V = 13143.3 (6) Å^3. The fit is displayed in Figure 24

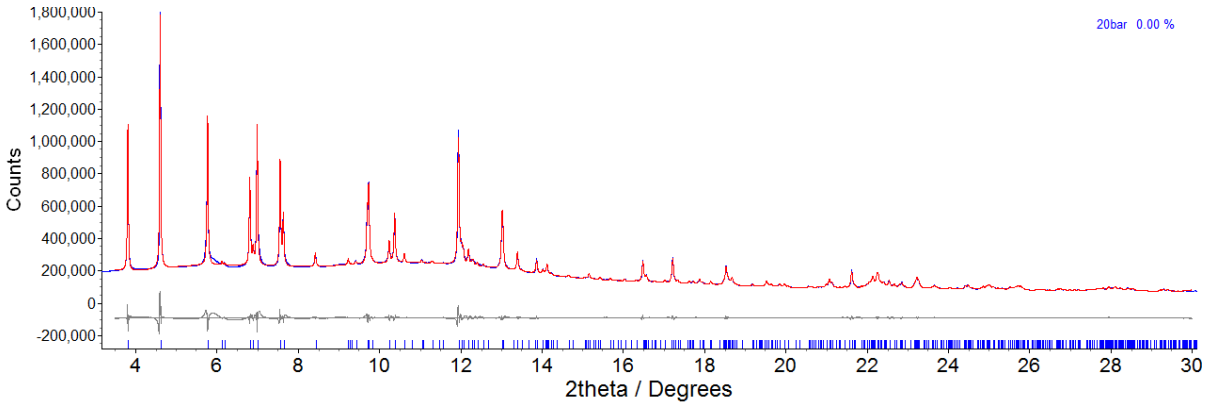

Figure 24 – Observed (blue) and calculated (red) and difference plot [I_{obs} - I_{calc}] (grey) of the Pawley[15] refinement of partially desolvated as-synthesised MOF $(Me_2NH_2)[In(ABDC)_2]$ under 20 bar CO_2 (**I4.5**) (2θ range 3.0 – 30.0 °, d_{min} = 1.6Å).

Powder diffraction experiment 2 (**I5**)

A powdered sample of as-synthesised MOF $(Me_2NH_2)[In(ABDC)_2]$ was heated at 120 °C in air for 30 mins inside a tube furnace. The sample was immediately transferred into an argon containing glovebox where it was packed into a 0.7 mm quartz capillary. The capillary was then fixed into the I11 gas cell using araldite adhesive. The procedure was designed to minimise exposure to atmospheric water vapour. The sample was placed under dynamic vacuum (≈10^{-5}mbar) for 30mins before collecting a powder pattern on the I11 beamline (**I5.1**), λ = 0.826210(5) Å.[11, 12] The sample was then loaded with successive pressures of CO_2 in 1 bar intervals between 5 and 10 bar (**I5.2 - I5.7**). The powder was allowed to equilibrate for 2.5 hours at 5 bar, 1 hour at 6-8 bar and 30 minutes at higher pressures. These times were sufficient to ensure that the patterns displayed no further change, *i.e.* equilibration at each pressure had taken place. After recording data at 10 bar the pressure was decreased in 1 bar steps to 3 bar CO_2, allowing 30 min equilibration times before recording data (**I5.8 - I5.14**). The collected powder patterns (**I5.1 - I5.14**) are displayed in Figure 25. After the experiment was completed the sample was additionally loaded with 20 and 40 bar CO_2 and the powder patterns recorded at these pressures (**I5.15** & **I5.16**). The unit cell values from Pawley refinements of all patterns are provided in

Table **5**. The progression along the known breathing trend line is discussed in section 4.4.3. All data was recorded at room temperature.

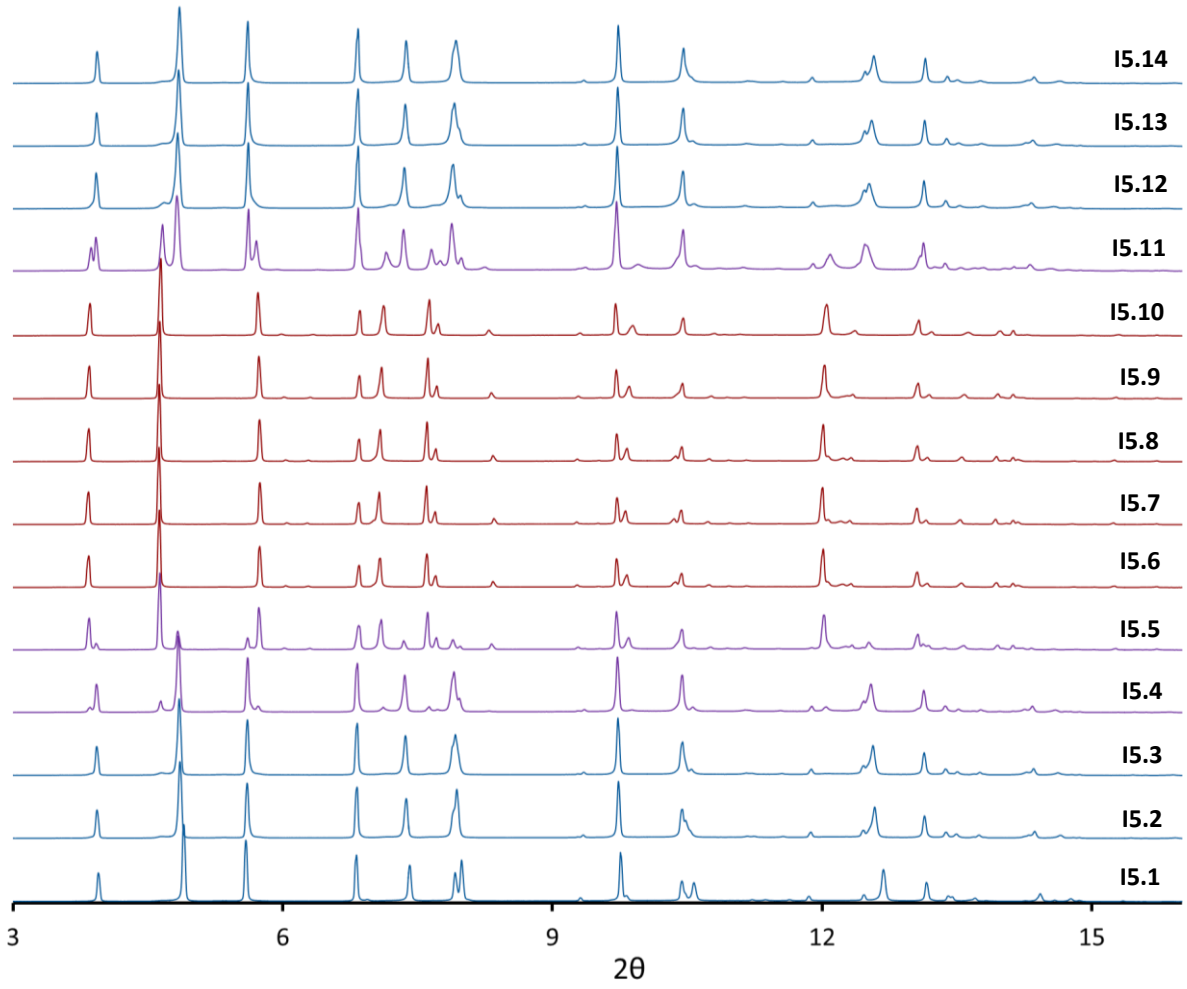

Figure 25 - Powder diffraction patterns obtained during *in situ* crystallographic gas uptake experiment **I5** on a partially desolvated as-synthesised MOF $(Me_2NH_2)[In(ABDC)_2]$

Table 5 - Unit cell parameters determined during crystallographic studies of CO_2 uptake in partially desolvated as-synthesised MOF $(Me_2NH_2)[In(ABDC)_2]$ (**I5**)

Sample Description	Data set Code	*a* (Å)	*b* (Å)	*c* (Å)	*V* (Å^3)
Vacuum after heat treatment	**I5.1**	15.2073(3)	23.4613(5)	33.8352(7)	12071.8(4)
5 bar CO_2 (adsorb)	**I5.2**	15.2206(3)	23.8527(8)	33.589(1)	12194.7(7)
6 bar CO_2 (adsorb)	**I5.3**	15.2230(4)	23.9300(9)	33.537(1)	12217.3(7)
7 bar CO_2 (adsorb)	**I5.4_1**	15.2223(2)	24.0228(4)	33.4804(5)	12243.1(3)
7 bar CO_2 2nd phase	**I5.4_2**	15.343(1)	26.627(2)	31.631(3)	12922(2)
8 bar CO_2 (adsorb)	**I5.5_1**	15.2273(3)	24.0715(6)	33.4138(9)	12247.6(6)
8 bar CO_2 2nd phase	**I5.5_2**	15.3689(2)	26.8112(3)	31.3995(4)	12938.5(3)
9 bar CO_2 (adsorb)	**I5.6**	15.3914(2)	26.9113(5)	31.3230(7)	12974.1(4)
10 bar CO_2 (adsorb)	**I5.7**	15.4054(2)	26.9771(4)	31.2639(5)	12993.0(3)
9 bar CO_2 (desorb)	**I5.8**	15.3878(2)	26.9061(4)	31.3277(6)	12970.4(4)
8 bar CO_2 (desorb)	**I5.9**	15.3647(2)	26.7931(5)	31.4269(7)	12937.5(5)
7 bar CO_2 (desorb)	**I5.10**	15.3323(4)	26.6173(9)	31.577(1)	12886.7(7)
6 bar CO_2 (desorb)	**I5.11_1**	15.2997(5)	26.248(1)	31.784(1)	12764.1(8)
6 bar CO_2 2nd phase	**I5.11_2**	15.2132(3)	24.1772(6)	33.3382(9)	12262.2(5)
5 bar CO_2 (desorb)	**I5.12**	15.2178(6)	24.123(1)	33.414(2)	12266(1)
4 bar CO_2 (desorb)	**I5.13**	15.2086(5)	24.009(1)	33.480(1)	12225.4(9)
3 bar CO_2 (desorb)	**I5.14**	15.2033(4)	23.9034(9)	33.539(1)	12188.3(7)
20 bar CO_2	**I5.15**	15.5118(2)	27.2977(4)	30.9634(5)	13111.1(3)
40 bar CO_2	**I5.16**	15.5775(2)	27.4832(4)	30.7895(4)	13181.6(3)

The unit cells of the framework were initially determined by analysis of the positions of the first few Bragg reflections and their known Miller indices. These unit cell parameters were used as a starting point for Pawley[15] refinements. Representative fits for vacuum (**I5.1**), 7 bar (**I5.4**) and 10 bar (**I5.7**) are detailed below. **I5.4**, **I5.5** and **I5.11** were fit using two-phase refinements but the rest of the patterns were fit with single-phase refinements.

The single-phase refinement of **I5.1** employed 1,782 parameters (7 background, 1 zero error, 5 profile, 3 cell and 1,766 reflections), resulting in final indices of fit R_{wp} = 6.903, $R_{wp'}$ = 12.617. The final unit cell parameters were orthorhombic *a* = 15.2073 (3) Å, *b* = 23.4613 (5) Å, *c* = 33.8352 (7) Å, *V* = 12071.8 (4) Å^3. The fit is displayed in Figure 26

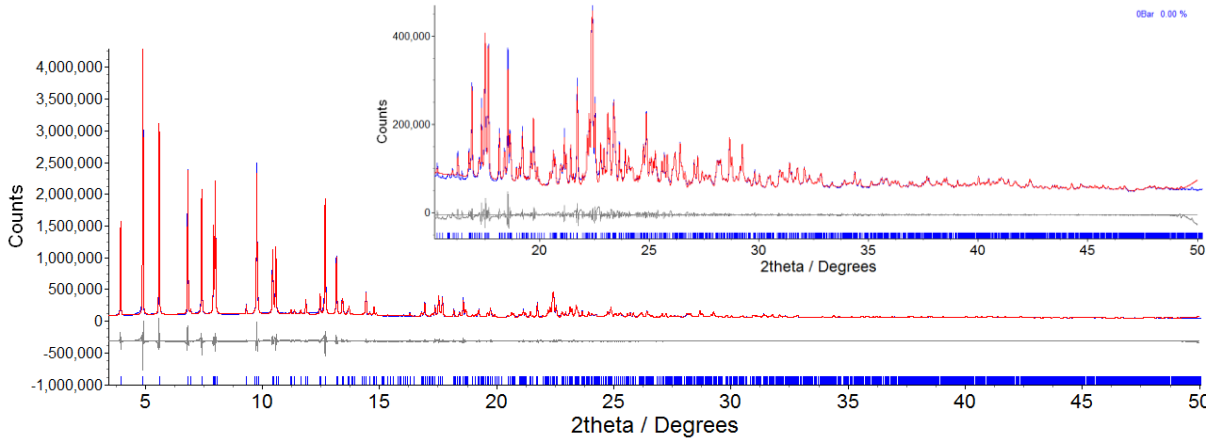

Figure 26 – Observed (blue) and calculated (red) and difference plot [I_{obs} - I_{calc}] (grey) of the Pawley[15] refinement of partially desolvated as-synthesised MOF $(Me_2NH_2)[In(ABDC)_2]$ under vacuum (**I5.1**) (2θ range 3.0 – 50.0 °, d_{min} = 0.97Å).

The two-phase refinement of **I5.4** employed 3,668 parameters (7 background, 1 zero error, 9 profile, 6 cell and 3,645 reflections), resulting in final indices of fit R_{wp} = 7.170, $R_{wp'}$ = 11.958. The final unit cell parameters were orthorhombic a = 15.2223 (2) Å, b = 24.0228 (4) Å, c = 33.4804 (5) Å, V = 12243.1 (3) Å^3, and orthorhombic a = 15.343 (1) Å, b = 26.627 (2) Å, c = 31.631 (3) Å, V = 12922 (2) Å^3. The fit is displayed in Figure 27

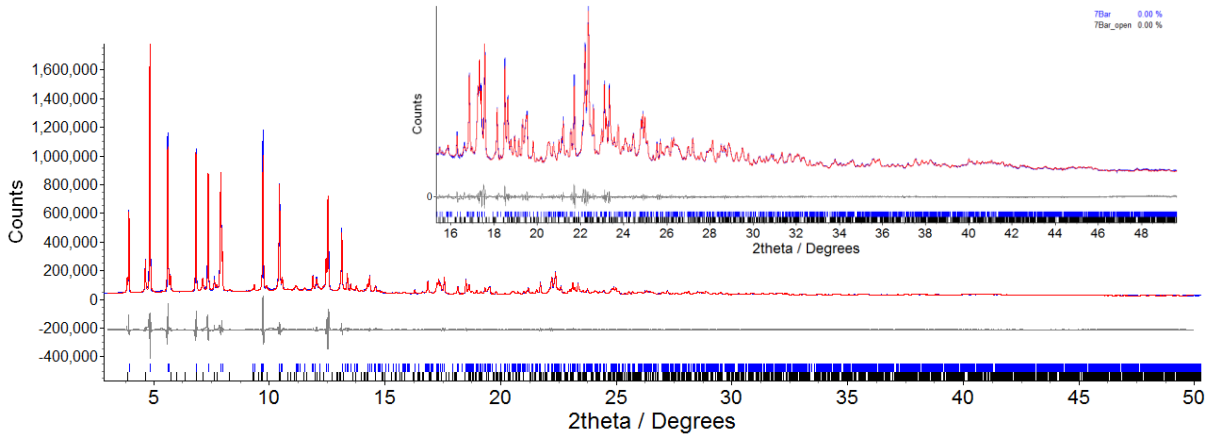

Figure 27 – Observed (blue) and calculated (red) and difference plot [I_{obs} - I_{calc}] (grey) of the Pawley[15] refinement of partially desolvated as-synthesised MOF $(Me_2NH_2)[In(ABDC)_2]$ under 7 bar CO_2 (**I5.4**) (2θ range 3.0 – 50.0 °, d_{min} = 0.97Å).

The single phase refinement of **I5.7** employed 1,926 parameters (12 background, 1 zero error, 5 profile, 3 cell and 1,905 reflections), resulting in final indices of fit R_{wp} = 6.188, $R_{wp'}$ = 12.899. The final unit cell parameters were orthorhombic a = 15.4054 (2) Å, b = 26.9771 (4) Å, c = 31.2639 (5) Å, V = 12993.0 (3) Å^3. The fit is displayed in Figure 28

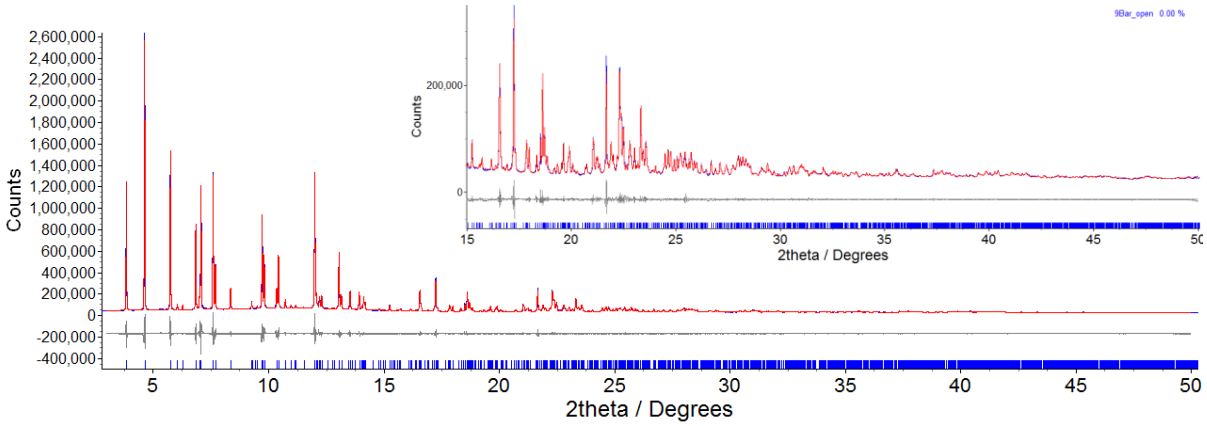

Figure 28 – Observed (blue) and calculated (red) and difference plot [I_{obs} - I_{calc}] (grey) of the Pawley[15] refinement of partially desolvated as-synthesised MOF $(Me_2NH_2)[In(ABDC)_2]$ under 10 bar CO_2 (**I5.7**) (2θ range 3.0 – 50.0 °, d_{min} = 0.97Å).

Powder diffraction experiment 3 (**I6**)

A powdered sample of as-synthesised MOF $(Me_2NH_2)[In(ABDC)_2]$ was heated at 150 °C for 20 mins inside a Schlenck tube under constant nitrogen flow. The sample was evacuated and transferred into an argon containing glovebox where it was packed into a 0.7 mm quartz capillary. The capillary was then fixed into the I11 gas cell using araldite adhesive. The sample was placed under dynamic vacuum (≈10^{-5}mbar) for 30 mins before collecting a powder pattern on the I11 beamline (**I6.1**), λ = 0.82582(2) Å.[11, 12] The sample was then loaded with successive pressures of CO_2 ; 1 bar, 5 bar, 10 bar and 20 bar, and allowed to equilibrate for 30 mins before collected powder patterns (**I6.2 – I6.5**). The powder patterns are displayed in Figure 29 and the unit cell values from Pawley refinements of all patterns are shown in Table 6. The progression along the known breathing trend line can be found in section 4.4.3. All data was recorded at room temperature.

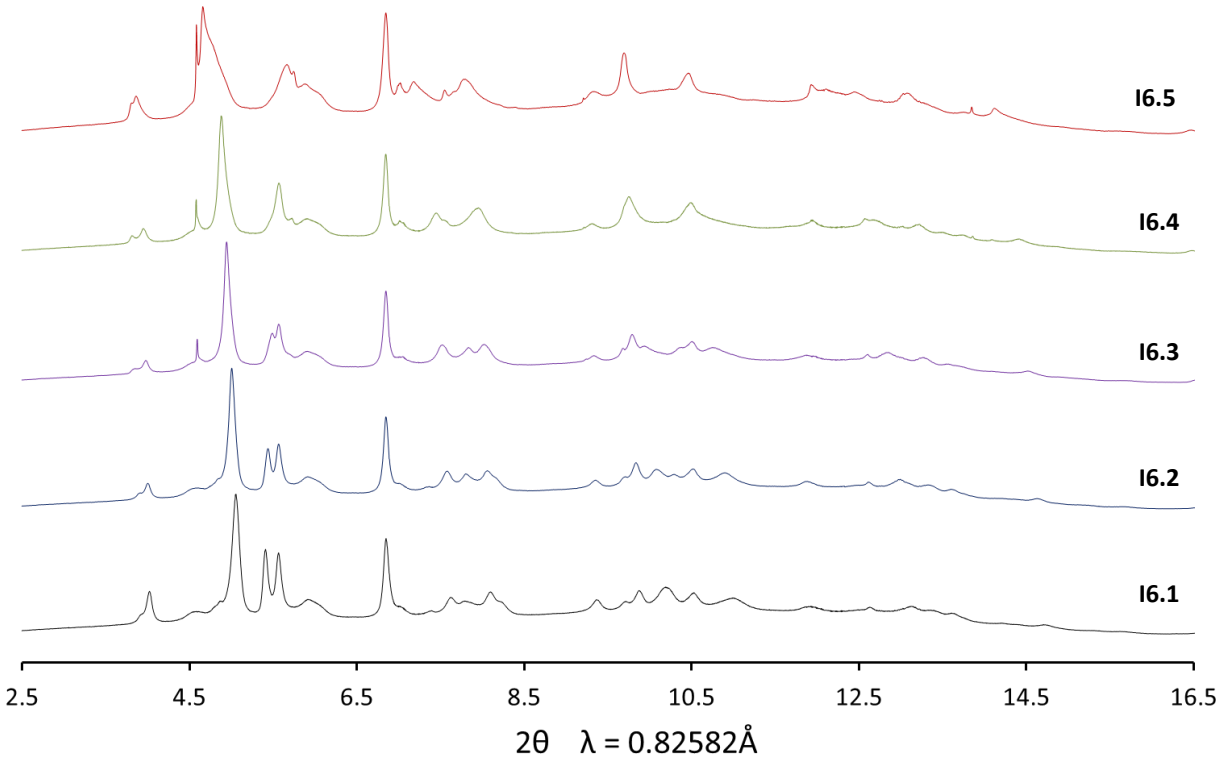

Figure 29 - Powder diffraction patterns obtained during *in situ* crystallographic gas uptake experiment **I6** on a partially desolvated as-synthesised MOF $(Me_2NH_2)[In(ABDC)_2]$

Table 6 - Unit cell parameters determined during crystallographic studies of CO_2 uptake in partially desolvated as-synthesised MOF $(Me_2NH_2)[In(ABDC)_2]$ (**I6**)

Sample Description	Data set Code	*a* (Å)	*b* (Å)	*c* (Å)	*V* (Å^3)
Vacuum after heat treatment	**I6.1**	14.961(4)	22.016(8)	34.71(1)	11433(6)
1 bar CO_2	**I6.2**	14.974(4)	22.324(8)	34.50(1)	11532(6)
5 bar CO_2	**I6.3_1**	15.029(6)	22.82(1)	34.31 (1)	11763(8)
5 bar CO_2 (2nd phase)	**I6.3_2**	15.314(5)	26.98(1)	31.47(1)	13000(10)
10 bar CO_2	**I6.4_1**	15.023(5)	23.176(5)	33.90(1)	11804(6)
10 bar CO_2 (2nd phase)	**I6.4_2**	15.278(2)	26.916(7)	31.256(6)	12853(5)
20 bar CO_2	**I6.5**	15.25(2)	25.56(4)	32.24(5)	12570(31)

The unit cells of the framework were initially determined by analysis of the positions of the first few Bragg reflections and their known Miller indices. These unit cell parameters were used as a starting point for Pawley[15] refinements. Representative fits for vacuum (**I6.1**), 5 bar (**I6.3**) and 20 bar (**I6.5**) are detailed below. **I6.1**, **I6.2** and **I6.5** were fit with single-phase refinements and **I6.3 a**nd **I6.4** were fit using two-phase refinements. **I6.5** was attempted to be fit with a two-phase refinement but the

phases were too similar in unit cell parameters to give a sufficiently reliable two-phase fit. **I6.5** was also seen to show peaks shapes implying a large distribution of phases rather than a one or two distinct crystalline environments. This led to a poor fit and bad crystallographic model and will be discussed in more detail in section 4.4.3.

The single-phase refinement of **I6.1** employed 264 parameters (16 background, 1 zero error, 5 profile, 3 cell and 239 reflections), resulting in final indices of fit R_{wp} = 4.174, $R_{wp'}$ = 23.845. The final unit cell parameters were orthorhombic a = 14.961 (4) Å, b = 22.016 (8) Å, c = 34.71 (1) Å, V = 11433 (6) Å^3. The fit is displayed in Figure 30

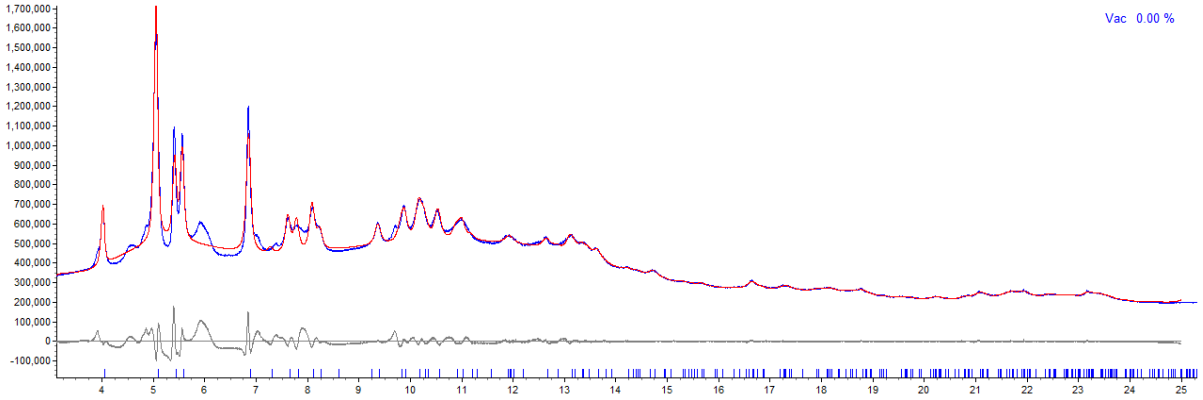

Figure 30 – Observed (blue) and calculated (red) and difference plot [I_{obs} - I_{calc}] (grey) of the Pawley[15] refinement of partially desolvated as-synthesised MOF $(Me_2NH_2)[In(ABDC)_2]$ under vacuum (**I6.1**) (2θ range 3.0 – 25.0 °, d_{min} = 1.9Å).

The two-phase refinement of **I6.3** employed 537 parameters (16 background, 1 zero error, 9 profile, 6 cell and 505 reflections), resulting in final indices of fit R_{wp} = 2.646, $R_{wp'}$ = 13.770. The final unit cell parameters were orthorhombic a = 15.029 (6) Å, b = 22.82 (1) Å, c = 34.31 (1) Å, V = 11763 (8) Å, and orthorhombic a = 15.314 (5) Å, b = 26.98 (1) Å, c = 31.47 (1) Å, V = 13000 (10) Å^3. The fit is displayed in Figure 31

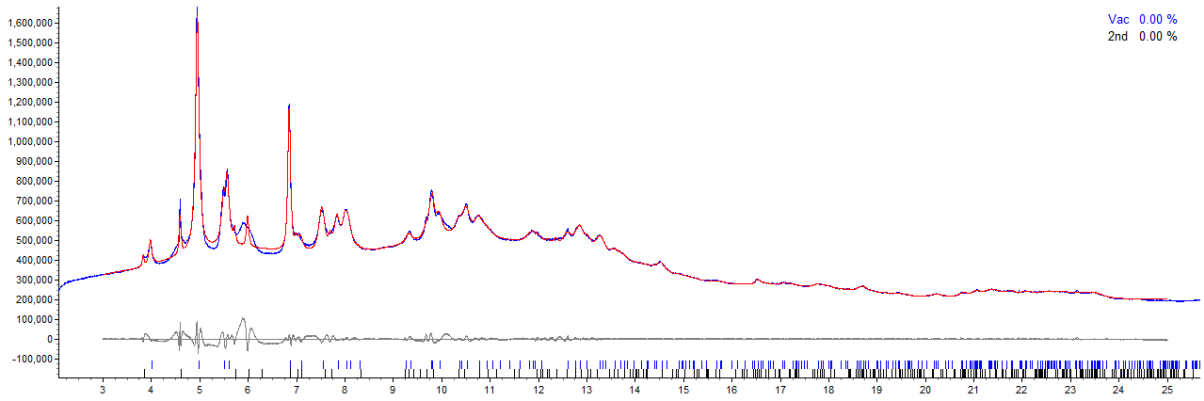

Figure 31 – Observed (blue) and calculated (red) and difference plot [I_{obs} - I_{calc}] (grey) of the Pawley[15] refinement of partially desolvated as-synthesised MOF $(Me_2NH_2)[In(ABDC)_2]$ under 5 bar CO_2 (**I6.3**) (2θ range 3.0 – 25.0 °, d_{min} = 1.9Å).

The single phase refinement of **I6.5** employed 288 parameters (16 background, 1 zero error, 5 profile, 3 cell and 263 reflections), resulting in final indices of fit R_{wp} = 4.758, $R_{wp'}$ = 22.149. The final unit cell parameters were orthorhombic a = 15.25 (2) Å, b = 25.56 (4) Å, c = 32.24 (5) Å, V = 12570 (31) Å. The fit is displayed in Figure 32

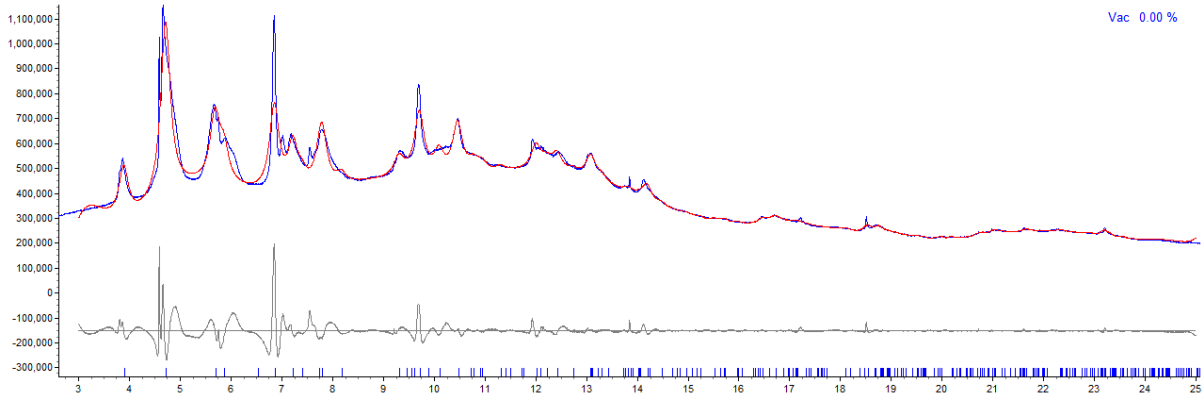

Figure 32 – Observed (blue) and calculated (red) and difference plot [I_{obs} - I_{calc}] (grey) of the Pawley[15] refinement of partially desolvated as-synthesised MOF $(Me_2NH_2)[In(ABDC)_2]$ under 20 bar CO_2 (**I6.5**) (2θ range 3.0 – 25.0 °, d_{min} = 1.9Å).

4.3.9 *In situ* crystallographic studies of CH_4 sorption in partially desolvated as-synthesised $(Me_2NH_2)[In(ABDC)_2]$

Single crystal diffraction experiment (**I7**)

Single crystals of as-synthesised MOF $(Me_2NH_2)[In(ABDC)_2]$ were removed from the DMF mother-liquor, dried in air for 15 minutes, and heated to 150 °C in a temperature-controlled oven. The sample was held at 150 °C for 15 minutes and the removed from the oven while still at 150 °C. A crystal was then chosen and mounted in the gas cell at beamline I19[4] as detailed in section 4.3.2, λ = 0.6889Å. The sample was placed under vacuum and an initial data collection was recorded (**I7.1**). 5 bar CH_4 was then introduced and the sample was removed from the diffractometer and held at 5 bar CH_4 for 16 hours, before returning to the diffractometer and recording a second data set (**I7.2**). Full structure solutions were not achievable but unit cell parameters for these measurements were able to be determined using all of the reflections collected. Table 7 shows the refined unit cell parameters during the study and Figure 38 shows the data points in comparison to the known breathing trend line.

Table 7 - Unit cell parameters determined during crystallographic studies of CH_4 uptake in partially desolvated as-synthesised MOF $(Me_2NH_2)[In(ABDC)_2]$ (**I7**)

Sample Description	Data set Code	*a* (Å)	*b* (Å)	*c* (Å)	*V* (Å^3)
Vacuum after heat treatment	**I7.1**	14.959(3)	22.980(5)	34.118(4)	11728(4)
5 bar CH_4 (16 hours equilibration)	**I7.2**	14.931(2)	23.933(8)	33.523(5)	11979(5)

All data recorded at 298K

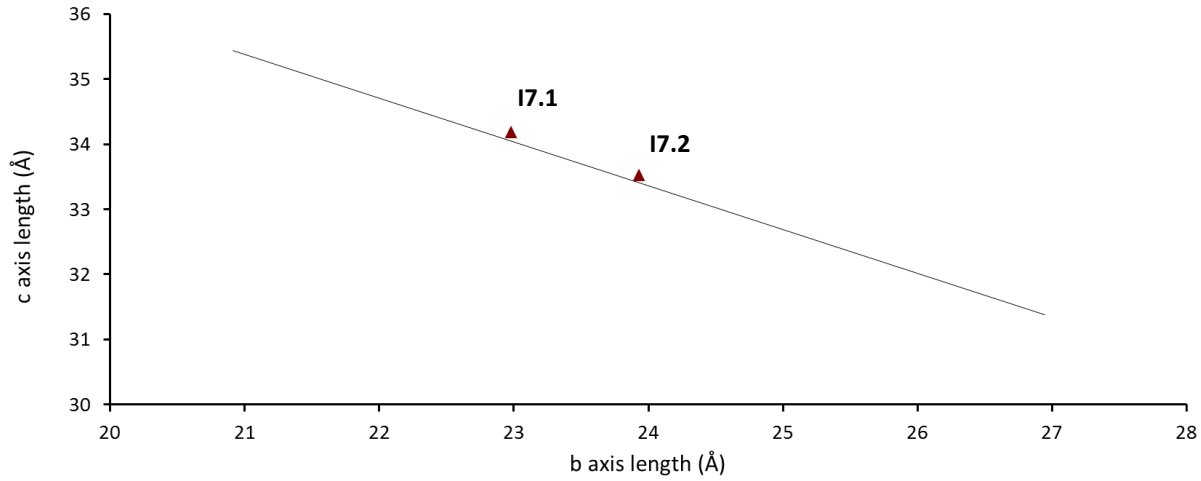

Figure 33 – *b*- and *c*-axis values for *in situ* single crystal diffraction experiment under CH_4 atmospheres **I7** on a partially desolvated as-synthesised $(Me_2NH_2)[In(ABDC)_2]$ in comparison to the trend line from single crystal desolvation studies of as-synthesised $(Me_2NH_2)[In(ABDC)_2]$ (**1-10**)

Powder diffraction experiment (**I8**)

The powder diffraction experiment was carried out directly after experiment **I4** using the same sample. The 20 bar CO_2 loaded sample **I4.5** was placed under dynamic vacuum (≈10^{-5} mbar) for 30 mins to remove the contained CO_2 before collecting a powder pattern on the I11 beamline (**I8.1**), λ = 0.82562(2) Å.[11, 12] The sample was then loaded with successive pressures of CH_4; 5 bar, 10 bar and 20 bar, and allowed to equilibrate for 30 mins before collected powder patterns (**I8.2 – I8.4**). The unit cell values from Pawley refinements are shown in Table 8, the progression along the known breathing trend line is shown in Figure 34 and the powder patterns are displayed in Figure 35. All data was recorded at room temperature.

Table 8 - Unit cell parameters determined during crystallographic studies of CH_4 uptake in partially desolvated as-synthesised MOF $(Me_2NH_2)[In(ABDC)_2]$ (**I8**)

Sample Description	Data set Code	*a* (Å)	*b* (Å)	*c* (Å)	*V* (Å^3)
Vacuum after CO_2 measurements (**I4**)	**I8.1**	15.1967(7)	23.655(2)	33.715(3)	12119(1)
5 bar CH_4	**I8.2**	15.2025(7)	23.773(2)	33.643(4)	12158(2)
10 bar CH_4	**I8.3**	15.2063(7)	23.839(2)	33.599(4)	12179(2)
20 bar CH_4	**I8.4**	15.2138(8)	23.927(2)	33.533(3)	12206(2)

All data recorded at 298K

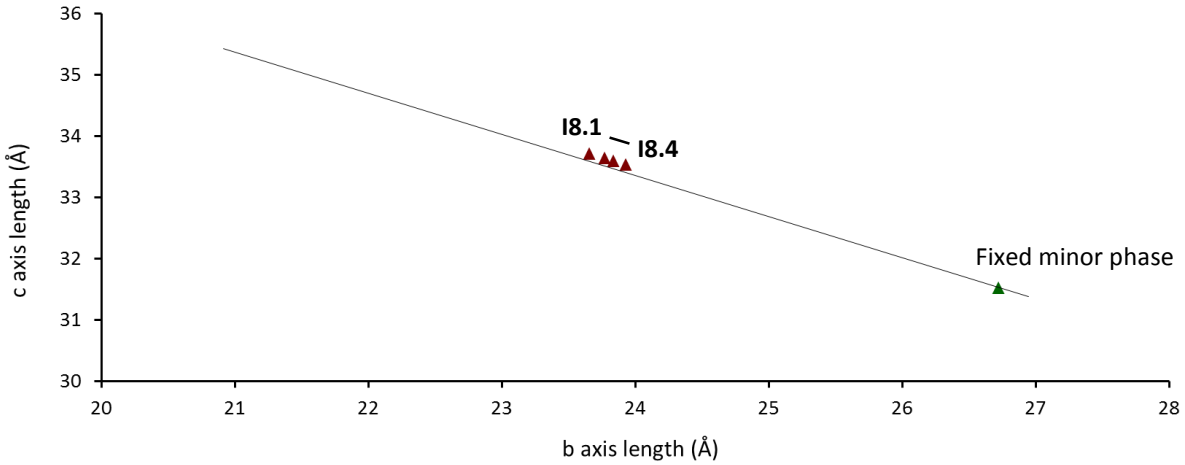

Figure 34 – *b*- and *c*-axis values for *in situ* powder diffraction experiment under CH_4 atmospheres **I8** on a partially desolvated as-synthesised $(Me_2NH_2)[In(ABDC)_2]$ in comparison to the trend from single crystal desolvation studies of as-synthesised $(Me_2NH_2)[In(ABDC)_2]$ (**1-10**). Red triangles; major phase at different pressures, green triangle; fixed minor phase

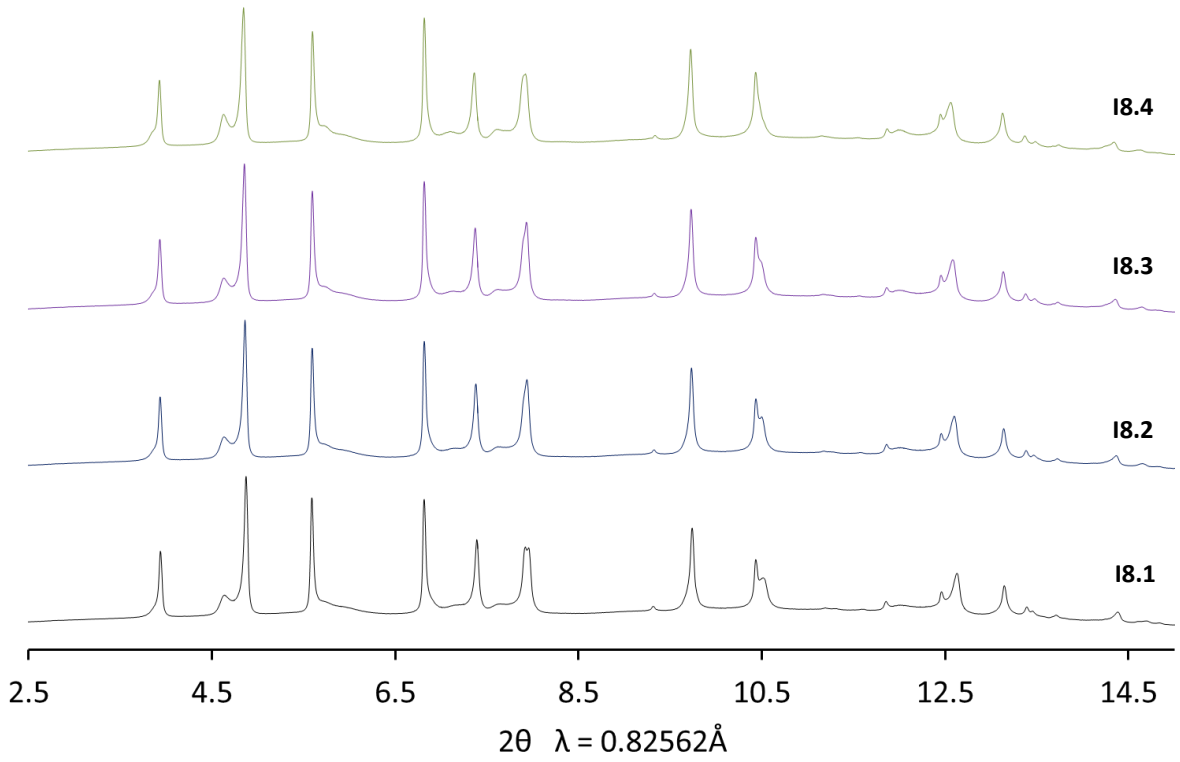

Figure 35 - Powder diffraction patterns obtained during *in situ* crystallographic CH_4 uptake experiment **I8** on a partially desolvated as-synthesised sample of MOF $(Me_2NH_2)[In(ABDC)_2]$

The unit cells of the framework were initially determined by analysis of the positions of the first few Bragg reflections and their known Miller indices. These unit cell parameters were used as a starting point for Pawley[15] refinements. Representative fits for vacuum (**I8.1**), and 20 bar (**I8.4**) are detailed below. All patterns were fit using two-phase refinements .The minor component was fixed as orthorhombic a = 15.317 Å, b = 26.723 Å, c = 31.522 Å, V = 12903 Å^3 based on the 5 bar measurement of the preceding CO_2 experiment (**I4.3_2**).

The two-phase Pawley refinement of **I8.1** employed 886 parameters (16 background, 1 zero error, 9 profile, 3 cell and 857 reflections), resulting in final indices of fit R_{wp} = 2.997, $R_{wp'}$ = 9.431. The final unit cell parameters of the refined phase were orthorhombic a = 15.1967 (7) Å, b = 23.655 (2) Å, c = 33.715 (3) Å, V = 12119 (1) Å^3. The fit is displayed in Figure 36.

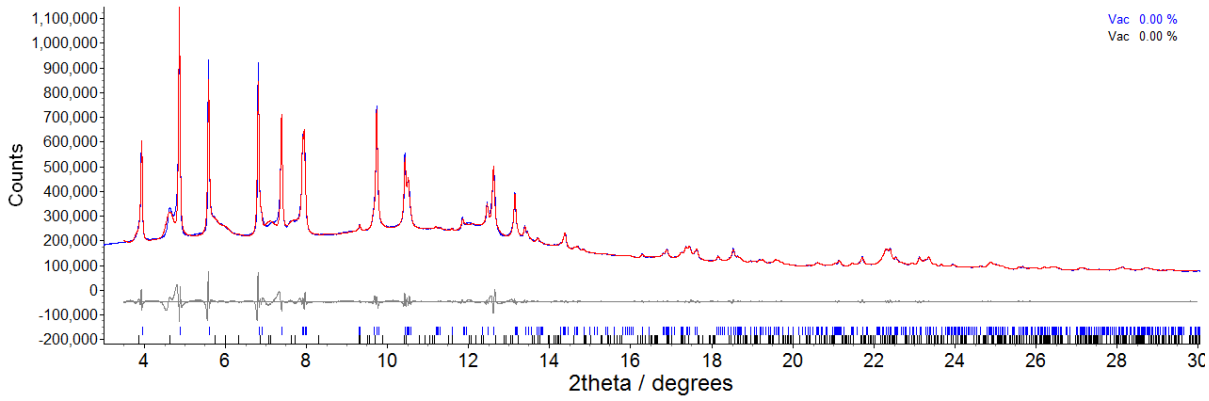

Figure 36 – Observed (blue) and calculated (red) and difference plot [I_{obs} - I_{calc}] (grey) of the Pawley[15] refinement of partially desolvated as-synthesised MOF $(Me_2NH_2)[In(ABDC)_2]$ under vacuum (**I8.1**) (2θ range 3.0 – 30.0 °, d_{min} = 1.6Å).

The two-phase refinement of **I8.4** employed 888 parameters (16 background, 1 zero error, 9 profile, 3 cell and 859 reflections), resulting in final indices of fit R_{wp} = 3.170, $R_{wp'}$ = 11.371. The final unit cell parameters of the refined phase were orthorhombic a = 15.2138 (8) Å, b = 23.927 (2) Å, c = 33.533 (3) Å, V = 12206 (2) Å^3. The fit is displayed in Figure 37.

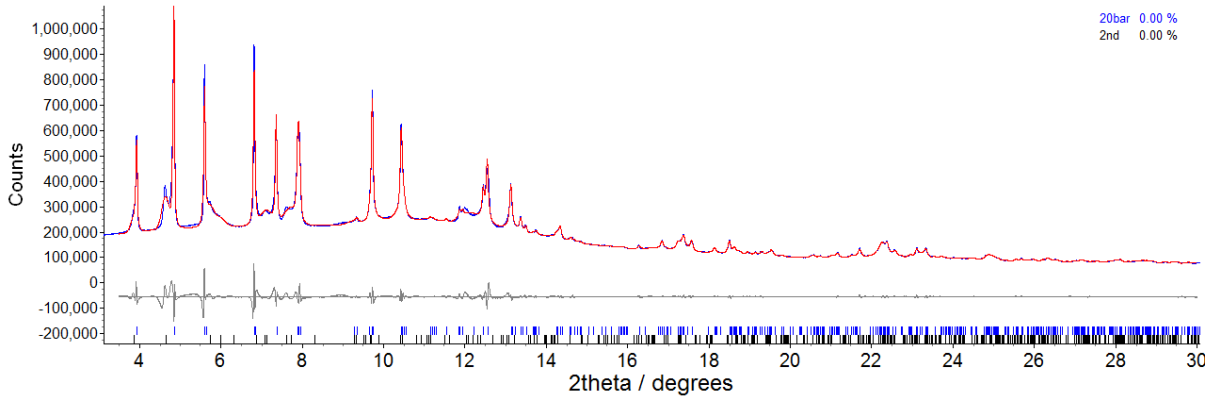

Figure 37 – Observed (blue) and calculated (red) and difference plot [I_{obs} - I_{calc}] (grey) of the Pawley[15] refinement of partially desolvated as-synthesised MOF $(Me_2NH_2)[In(ABDC)_2]$ under 20 bar CH_4 (**I8.4**) (2θ range 3.0 – 30.0 °, d_{min} = 1.6Å).

4.3.10 *In situ* crystallographic studies of CO_2 sorption in $(Me_2NH_2)[In(ABDC)_2(H_2O)]$

A powdered sample of $CHCl_3$-exchanged MOF $(Me_2NH_2)[In(ABDC)_2]$ was packed into a 0.5 mm quartz capillary and fixed into the I11 gas cell using araldite adhesive. The sample was placed under dynamic vacuum (≈10^{-5}mbar) for 2 hours before collecting a powder pattern on the I11 beamline (**I9.1**), λ = 0.82665(5) Å.[11, 12] The sample was seen to be predominantly the water-coordinated MOF $(Me_2NH_2)[In(ABDC)_2(OH_2)]$. The sample was then loaded with successive pressures of CO_2; 1 bar, 3 bar, 5 bar, 10 bar and 20 bar, and allowed to equilibrate for 30mins before collected powder patterns (**I9.2 – I9.6**). The sample was the returned to vacuum and a final measurement recorded (**I9.7**). The powder patterns are displayed in Figure 29. The peaks corresponding to the water-coordinated phase (**C2**) are labelled with triangles, and the peaks of open pore MOF (**1**) are labelled with asterisks. All data was recorded at room temperature.

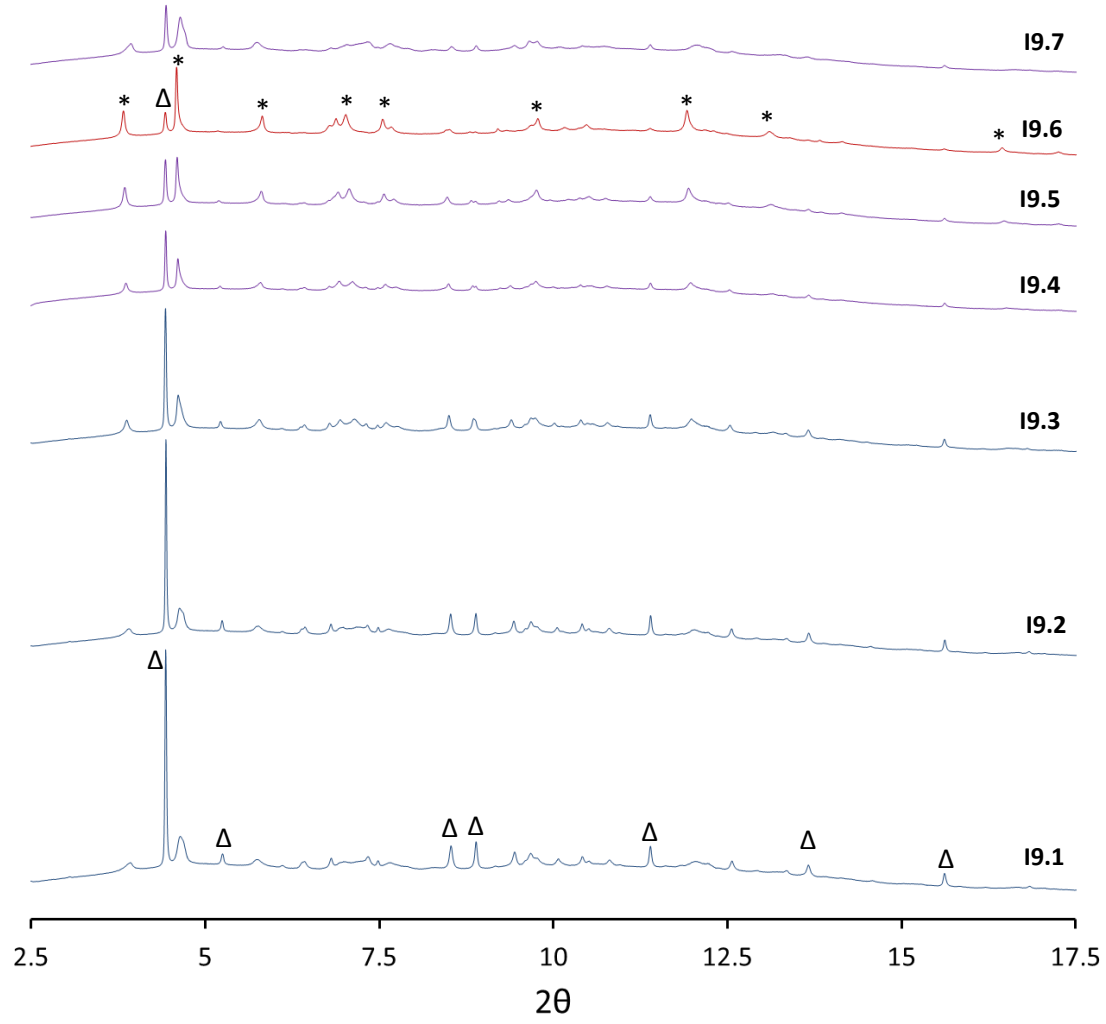

Figure 38 - Powder diffraction patterns obtained during *in situ* crystallographic CO_2 uptake experiment on a water-coordinated MOF $(Me_2NH_2)[In(ABDC)_2(H_2O)]$ (**I9**)

4.3.11 Complementary techniques used to characterise the as-synthesised $(Me_2NH_2)[In(ABDC)_2]$

NMR spectroscopy after gravimetric measurements

A solution-phase ^1H NMR spectrum of the as-synthesised framework after gravimetric measurement **G8** was collected. The MOF was digested using the method detailed in section 4.3.2. The spectrum is shown together with an enlarged section showing only the aromatic protons in Figure 39. The spectra show no peaks associated with the proton on the carbonyl carbon of the DMF, suggesting its complete removal in the desolvation process. Two proton environments however are seen between 2 and 3 ppm where only 1 cation peak is expected. Unfortunately one of the peaks doesn't quite have baseline separation with the DMSO, but neither peak appears provides suitable integration for the cation on its own, whereas the sum of the two environments does. Possible deprotonation of the cation is a suspected cause of the two different peaks.

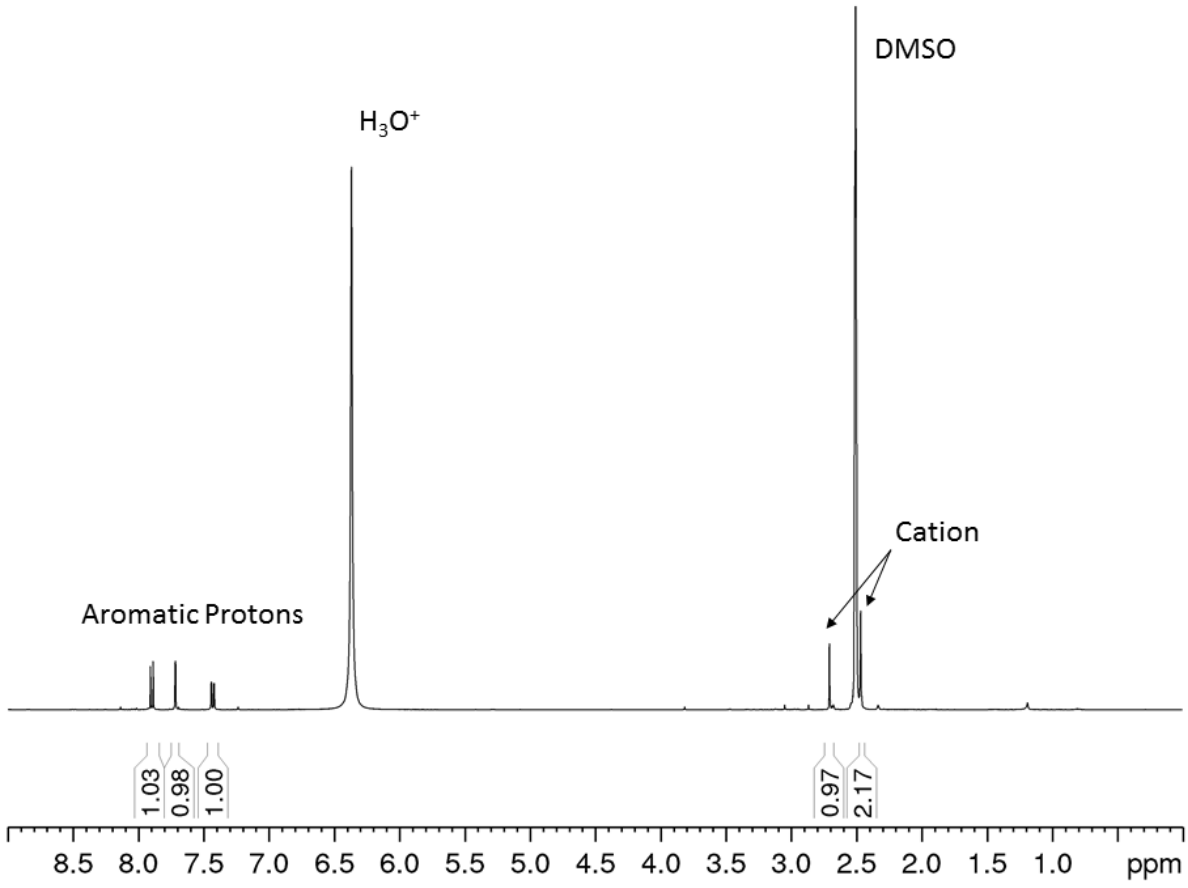

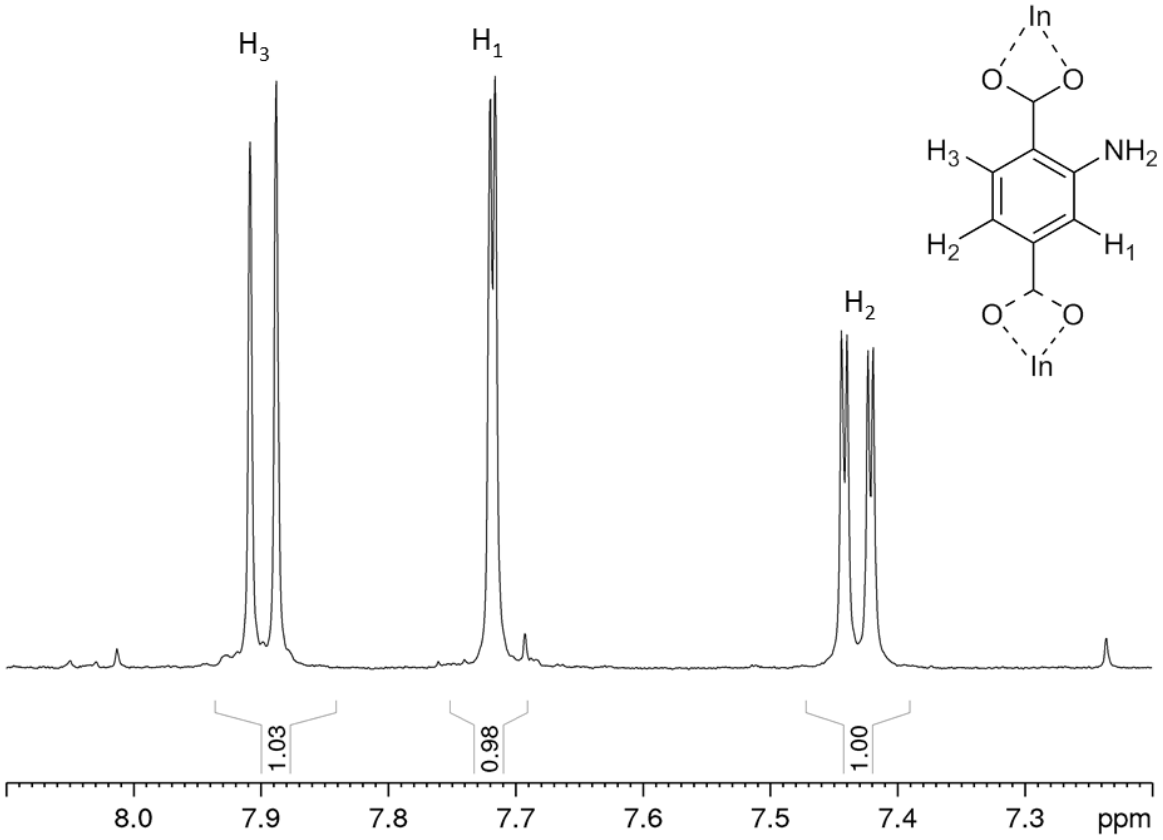

Figure 39 – Solution-phase ^{1}H NMR spectrum of digested as-synthesised MOF $(Me_2NH_2)[In(ABDC)_2]$ after gravimetric CO_2 adsorption study **G8** (Full spectrum previous page; aromatic region of spectrum this page).

The removal of the DMF was also confirmed by recording solid-state ^{13}C NMR of the as-synthesised framework before and after gravimetric CO_2 adsorption measurement **G8**. The spectra are shown in Figure 40 and Figure 41, respectively. The carbonyl peak of the DMF is no longer present in the spectrum after the adsorption measurements, suggesting it has been removed. The two peaks seen in Figure 41 between 30 and 50 ppm are suspected to be due to the two separate cation environments, which are often observed crystallographically, and not residual solvent or neutral dimethyl ammonia molecules.

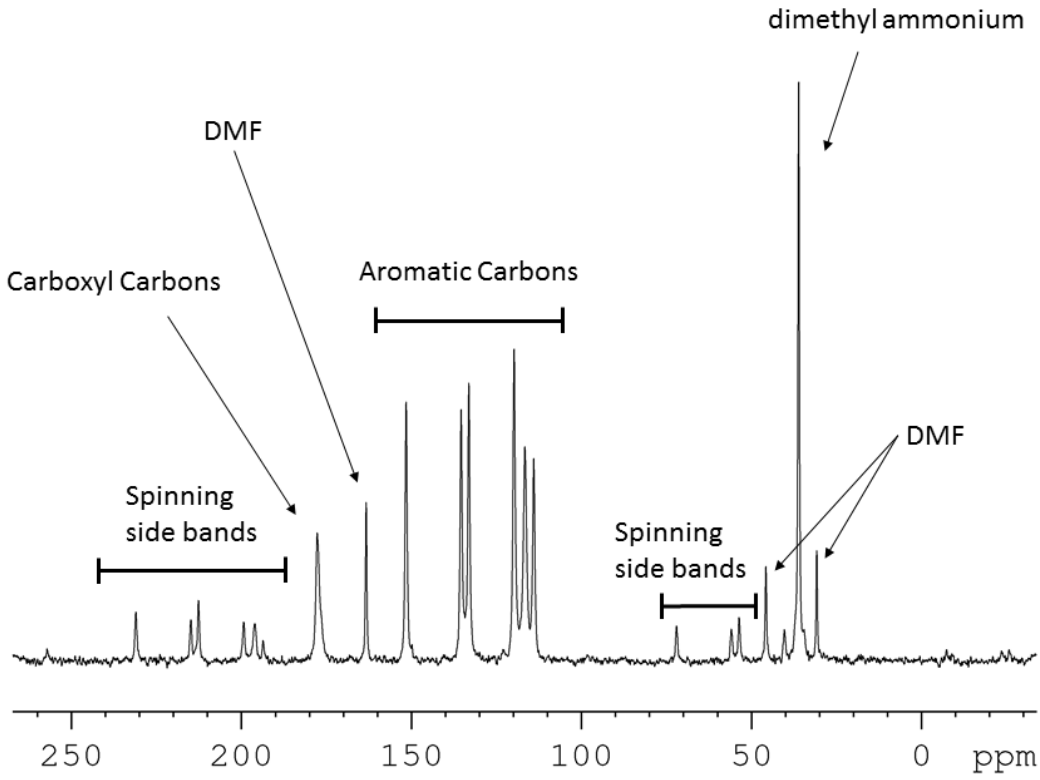

Figure 40 - Solid-state ^{13}C NMR spectrum of as-synthesised MOF $(Me_2NH_2)[In(ABDC)_2]$

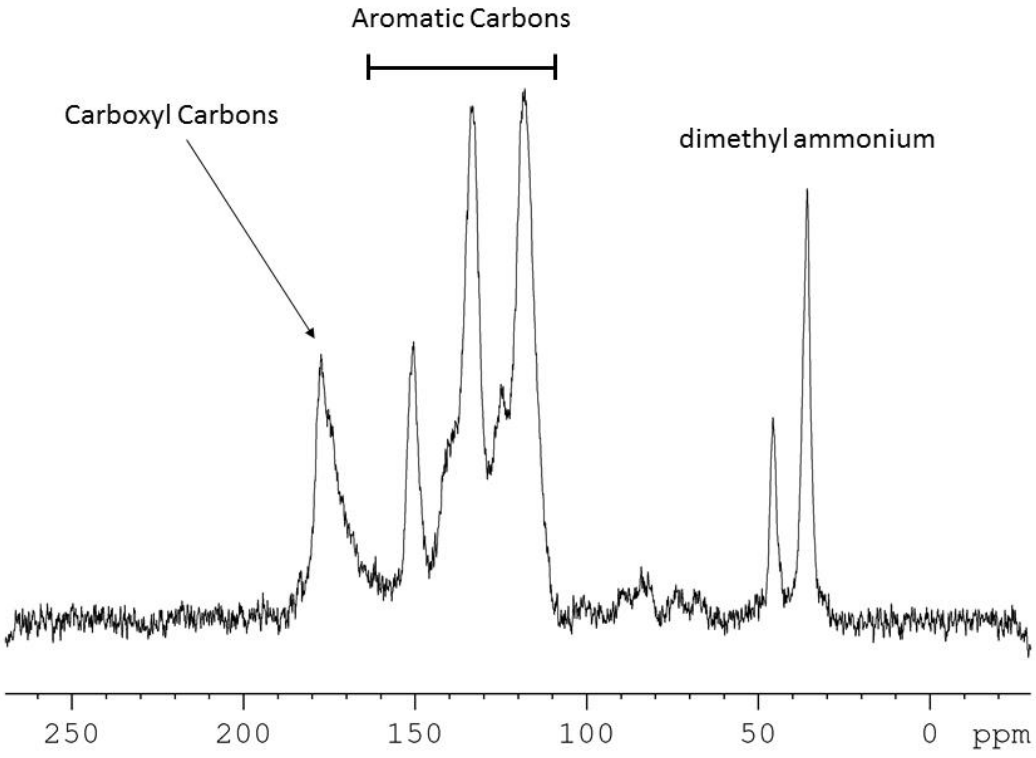

Figure 41 - Solid-state ^{13}C NMR spectrum of as-synthesised MOF $(Me_2NH_2)[In(ABDC)_2]$ after gravimetric adsorption isotherm **G8**

NMR spectroscopy after *in situ* crystallographic measurements

A solution-phase ^{1}H NMR spectrum of the as-synthesised framework was measured after the *in situ* crystallographic CO_2 uptake study **I5**. The framework was digested by the method detailed in section 4.2.2. The spectrum is shown together with an enlarged section showing only the aromatic protons in Figure 42.The spectrum shows that the framework contains roughly 1.6 DMF per indium unit, and also appears to show to two cation environments, but both peaks overlap with other protons.

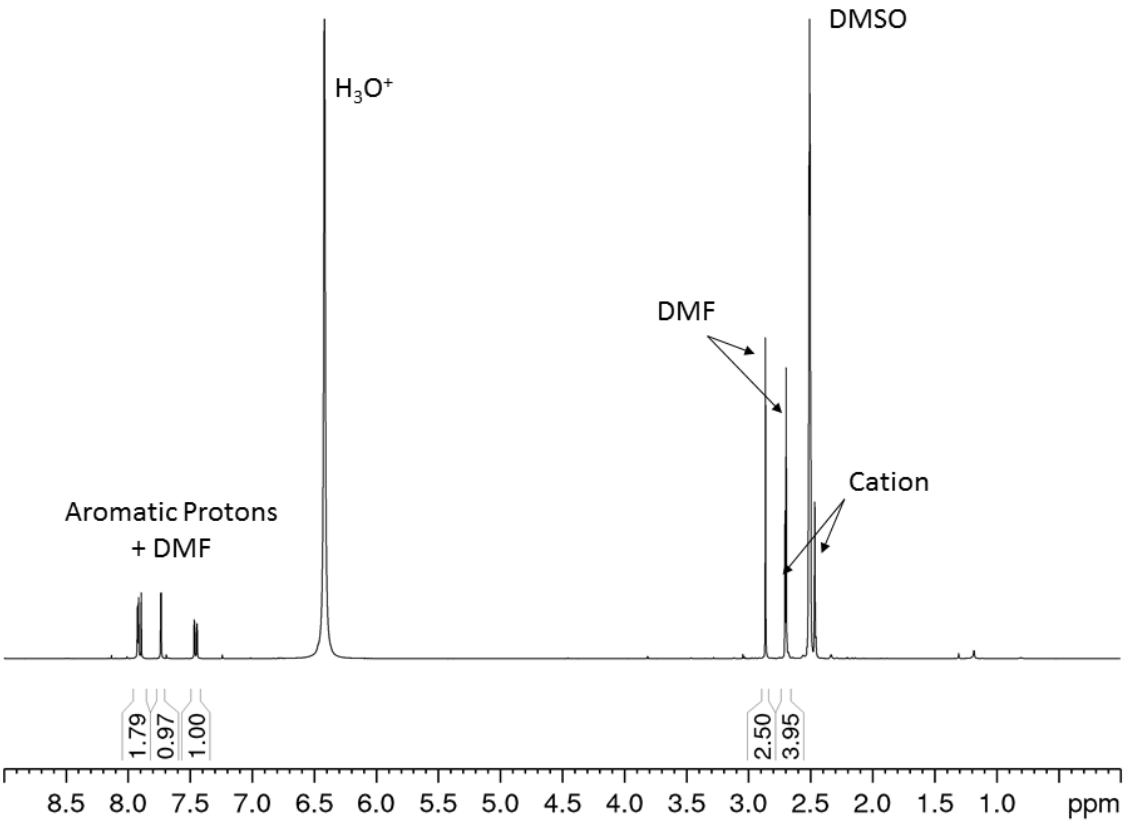

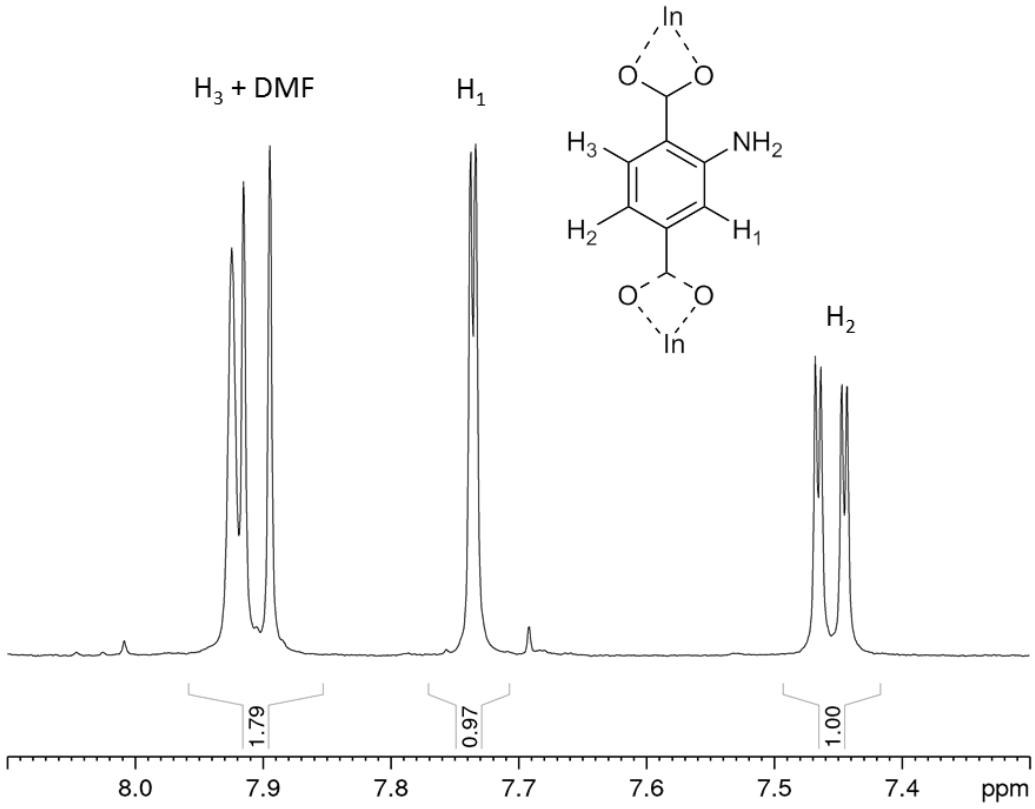

Figure 42 – Solution-phase ^{1}H NMR spectrum of digested as-synthesised MOF $(Me_2NH_2)[In(ABDC)_2]$ after *in situ* crystallographic CO_2 adsorption study **I5** (Full spectrum previous page; aromatic region of spectrum this page).

Infra-red spectroscopy

Solid-state infrared spectra were recorded for the as-synthesised MOF, the sample after gravimetric CO_2 adsorption study **G8** and the sample after *in situ* crystallographic study **I5**. The spectra are shown in Figure 43. The relative ratios of the DMF can be seen in the carbonyl stretching bang at ≈ 1650 cm^{-1}

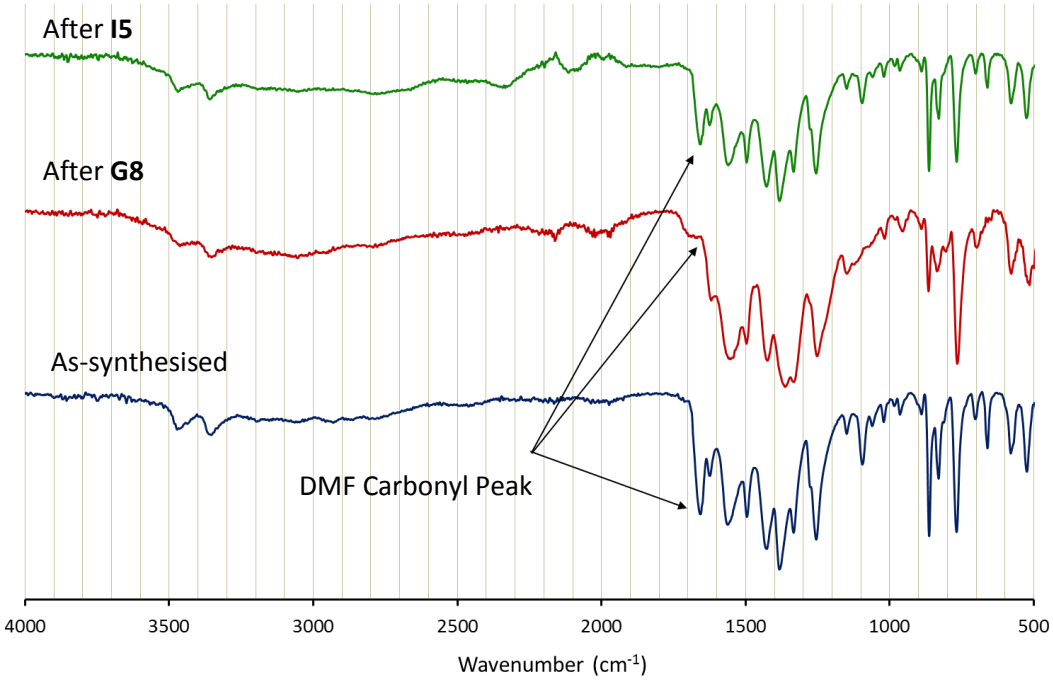

Figure 43 - Solid-state IR spectra of as-synthesised MOF $(Me_2NH_2)[In(ABDC)_2]$ (blue), sample after gravimetric CO2 adsorption measurements **G8** (red) and after *in situ* crystallographic study **I5** (green)

4.4 Results and Discussion

4.4.1 CO_2 adsorption studies on desolvated $(Me_2NH_2)[In(ABDC)_2]$

Gravimetric adsorption data

The gravimetric CO_2 adsorption isotherms were obtained for both the as-synthesised and $CHCl_3$-exchanged MOF. Prior to the measurements the $CHCl_3$-exchanged compound was desolvated by heating at 80 ^oC and applying high vacuum to mimic the literature procedure.[1] The as-synthesised version was evacuated at 150 ^oC under nitrogen flow, based on the previous desolvation studies. In each case total mass loss was consistent with full desolvation and the residual mass stabilised. A comparison of the isotherms is displayed in Figure 44, showing a significantly higher CO_2 uptake from the desolvated $CHCl_3$-exchanged MOF (blue circles) than from the desolvated as-synthesised MOF (red circles). The measurement on the $CHCl_3$-exchanged MOF shows a reasonable correlation to the reported value (after conversion from volumetric units) although is slightly lower in total uptake (6.24 mmol g^{-1} compared to ≈ 7 mmol g^{-1}). This uptake is comparable with dehydrated MIL-53(Cr) [Cr(OH)(BDC)] which exhibits a CO_2 uptake of ≈ 9 mmol g^{-1}, at 20 bar and 304K,[22] but is substantially lower than the well-known frameworks MOF-5 $[Zn_4O(BDC)_3]$ (≈ 18 mmol g^{-1})[23] and Mil-101(Cr) $[Cr_3F(H_2O)_2(\mu_3\text{-}O)(BDC)_3]$ (≈ 19 mmol g^{-1})[24] (recorded at 298K). The maximum uptake capacities of MOFs under 20 bar CO_2 have so far been shown at around 25 mmol g^{-1} (MOF-177 $[Zn_4O(BTB)_3]$ BTB = 4,4',4''-benzene-1,3,5-triyl-tribenzoate).[25]

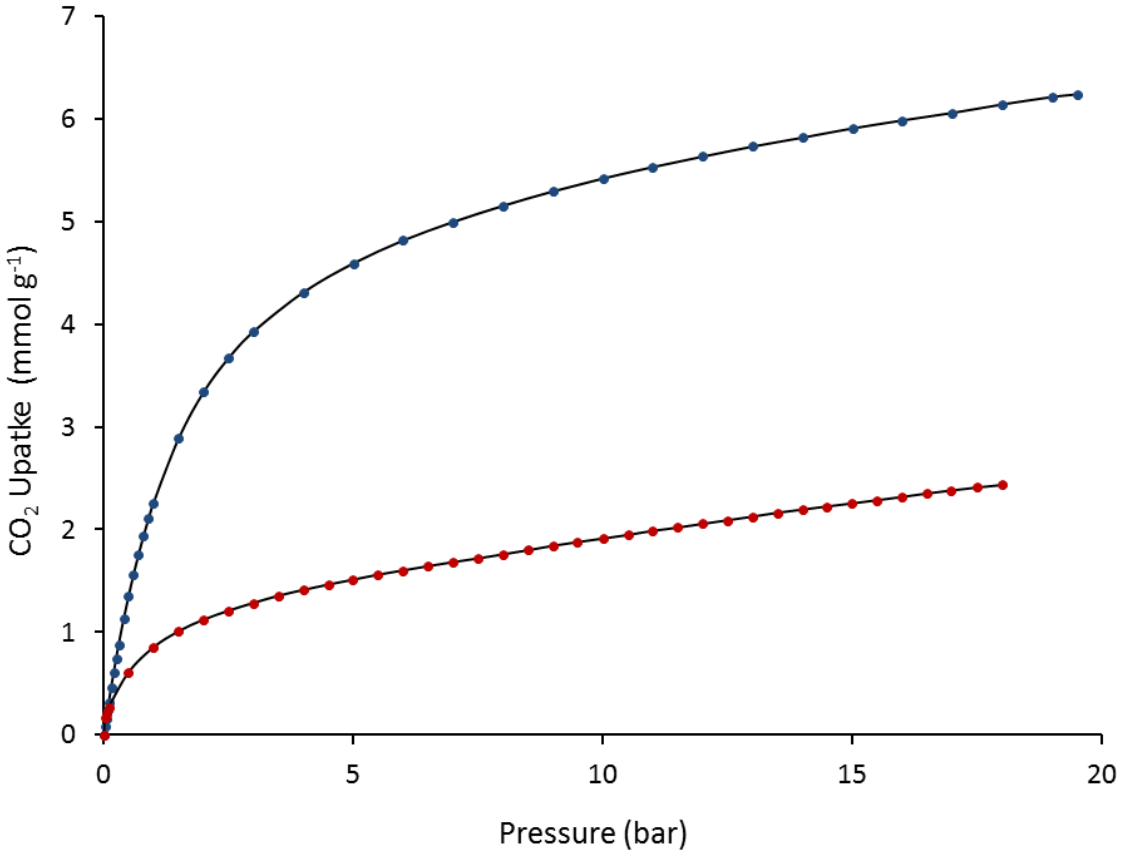

Figure 44 – Gravimetric CO_2 adsorption isotherms for desolvated $CHCl_3$ exchanged MOF $(Me_2NH_2)[In(ABDC)_2]$ (**G4**) (blue circles) and desolvated as-synthesised MOF $(Me_2NH_2)[In(ABDC)_2]$ (**G1**) (red circles)

The gravimetric CO_2 adsorption data were numerically fitted to known adsorption models; the $CHCl_3$-exchanged framework matches a Langmuir model but the as-synthesised framework fits a BET model (Figure 45). The Langmuir model implies monolayer formation of gas molecules only interacting with the walls of the channels, common in large pore materials, whereas a BET model represents multilayer formation, with interactions to both the walls of the channel and other gas molecules, often observed in narrow pore materials. Two representations of pore shapes likely to lead to Langmuir and BET models are illustrated in Figure 46.

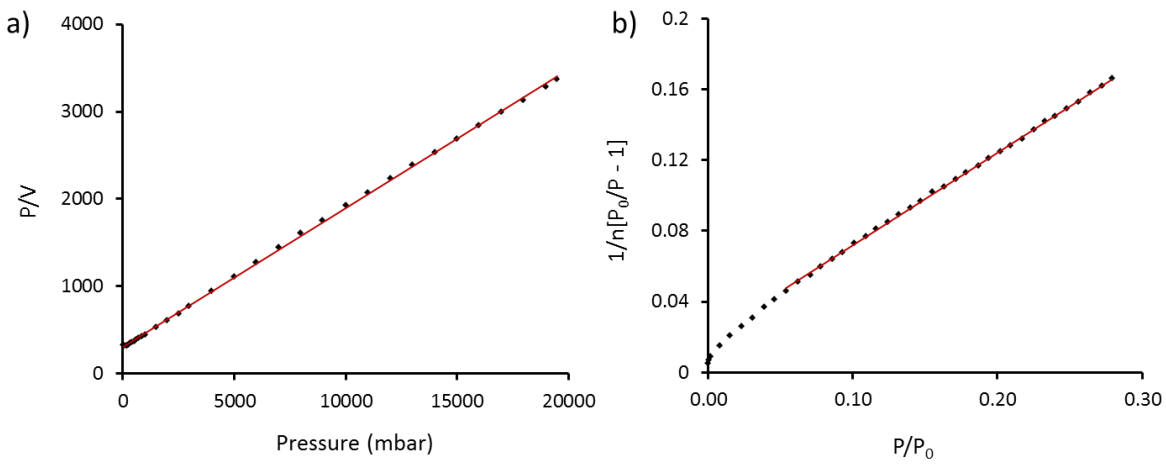

Figure 45 – Numerical fits of adsorption models to the gravimetric CO_2 uptake for a) desolvated $CHCl_3$ exchanged MOF $(Me_2NH_2)[In(ABDC)_2]$ - Langmuir fit, and b) desolvated as-synthesised MOF $(Me_2NH_2)[In(ABDC)_2]$ - BET fit in the P/P_0 range 0.05 to 0.279

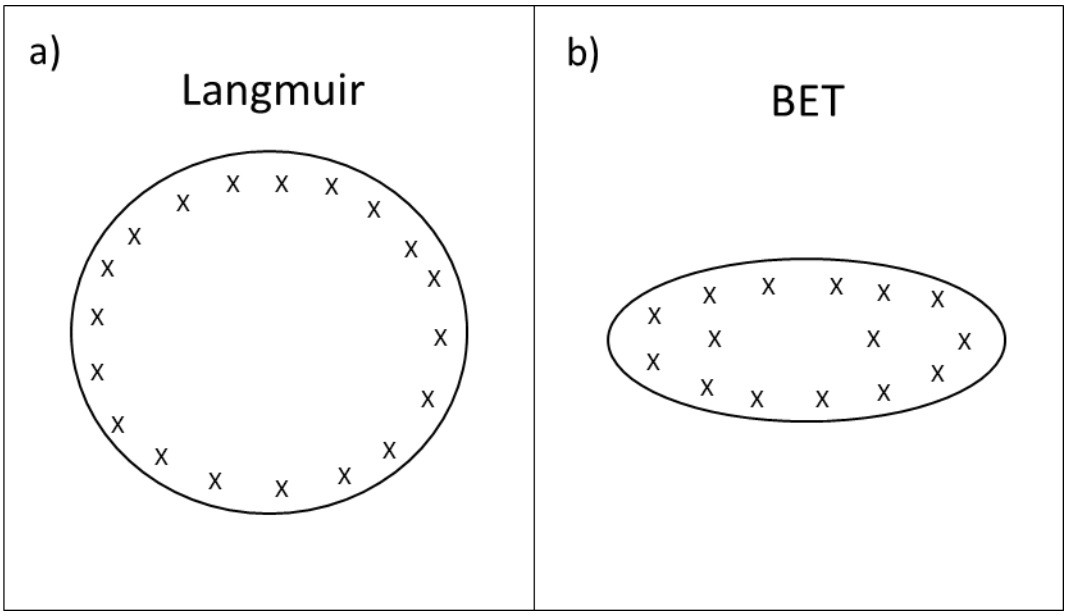

Figure 46 – Pore shape representations leading to a) Langmuir (monolayer) behaviour and b) BET (multilayer) behaviour

Analysis

The differences observed in the gravimetric data imply a change to accessible pore space due to structural differences between the frameworks after removal of the two different solvents. This can be directly related to the findings of chapters 2 and 3 which suggest that the $CHCl_3$ version remains in an open-pore form during desolvation, whereas the as-synthesised framework exhibits a significant pore closing. Volumetric nitrogen isotherms at 77K (Figure 47) were used to measure the accessible surface area of the framework and show that the as-synthesised version is almost non-

porous, and therefore highly closed, whereas the $CHCl_3$-exchanged version displays a reasonably large surface area, and therefore can be considered to be in open-pore form.

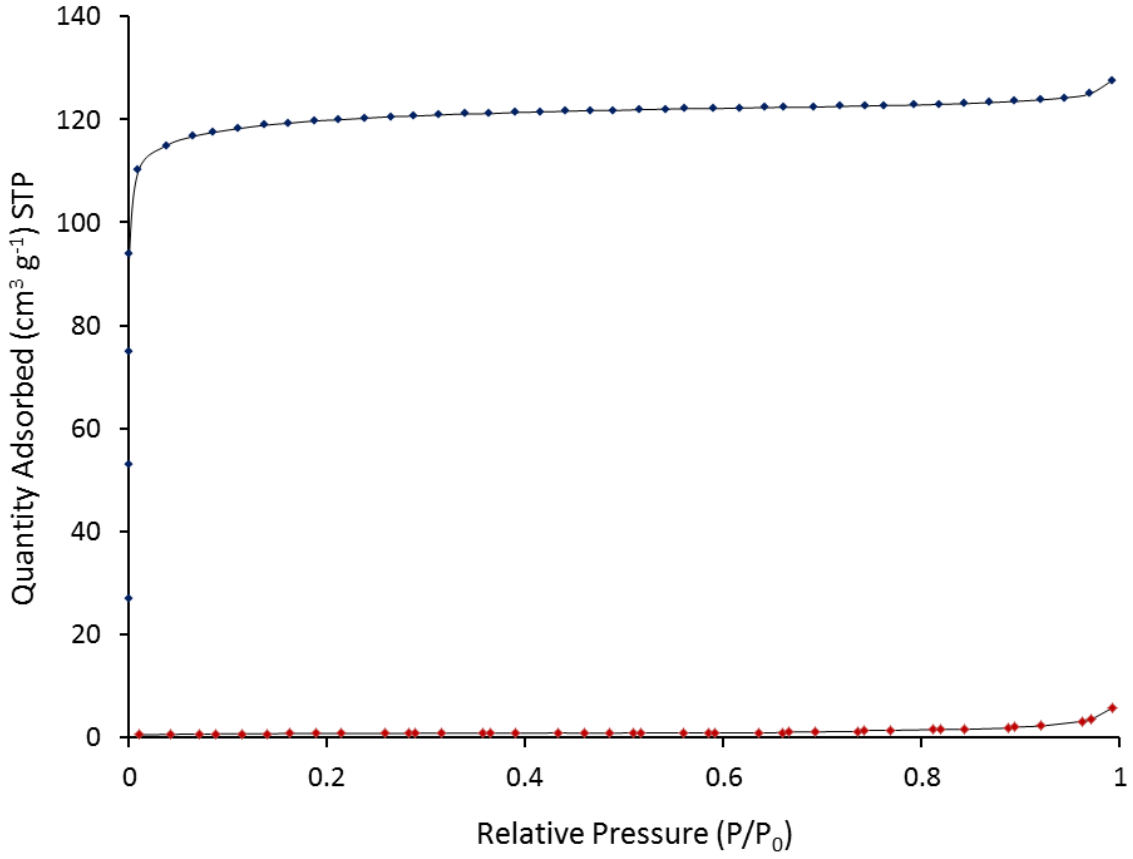

Figure 47 - Volumetric N_2 adsorption isotherms for desolvated $CHCl_3$-exchanged MOF $(Me_2NH_2)[In(ABDC)_2]$ (blue circles) (**V2**) and desolvated as-synthesised MOF $(Me_2NH_2)[In(ABDC)_2]$ (red circles) (**V1**) recorded at 77K

Chapter 3 discussed the idea that the remaining solvent within the pores of the closed as-synthesised MOF could be responsible for holding it shut, and if this is then removed the framework returns to an open-pore form, as demonstrated by the dehydration of MIL-53, which is held in closed- pore form by water molecules.[26] Such a scenario would suggest that on full desolvation both the $CHCl_3$ and DMF versions should be identical, which is clearly not the case. The full desolvation of the as-synthesised MOF can be confirmed by comparing the mass loss during the desolvation step of the gravimetric measurements to the solvent content identified by elemental analysis and TGA. These results in chapter 2 suggested that the solvent content lies in the range of 1.75 - 2 DMF molecules and 1.25 - 1.5 water molecules, giving an expected mass loss between 23-25%. This correlates well to the mass loss prior to the adsorption measurements of 24.3%. This mass loss is illustrated in Figure 48 compared to an example TGA trace, and shows a reasonably good match

considering the potential variability in solvent content. Further evidence of solvent removal was provided by solution-phase ^{1}H NMR and solid-state ^{13}C NMR analysis revealing a complete loss of the DMF peaks. It can therefore be concluded that the framework is not being held shut by any residual solvent.

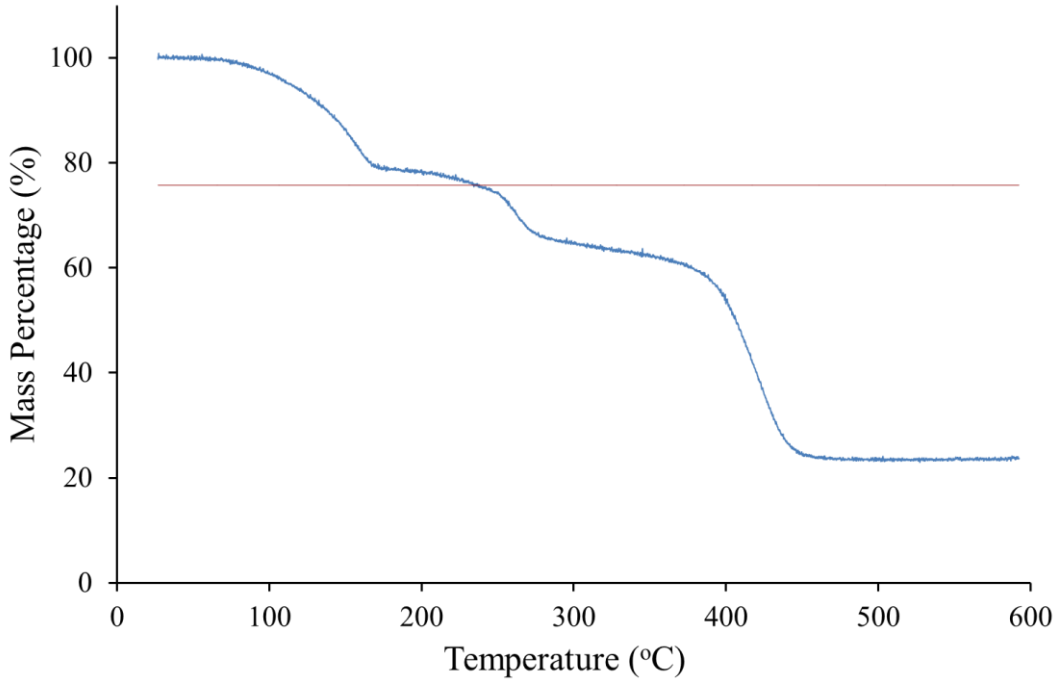

Figure 48 - Thermogravimetric analysis of as-synthesised $(Me_2NH_2)[In(ABDC)_2]$ (blue line) in comparison to the mass loss observed during desolvation prior to gravimetric CO_2 measurement (**G1**)

The MOF can be considered as having two different desolvated pore structures, resulting in the two different gas sorption behaviours. The isotherms show no evidence of step behaviour, and the uptake for the as-synthesised version consistently remains lower than the $CHCl_3$ version, suggesting that there is no transition of the closed-pore to the open-pore material during the CO_2 uptake. This has been confirmed for the majority of the accessible P/P_0 range for CO_2 by collection an isotherm up to 20 bar at -15 °C ($P/P_0 \approx 0.9$) (**G2**). The non-porous structure of the closed desolvated as-synthesised MOF is, however, suspected to open slightly to allow accommodation of the CO_2 molecules. This most likely occurs in a continuous manner, similar to the observed water uptake.

The behaviour described above suggests two reasonably stable thermodynamic minima for the framework that do not readily interconvert. The MOF is thought to be held closed by strong framework-framework or framework-cation interactions that only form once the framework has narrowed to certain point and all the solvent has been removed. The interactions must be substantial to avoid being broken by the high CO_2 pressure. The initial narrowing of the pores

appears to require the presence of a more strongly interacting guest than CO_2, such as DMF, and therefore, unlike MIL-53,[27, 22, 28] loading the open-pore MOF with CO_2 does not induce a closing of the pore. This behaviour is verified by the *in situ* diffraction experiments.

In situ diffraction studies

To further understand the effect of gas sorption in the framework, the structural changes of the desolvated $CHCl_3$-exchanged MOF during gas sorption was studied by *in situ* crystallographic techniques. A powder pattern of the activated (desolvated) material was obtained under vacuum and at 20 bar CO_2 (**I1.1** & **I1.2**). The data showed a small closing of the pores under vacuum, followed by an expansion of the structure along the known breathing trend line during the CO_2 adsorption. This is illustrated in Figure 49 using the *b* and *c* unit cell axis values. The relatively open framework structure of the $CHCl_3$ exchanged MOF is therefore not rigid but displays a small dynamic response to the guest uptake. A similar behaviour is expected for the fully desolvated as-synthesised framework, but starting from the narrow pore and displaying a higher energy barrier to opening due to the strong framework interactions holding it closed. Unfortunately this could not yet be studied as the fully desolvated as-synthesised version has not yet been able to be characterised crystallographically. The isotherms for both frameworks show no evidence of a plateau at higher CO_2 pressures which would be expected in normal type I materials. This implies that within the pressure range of the measurements a saturation point has not been reached, due to the continuous expansion of the structures during increasing CO_2 uptake.

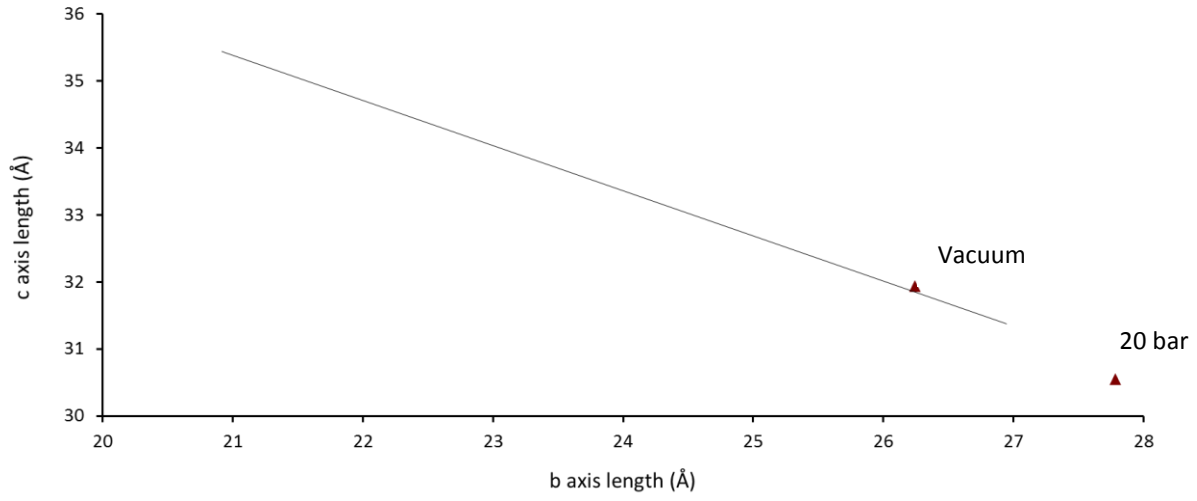

Figure 49 - Comparison of the *b* and *c* unit cell axis lengths of an *in situ* crystallographic study on $CHCl_3$-exchanged MOF$(Me_2NH_2)[In(ABDC)_2]$ (**I1**). The trend line is from single crystal desolvation studies of as-synthesised $(Me_2NH_2)[In(ABDC)_2]$ (**1-10**)

4.4.2 CH_4 adsorption studies on desolvated $(Me_2NH_2)[In(ABDC)_2]$

Gravimetric CH_4 adsorption data were also collected for both the desolvated as-synthesised MOF and the desolvated $CHCl_3$-exchanged MOF. The results are displayed in Figure 50 compared to the previously shown CO_2 isotherms. The uptake of CH_4 by the $CHCl_3$-exchanged MOF is higher than in the as-synthesised MOF, which would be expected due to the difference in pore size. There is, however, also a difference in the CO_2 vs CH_4 selectivity. The CH_4 uptake for the direct activation of the as-synthesised MOF approximately matched its CO_2 uptake at the highest pressure recorded (4.5 bar), and is suggestive of potentially reversing the selectivity at higher pressures. Unfortunately the experiments using CH_4 were limited to 5 bar so it has not yet been possible to pursue this further. The $CHCl_3$ version in contrast showed significantly reduced CH_4 adsorption compared to its CO_2 uptake, exhibiting selectivity of CO_2 over CH_4, as reported in the original publication.[1] Our results, however, call into question the extent of the selectivity asserted in the original report; our recorded CH_4 isotherm showed an uptake >2.5mmol g^{-1} at 4.5 bar in comparison to the value quoted as "below the detection limit of the apparatus" in the original publication.[1] The CH_4 uptake recorded is similar to dehydrated MIL-53 (ca. 2 mmol g^{-1} at 304K) which is known to be in its large pore form, similar to the desolvated $CHCl_3$-exchanged framework, and exhibit a similar scale CO_2 uptake.[22] Our recorded uptake and CO_2 *vs* CH_4 selectivity therefore doesn't seem unreasonable. Full kinetic analysis of the adsorption data has not yet been completed, but the uptake of the CH_4 uptake was observed to be very slow. The difference between the original report and our gravimetric studies is therefore thought to originate from insufficient times being used to permit equilibration in the published study. Under practical conditions slower adsorption kinetics for CH_4 could still lead to the selectivity observed in the reported mixed gas stream experiment, particularly as no evidence was provided to show no CH_4 was adsorbed during that experiment. On a purely kinetic diameter analysis the narrower pore shape of the desolvated as-synthesised MOF would be thought to improve CO_2 *vs* CH_4 selectivity rather than reverse it. This implies that either multilayer formation is more beneficial for the CH_4 adsorption than for CO_2, or that the CH_4 triggers a larger dynamic response. The behaviour is opposite to hydrated MIL-53(Cr) (closed pore), which exhibits excellent CO_2 *vs* CH_4 selectivity at high pressures because CH_4, unlike CO_2, is unable to enter the narrow pore or reopen the framework.[22]

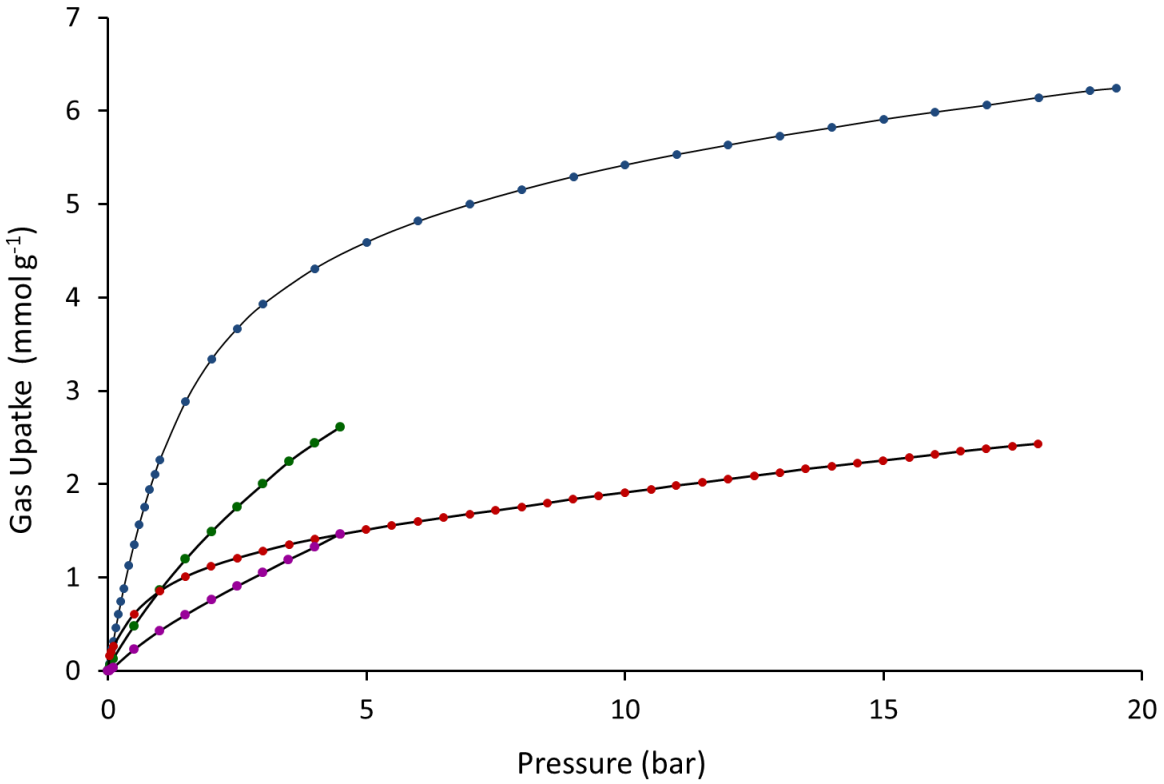

Figure 50 – Gravimetric CO_2 and CH_4 adsorption isotherms for desolvated $CHCl_3$ exchanged MOF $(Me_2NH_2)[In(ABDC)_2]$ (blue and green circles respectively) (**G4** & **G6**) and desolvated as-synthesised MOF $(Me_2NH_2)[In(ABDC)_2]$ (red and purple circles respectively) (**G1** & **G3**)

4.4.3 Effect of partial desolvation on CO_2 uptake

Concept

The isotherms displayed above were obtained after fully desolvating the as-synthesised or $CHCl_3$-exchanged framework to give the two different solvent-free structures, containing only counterions in their pores. The continuous breathing effect of the as-synthesised framework during the desolvation, however, suggests there are an infinite number of structures within the breathing range, based on the amount or type of residual solvent. In these structures solvent-framework interactions are believed to be responsible for holding the framework closed, instead of the framework-framework or framework-cation interactions in the fully desolvated framework. The solvent-framework interactions are likely to be significantly weaker and present an opportunity to probe the reopening of the framework via gas pressure. Parallels to this concept can be drawn to CO_2 uptake experiments on the hydrated closed-pore version of MIL-53(Cr), which shows a gate pressure at about 12 bar CO_2, where the hydrogen bonding interactions with its guest water

molecules are broken leading to sudden pore opening.[22] The hydrated version of MIL-53(Cr), however, is the fully solvated version of the MOF on exposure to water, and to the author's knowledge no analogous studies of CO_2 uptake in deliberately designed partially-desolvated MOFs exist in the literature.

Gravimetric Studies

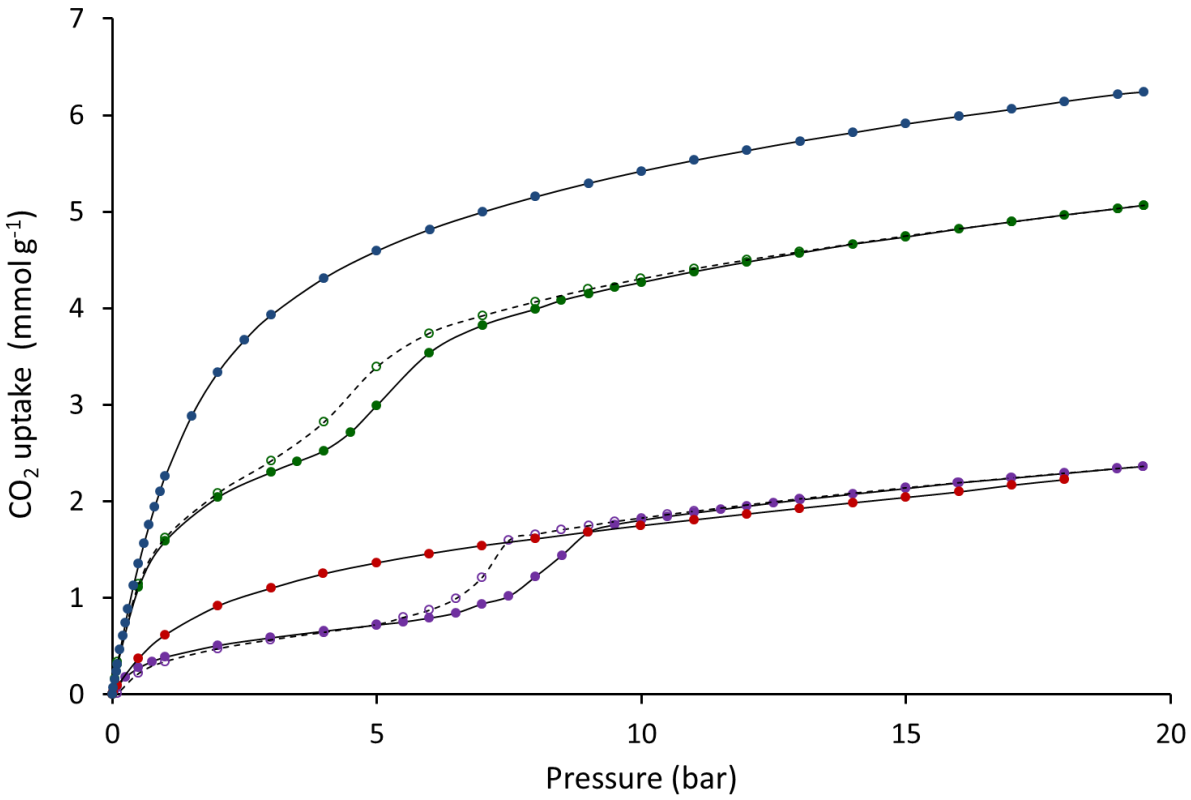

Figure 51 – Gravimetric CO_2 adsorption isotherms after various levels of desolvation in $(Me_2NH_2)[In(ABDC)_2]$. Blue Circles; CO_2 adsorption of fully desolvated $CHCl_3$-exchanged MOF (**G4**), Red Circles; CO_2 adsorption of fully desolvated as-synthesised MOF (**G1**), Purple Circles; CO_2 adsorption of a 33% desolvated as-synthesised MOF (**G7.1**), Green Circles; CO_2 adsorption of 66% desolvated as-synthesised MOF (**G7.2**). Filled data points are during adsorption and open data points desorption. All isotherms are measured at 298 K.

The gravimetric adsorption isotherms for a 33% desolvated (**G7.1**) and a 66% desolvated as-synthesised MOF (**G7.2**), shown in purple and green respectively, are compared to the fully desolvated as-synthesised (red) and $CHCl_3$ exchanged (blue) frameworks in Figure 51. The isotherms show distinct step change behaviour indicating a transition to the open-pore framework at a particular gate pressure. The transition causes the final uptake in the 33% desolvated framework to be similar to the fully desolvated as-synthesised version despite it still containing 66% of the solvent

molecules. The uptake of the 66% desolvated is significantly higher than the corresponding fully-desolvated framework but lower than the desolvated $CHCl_3$-exchanged MOF which is also in an open-pore form but without any residual solvent. The gate pressure of the two different levels of partial solvation is seen to change from about 7 bar to 5 bar due to the different amount (and potentially ratio) of DMF and H_2O molecules in the pore, resulting in a different overall barrier to re-opening. The isotherms also display hysteretic behaviour on desorption suggesting the transition back to the closed MOF occurs at lower pressures than the originally opening. A repeat measurement of the adsorption curve from the 33% desolvated material (**G8.1**) shows that the gate pressure, even for similar desolvated materials, is slightly variable, which is most likely due to changes in the relative solvent content (DMF *vs* H_2O). The two adsorption isotherms of the 33% desolvated material are shown in Figure 52.

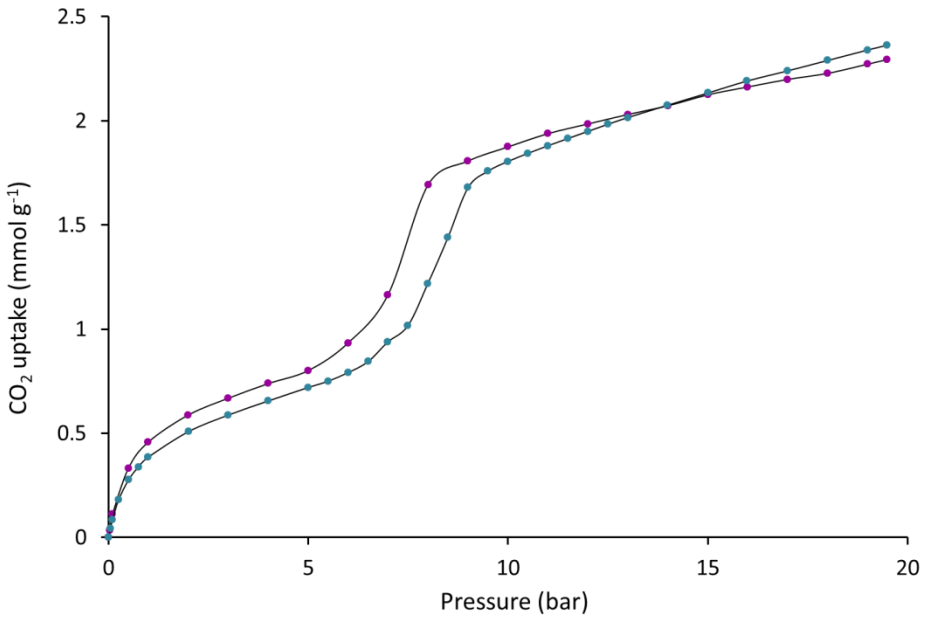

Figure 52 - Gravimetric CO_2 adsorption isotherms for two different samples of 33% desolvated as-synthesised MOF $(Me_2NH_2)[In(ABDC)_2]$.

In situ diffraction studies

The structural changes occurring during gas uptake in the partial solvated frameworks were followed through a number of different *in situ* crystallographic studies on both single crystal and powder samples (**I2 - I6**). These types of experiments are becoming well-known in the literature and have provided information relating to the gating effect of MIL-47,[29] [Co(BDP] (BDP = benzene-1,4-dippyrazolate),[30] [$Zn(BME\text{-}BDC)_2(dabco)$] (BME-BDC = 2,5-bis(2-methoxyethoxy)-1,4-

benzenedicarboxylate),[31] [VO(BPDC)] (BPDC = biphenyldicarboxylate),[32] and various analogues of MIL-53.[22, 28, 33–41] The majority of the *in situ* studies on partially desolvated $(Me_2NH_2)[In(ABDC)_2]$ (**I2 - I6**) confirmed the return to the open pore structure under increasing gas pressures and showed gating pressures between 5-8 bar consistent with gravimetric data. The gate pressure was seen to be variable within this range even from frameworks of similar pore opening. The full details of all the *in situ* diffraction studies can be found in section 4.3.8 and illustrative examples will be used in the following discussion.

Figure 53 shows one particular powder diffraction study (**I5**) where a partially desolvated framework was studied during CO_2 adsorption around the stepped region of the gravimetric isotherm. The powder patterns show that the sample remains in a partially closed phase (blue) up to CO_2 pressures of 6 bar, the pattern then becomes two-phase at 7 and 8 bar (purple), and finally is exhibits a single open-pore phase at 9 bar or above (red). This corresponds well to the step observed in the corresponding gravimetric isotherm. The powder diffraction patterns on desorption convert back to the partially closed phase via a mixed phase pattern at 6 bar, which also agrees with the hysteresis seen gravimetrically.

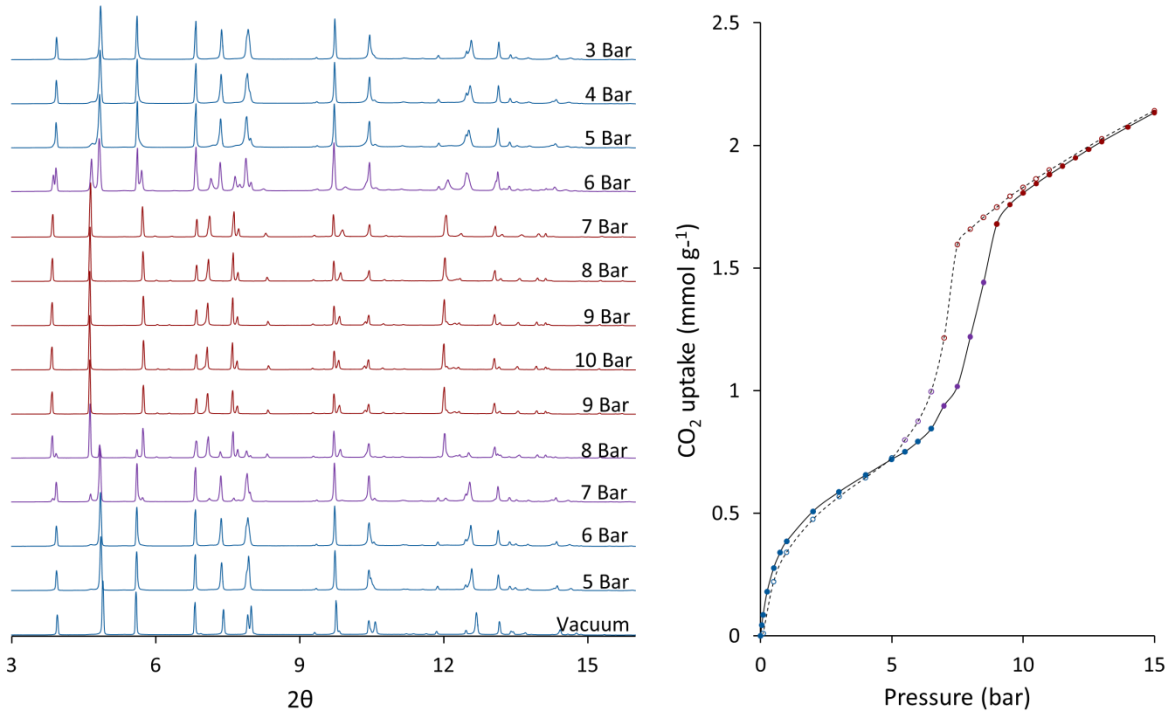

Figure 53 - Comparison of an *in situ* powder diffraction study of CO_2 adsorption on a partially desolvated as-synthesised MOF $(Me_2NH_2)[In(ABDC)_2]$ (**I5**) (left) to the gravimetric CO_2 adsorption after removal of only 33% of the solvent from the as-synthesised MOF(**G7.1**) (right). Filled data points are during adsorption and open data points desorption.

Pawley refinements of the powder diffraction patterns confirm that the unit cell values lie along the known breathing trend line and that the gating occurs at the same point as the step in the gravimetric adsorption isotherm. This is displayed in Figure 54 by comparing the CO_2 uptake with the *b*-axis length. The refinements also reveal that the regions outside the gate pressure show a slow continuous opening of the framework, rather than remaining static. Figure 55 plots the continually evolving structure during adsorption along the known breathing trend line. Data recorded at 20 and 40 bar have also been included and show that even up to 40 bar the structure continues to open. This reinforces the theory that the lack of a plateau in the gravimetric isotherms is due to the materials continuous flexibility.

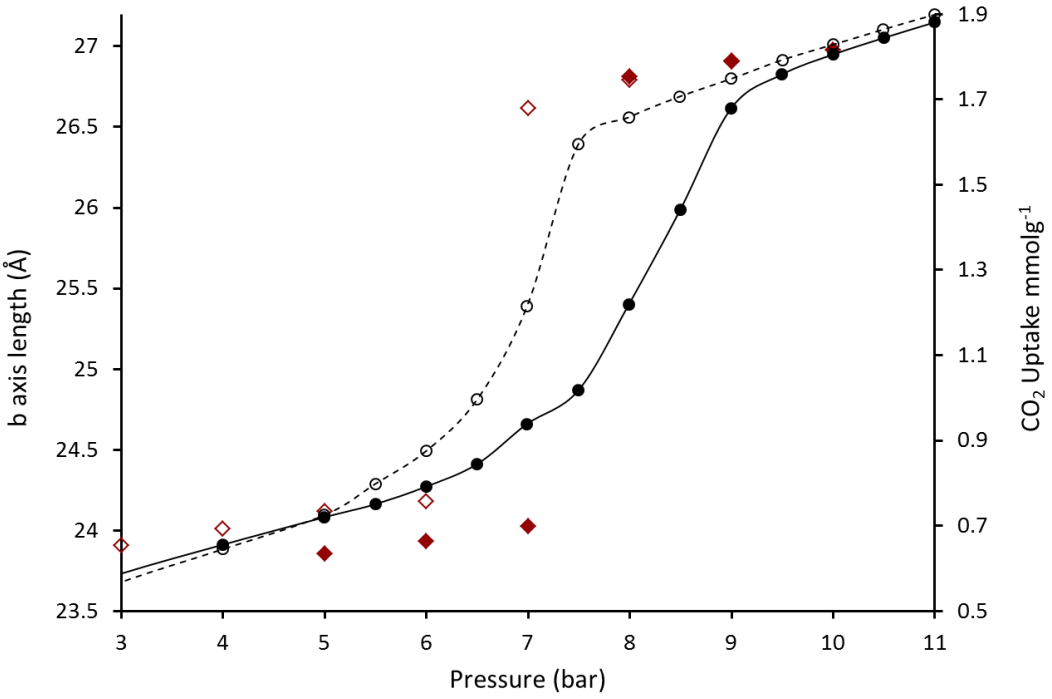

Figure 54 - Comparison of the refined b-axis unit cell lengths during an *in situ* CO_2 powder diffraction study (red diamonds) (**I5**) to the CO_2 isotherm of 33% desolvated as-synthesised MOF (black cirlces) (**G7.1**). Filled data points are during adsorption and open data points desorption.

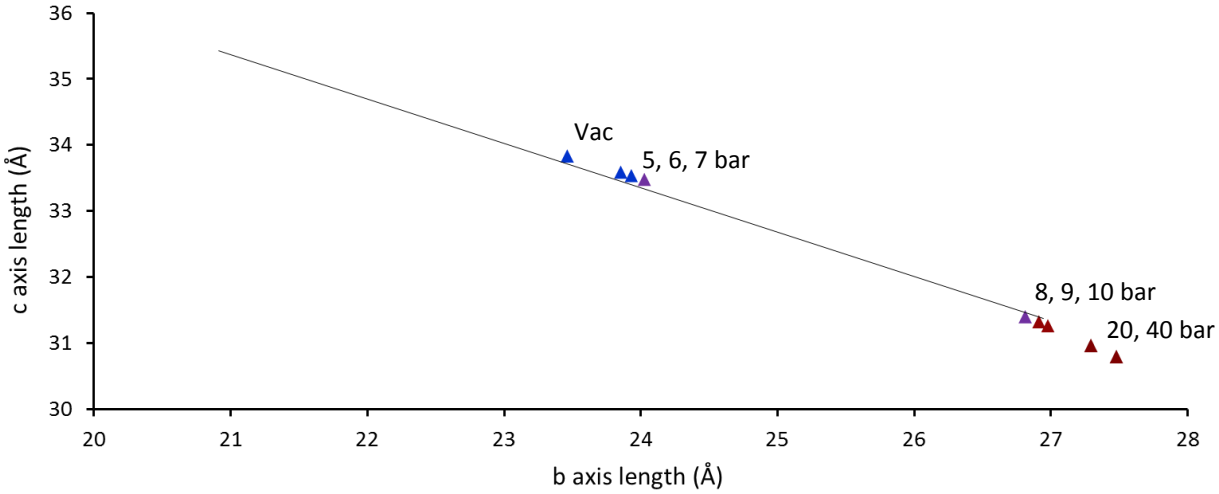

Figure 55 – Refined *b* and *c* unit cell axis lengths of an *in situ* crystallographic study during CO_2 adsorption on partially desolvated as-synthesised MOF$(Me_2NH_2)[In(ABDC)_2]$ (**I5**). The trend line is from single crystal desolvation studies of as-synthesised $(Me_2NH_2)[In(ABDC)_2]$ (**1-10**)

A second example is a CO_2 powder diffraction study carried out on a more highly-closed-pore MOF, obtained by heating the framework to higher temperatures, thereby removing more solvent (**I6**). Figure 56 shows the refined *b* and *c* unit cell parameters and initial inspection suggests a more continuous behaviour. The powder patterns (Figure 29 section 4.3.8) however show the introduction of a minor phase corresponding to the fully open framework at CO_2 pressures as low as 5 bar. The relative quantity of this minor open phase increases at 10 and 20 bar but unlike the study presented above (**I5**) the pattern does not fully convert and a continuous movement of the diffraction peaks of the closed phase are also observed.

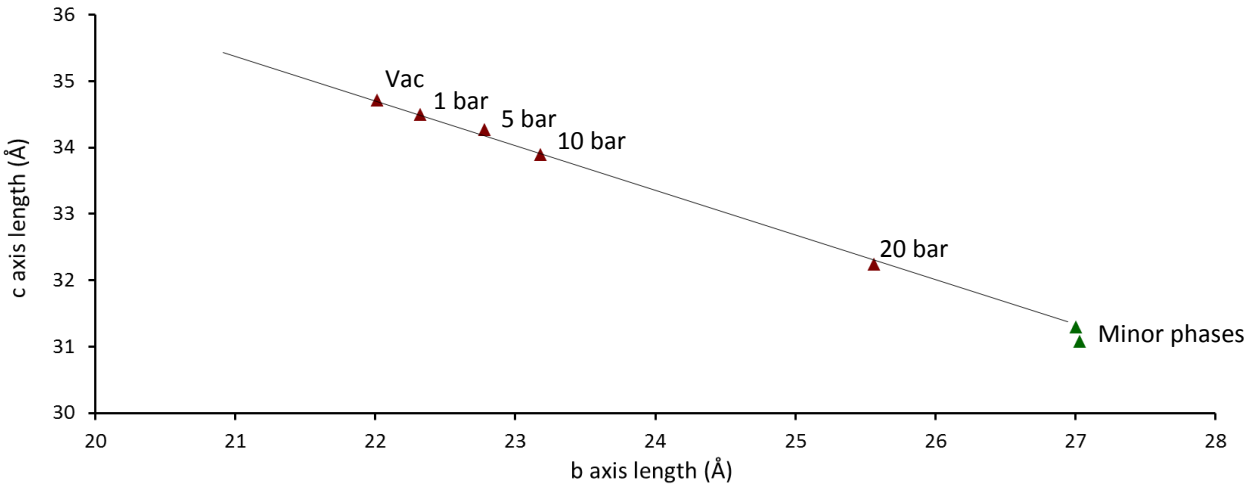

Figure 56 – Refined *b* and *c* unit cell axis lengths of a second *in situ* crystallographic study during CO_2 adsorption on partially desolvated as-synthesised MOF(Me_2NH_2)[In(ABDC)$_2$] (**I6**). The trendline is from single crystal desolvation studies of as-synthesised (Me_2NH_2)[In(ABDC)$_2$] (**1-10**)

The powder diffraction pattern at 20 bar CO_2 was very difficult to model, displaying a wide range of peak shapes. This is thought to occur because of a distribution of different crystalline phases along the breathing trend line resulting in a superposition of many different diffraction peaks. The breathing effect predominantly occurs in two dimensions causing certain reflections to be more strongly affected by the flexibility than others. The most notable case is 022 reflection. Figure 57; a)-c) shows attempts to fit the single reflection of the major and minor phases from the vacuum, 5 bar and 20 bar patterns respectively with simple Gaussian curves. The vacuum and 5 bar measurements, including the minor phase (purple), can be reasonably described by just one Gaussian function, but in the 20 bar measurement this is a poor model. Figure 57 d) shows that the major peak can be much better represented as the combination of 4 different Gaussian functions at different 2θ values. These would relate to 4 different unit cells, each in a different open- or closed-pore state. The data point presented in Figure 56 therefore only represents an average position for the 20 bar measurement based on the best fit that could be obtained using TOPAS[13] to model the pattern as a single phase. The actual behaviour is more likely a wide distribution of phases along the trend line. Unfortunately all the phases are too close together to be accurately modelled using multiphase fitting.

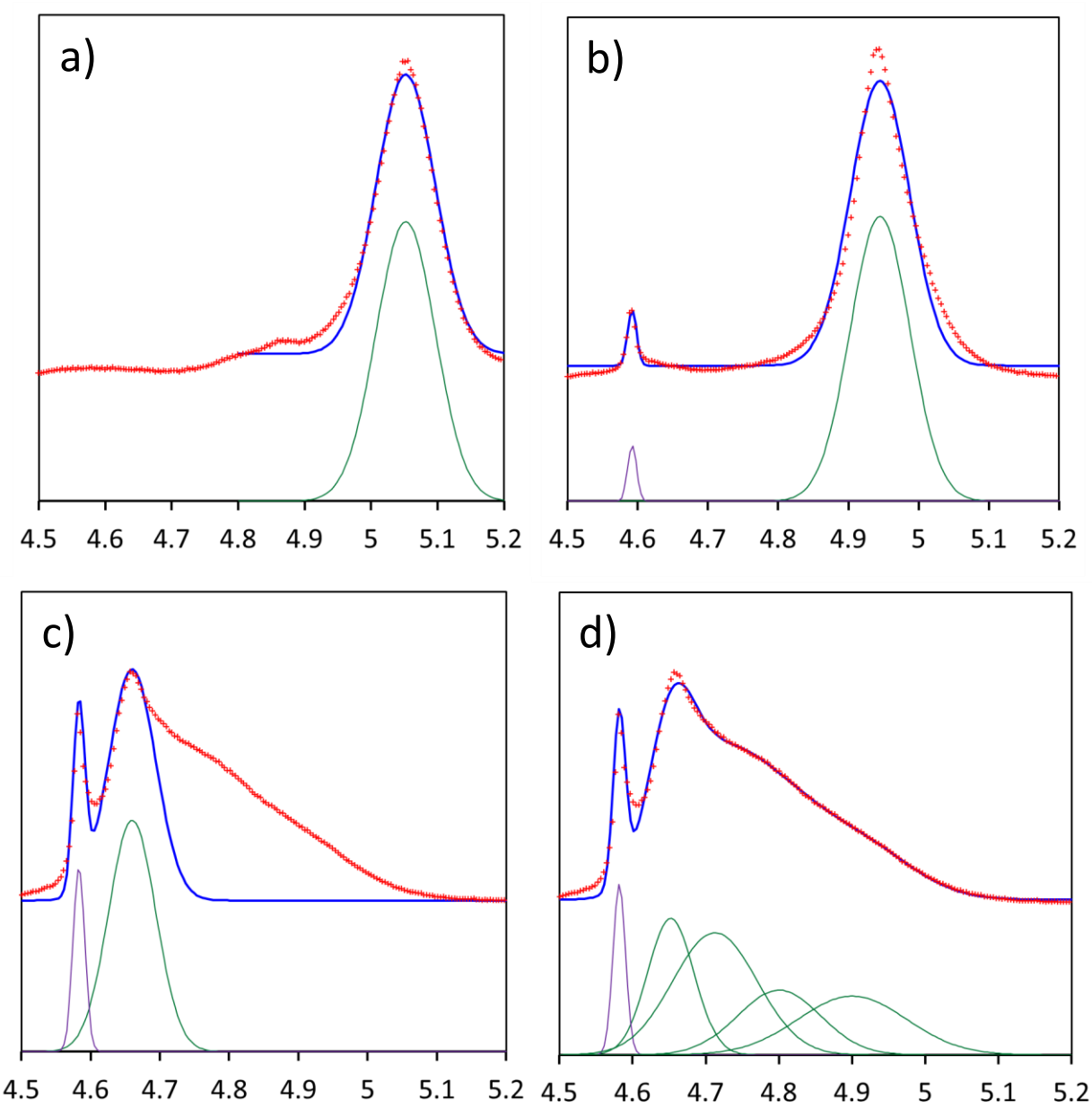

Figure 57 – Gaussian function fitting the 022 reflection of the major (green) and minor (purple) phases during *in situ* CO_2 sorption experiment **I6**. a) Vacuum (**I6.1**) b) 5 bar CO_2 (**I6.3**), c) 20 Bar CO_2 (**I6.5**) with one major phase, d) 20 bar CO_2 (**I6.5**) fitted with multiple major phases. Experimental data are displayed by red crosses and the calculated peak is displayed by the blue line.

The introduction of the minor phase at 5 bar suggests this is sufficient pressure to break the solvent-framework interactions in the MOF and return it to its open-pore form, agreeing with the gravimetric isotherm recorded at 66% desolvation. This, however, only occurs for some crystallites and the majority display more continuous behaviour resulting in the large distribution of phases. The most likely cause of this is poor equilibration kinetics inside the narrow pore material. This would also explain the disparity between a comparable single crystal diffraction study which starts from a

very similarly sized pore, but only shows a small progression along the trend line (**I3**) (Figure 58). The gas uptake kinetics in the single crystal experiment would be expected to be significantly slower due to the large crystallite size. The continuous movement seen would therefore be expected to be substantially larger if allowed to equilibrate over long periods. Unfortunately time constraints at synchrotron facilities don't allow such measurements. The range of structures seen in the powder patterns implies that although the opening is observed as a defined step in the isotherm, this can occur through continuous motions, transforming slowly rather than just snapping open.

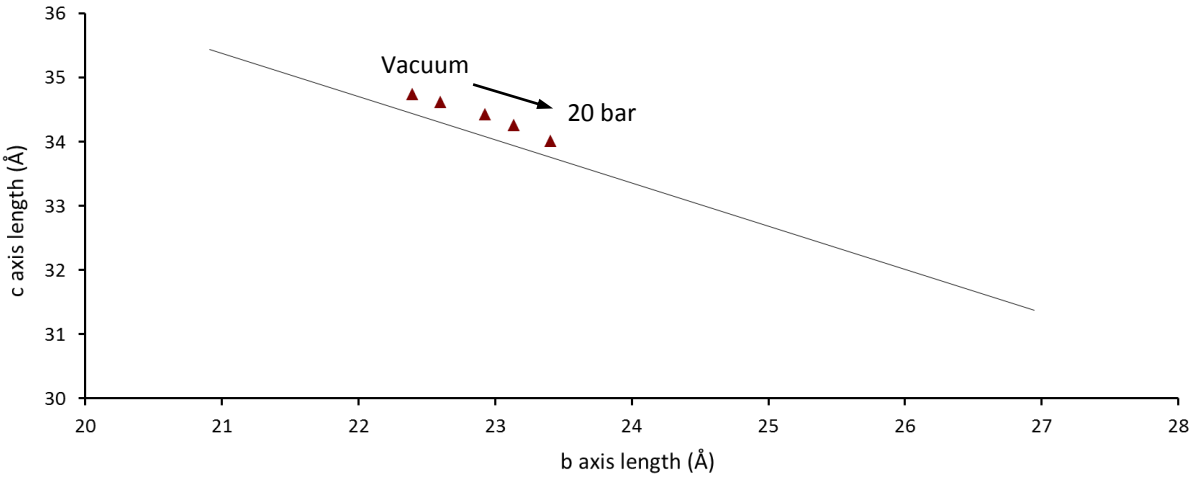

Figure 58 – Refined *b* and *c* unit cell axis lengths of a single crystal *in situ* crystallographic study during CO_2 adsorption on partially desolvated as-synthesised MOF$(Me_2NH_2)[In(ABDC)_2]$ (**I3**). The trend line is from single crystal desolvation studies of as-synthesised $(Me_2NH_2)[In(ABDC)_2]$ (**1-10**)

4.4.4 CH_4 adsorption studies in partially desolvated $(Me_2NH_2)[In(ABDC)_2]$

To understand the reasoning behind the change in CO_2/CH_4 selectivity in the framework, CH_4 uptake in the partially desolvated framework was also explored through crystallographic methods (**I7** & **I8**). Unfortunately comparable partially desolvated gravimetric isotherms have not yet been recorded for CH_4. Figure 59 shows a direct comparison between two analogous *in situ* crystallographic studies, CO_2 uptake and CH_4 uptake, carried out consecutively on the same sample (**I3** & **I8**). Adsorption of CO_2 can be seen to result in a transition back to the open-pore phase whereas very little effect on the structure is observed during CH_4 adsorption. This suggests very little dynamic motion and an inability of CH_4 to the break the solvent-framework interactions. The single crystal diffraction study (**I7**) did, however, show a progression of the unit cell along the known trend line, particularly if the

sample was allowed to equilibrate at a particular CH_4 pressure for much longer periods of time (≈16hrs). It is therefore thought that the CH_4 adsorption does occur with an opening of the structure but is likely very slow and difficult to study on a suitable timescale at a synchrotron facility.

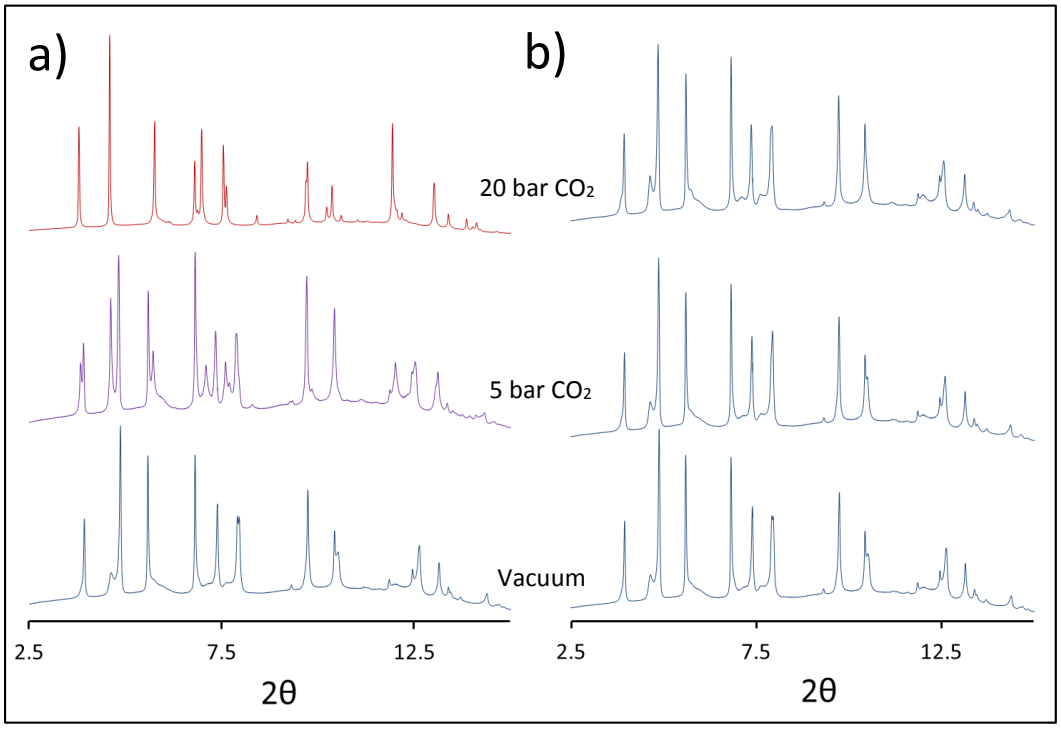

Figure 59 - Powder diffraction patterns obtained during *in situ* crystallographic studies of a) CO_2 uptake (**I4**) and b) CH_4 uptake (**I8**) on a partially desolvated as-synthesised MOF $(Me_2NH_2)[In(ABDC)_2]$

4.4.5 CO_2 adsorption studies on $(Me_2NH_2)[In(ABDC)_2(H_2O)]$

The gas adsorption properties of the new water-coordinated phase $(Me_2NH_2)[In(ABDC)_2(H_2O)]$ (see chapter 3), which occurs upon hydration of the solvent-free open-pore framework were also probed by *in situ* crystallographic experiments. This new phase involves the coordination of two water molecules to half of the indium centres and conversion of these indium centres to an octahedral environment, resulting in a contraction in the helical chains of the framework that run parallel to the pore and a consequent unit cell and void volume reduction. Heating the sample was found to convert this phase back to the original open-pore form but $CHCl_3$ solvent removal using only vacuum was found to enhance its relative composition (**I9.1**). This is suspected to be due to removal of the majority of the $CHCl_3$ molecules but not some residual uncoordinated water molecules, which then

become coordinated to the framework. The *in situ* crystallographic study of CO_2 adsorption involving this water-coordinated phase shows that a transformation back to the open-pore form occurs as CO_2 pressure is increased, higher pressures resulting in a higher conversion to the open-pore framework. This is displayed in the stacked powder patterns in Figure 38 (section 4.3.10). A comparison of the vacuum and 20 bar patterns (**I9.1** & **I9.6**) to the patterns calculated from single crystal structures of the water-coordinated and open-pore MOF are shown below in Figure 60. The conversion implies that forcing CO_2 inside the MOF causes the water-indium bonds to break and the bidentate carboxylic acid interaction to re-form. This rearrangement around the metal centre is unlikely to be due to direct interaction of the CO_2 with the water molecules or the indium ions, but one that occurs to provide more pore space for the guest CO_2 molecules to occupy. During the conversion back to the open-pore structure the bound water molecules are likely to become guests within the pore. The water molecules are subsequently seen to rebind to some of the indium centres and reform the water-coordinated phase when the CO_2 is removed by taking the sample back to vacuum (**I9.7**). The crystallographic gas sorption study was attempted to be studied analogously using gravimetric adsorption measurements by evacuating the $CHCl_3$-exchanged sample prior to the measurements only using vacuum (**G5**). The data in comparison to the isotherm obtained by desolvating under vacuum at 80 ^oC is shown in Figure 61 and appears to be very similar, but does show a slightly lower uptake. This lower uptake could be due to the water-bound phase returning to the open pore form but the coordinated water molecules becoming guests in the channels, therefore reducing the accessible void. The difference between the measurements however was not great, and it is possible that the stronger vacuum pump connected to the gravimetric machine was able to be pull out most of the water.

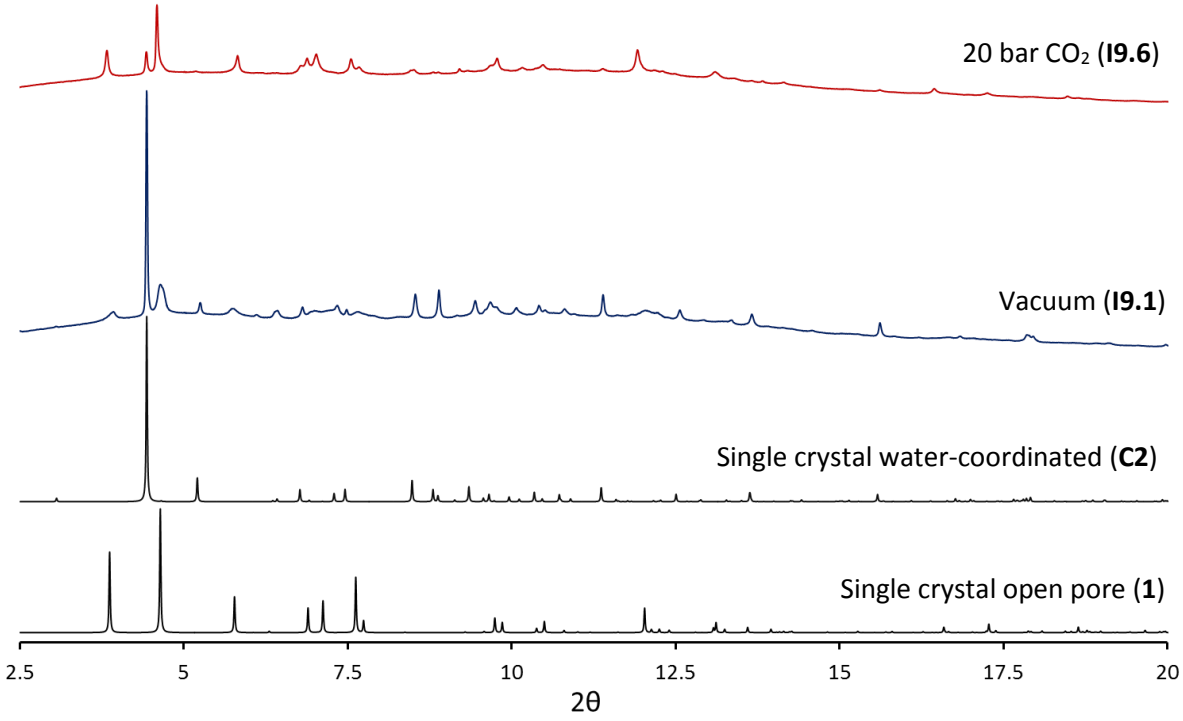

Figure 60 - Powder diffraction patterns of $(Me_2NH_2)[In(ABDC)_2(OH_2)]$ under vacuum (blue) (**I9.1**) and 20 bar CO2 (red) (**I9.6**), compared to predicted powder diffraction patterns from single crystal structures **1** and **C2**

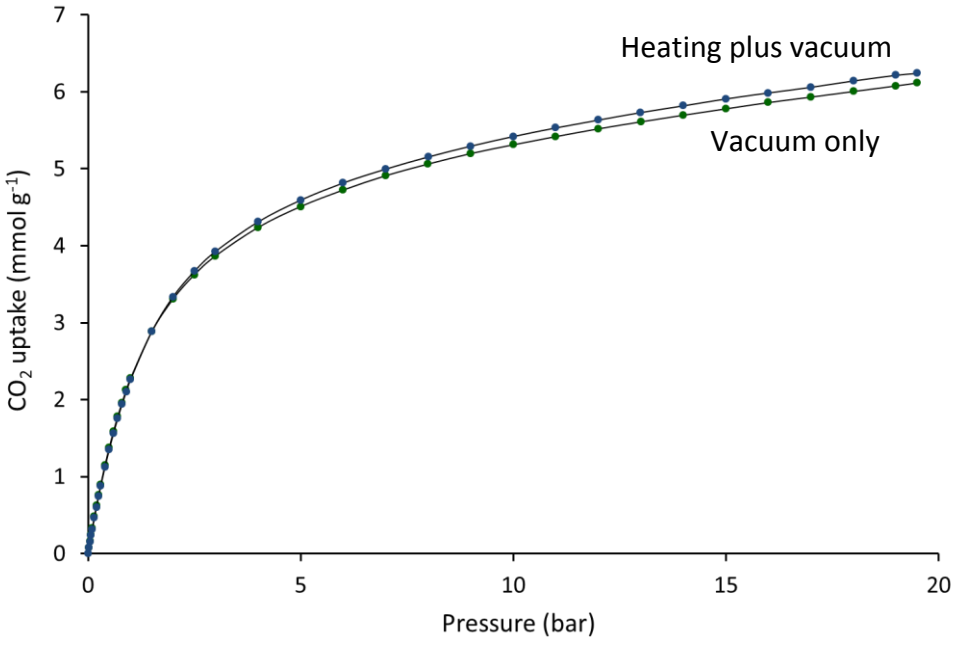

Figure 61 – Gravimetric adsorption isotherms of $CHCl_3$ exchanged MOF $(Me_2NH_2)[In(ABDC)_2]$ after desolvation using heating and vacuum (blue circles) (**G4**) and only using vacuum (red circles) (**G5**)

4.5 Conclusions

The gravimetric adsorption measurements have shown significant differences between the gas uptake properties of the fully desolvated as-synthesised MOF and $CHCl_3$-exchanged MOF. These changes can be accounted for by the solvent-dependent breathing behaviour of the material which results in two different solvent-free framework structures; open-pore or highly closed-pore. The closed-pore framework shows no evidence of a transition back to the open-pore form during gas uptake and is suggested to be held closed by strong framework-framework or framework-cation interactions. A gate pressure during CO_2 adsorption can be introduced by partially desolvating the as-synthesised material, replacing the framework-framework or framework-cation interactions in the closed-pore form with weaker solvent-framework interactions in a partially closed form. The gate pressure is seen to vary between 5-8 bar depending on the amount or type of solvent contained in the pores and the transition can be observed at the same gate pressures via *in situ* crystallographic techniques. The crystallographic characterisation in the *in situ* experiments also reveals that dynamic response of the material occurs through continuous motions when not in the gating region and that the equilibration times are important to consider in highly closed-pore systems. The overall behaviour for the system is described by the schematic in Figure 62.

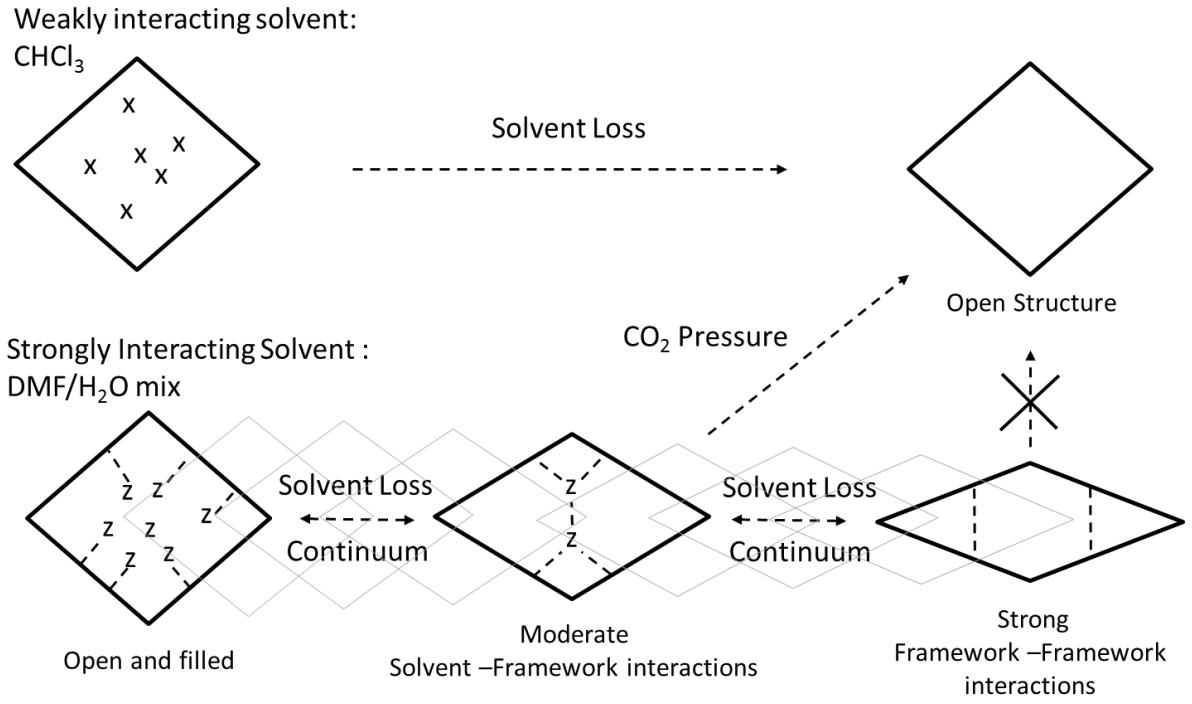

Figure 62 - Schematic showing the different behaviours of the $(Me_2NH_2)[In(ABDC)_2]$ during solvent loss and gas sorption, due to the varying interactions within the pore

The $CHCl_3$-exchanged framework showed a positive CO_2 *vs* CH_4 selectivity but at a significantly reduced value to the original report. This is most likely due to inadequate equilibration times used in the published report, although such details are not provided. The water-coordinated phase which can be generated from the $CHCl_3$-exchanged MOF was also tested for gas sorption and this framework showed a conversion back the open-pore form on increased gas loading, which is accompanied by a marked increase in unit cell volume. The next step to understand the change in selectivity and the difference to the literature would be to study the open-pore and water-coordinated phases during CH_4 adsorption, particularly with *in situ* crystallographic methods. Unfortunately this is likely to be problematical due to the slow kinetics. Overall the work shows the importance of accurately understanding the structural behaviour of porous materials using crystallographic techniques in conjunction with the gravimetric studies normally obtained. A wide range of different guest species, capable of interacting with the framework in different ways, should also be tested for all new framework materials to avoid large dynamic motions such as the ones displayed by $(Me_2NH_2)[In(ABDC)_2]$ being missed.

4.6 References

1 B. Yuan, D. Ma, X. Wang, Z. Li, Y. Li, H. Liu, and D. He, *Chem. Commun.*, 2012, 48, 1135–1137.

2 J. P. S. Mowat, S. R. Miller, A. M. Z. Slawin, V. R. Seymour, S. E. Ashbrook, and P. A. Wright, *Microporous Mesoporous Mater.*, 2011, 142, 322–333.

3 A. C. McKinlay, J. F. Eubank, S. Wuttke, B. Xiao, P. S. Wheatley, P. Bazin, J. C. Lavalley, M. Daturi, A. Vimont, G. De Weireld, P. Horcajada, C. Serre, and R. E. Morris, *Chem. Mater.*, 2013, 25, 1592–1599.

4 H. Nowell, S. a. Barnett, K. E. Christensen, S. J. Teat, and D. R. Allan, *J. Synchrotron Radiat.*, 2012, 19, 435–441.

5 R. H. Blessing, *Acta Crystallogr. A.*, 1995, 51, 33–38.

6 CrysAlisPro, Oxford Diffraction, UK.

7 O. V. Dolomanov, L. J. Bourhis, R. J. Gildea, J. a. K. Howard, and H. Puschmann, *J. Appl. Cryst.*, 2009, 42, 339–341.

8 G. M. Sheldrick, *Acta Crystallogr. A.*, 2008, 64, 112–122.

9 A. L. Spek, *Acta Crystallogr. D.*, 2009, 65, 148–155.

10 A. L. Spek, *Acta Crystallogr. C.*, 2015, 71, 9–18.

11 S. P. Thompson, J. E. Parker, J. Potter, T. P. Hill, A. Birt, T. M. Cobb, F. Yuan, and C. C. Tang, *Rev. Sci. Instrum.*, 2009, 80, 075107.

12 S. P. Thompson, J. E. Parker, J. Marchal, J. Potter, A. Birt, F. Yuan, R. D. Fearn, A. R. Lennie, S. R. Street, and C. C. Tang, *J. Synchrotron Radiat.*, 2011, 18, 637–648.

13 A. A. Coelho, *TOPAS Acad. Version 4.1, 2007, see http//www.topas-academic.net*.

14 A. A. Coelho, *J. Appl. Cryst.*, 2003, 36, 86–95.

15 G. S. Pawley, *J. Appl. Cryst.*, 1981, 14, 357–361.

16 H. M. Rietveld, *Acta Crystallogr.*, 1966, 20, 508–513.

17 H. M. Rietveld, *Acta Crystallogr.*, 1967, 22, 151–152.

18 H. M. Rietveld, *J. Appl. Cryst.*, 1969, 2, 65–71.

19 I. Langmuir, *J. Am. Chem. Soc.*, 1918, 40, 1361–1403.

20 S. Brunauer, P. H. Emmett, and E. Teller, *J. Am. Chem. Soc.*, 1938, 60, 309–319.

21 K. S. W. Sing, *Pure Appl. Chem.*, 1985, 57, 603–619.

22 P. L. Llewellyn, S. Bourrelly, C. Serre, Y. Filinchuk, and G. Férey, *Angew. Chem. Int. Ed.*, 2006, 45, 7751–7744.

23 J.-S. Choi, W.-J. Son, J. Kim, and W.-S. Ahn, *Microporous Mesoporous Mater.*, 2008, 116, 727–731.

24 Z. Zhang, S. Huang, S. Xian, H. Xi, and Z. Li, *Energy & Fuels*, 2011, 25, 835–842.

25 H. Furukawa, N. Ko, Y. B. Go, N. Aratani, S. B. Choi, E. Choi, a O. Yazaydin, R. Q. Snurr, M. O'Keeffe, J. Kim, and O. M. Yaghi, *Science.*, 2010, 329, 424–428.

26 C. Serre, F. Millange, C. Thouvenot, M. Noguès, G. Marsolier, D. Louër, and G. Férey, *J. Am. Chem. Soc.*, 2002, 124, 13519–13526.

27 T. Loiseau, C. Serre, C. Huguenard, G. Fink, F. Taulelle, M. Henry, T. Bataille, and G. Férey, *Chem. - A Eur. J.*, 2004, 10, 1373–1382.

28 C. Serre, S. Bourrelly, A. Vimont, N. A. Ramsahye, G. Maurin, P. L. Llewellyn, M. Daturi, Y. Filinchuk, O. Leynaud, P. Barnes, and G. Férey, *Adv. Mater.*, 2007, 19, 2246–2251.

29 H. Leclerc, T. Devic, S. Devautour-Vinot, P. Bazin, N. Audebrand, G. Férey, M. Daturi, A. Vimont, and G. Clet, *J. Phys. Chem. C*, 2011, 115, 19828–19840.

30 F. Salles, G. Maurin, C. Serre, P. L. Llewellyn, C. Knöfel, H. J. Choi, Y. Filinchuk, L. Oliviero, A. Vimont, J. R. Long, and G. Férey, *J. Am. Chem. Soc.*, 2010, 132, 13782–13788.

31 S. Henke, D. C. Florian Wieland, M. Meilikhov, M. Paulus, C. Sternemann, K. Yusenko, and R. a. Fischer, *CrystEngComm*, 2011, 13, 6399.

32 Y.-Y. Liu, S. Couck, M. Vandichel, M. Grzywa, K. Leus, S. Biswas, D. Volkmer, J. Gascon, F. Kapteijn, J. F. M. Denayer, M. Waroquier, V. Van Speybroeck, and P. Van Der Voort, *Inorg. Chem.*, 2013, 52, 113–120.

33 P. L. Llewellyn, G. Maurin, T. Devic, S. Loera-Serna, N. Rosenbach, C. Serre, S. Bourrelly, P. Horcajada, Y. Filinchuk, and G. Férey, *J. Am. Chem. Soc.*, 2008, 130, 12808–12814.

34 P. L. Llewellyn, P. Horcajada, G. Maurin, T. Devic, N. Rosenbach, S. Bourrelly, C. Serre, D. Vincent, S. Loera-Serna, Y. Filinchuk, and G. Férey, *J. Am. Chem. Soc.*, 2009, 131, 13002–13008.

35 N. Rosenbach, A. Ghoufi, I. Déroche, P. L. Llewellyn, T. Devic, S. Bourrelly, C. Serre, G. Férey, and G. Maurin, *Phys. Chem. Chem. Phys.*, 2010, 12, 6428–6437.

36 L. Hamon, P. L. Llewellyn, T. Devic, A. Ghoufi, G. Clet, V. Guillerm, G. D. Pirngruber, G. Maurin, C. Serre, G. Driver, W. van Beek, E. Jolimaître, A. Vimont, M. Daturi, and G. Férey, *J. Am. Chem. Soc.*, 2009, 131, 17490–17499.

37 N. A. Ramsahye, T. K. Trung, S. Bourrelly, Q. Yang, T. Devic, G. Maurin, P. Horcajada, P. L. Llewellyn, P. Yot, C. Serre, Y. Filinchuk, F. Fajula, G. Férey, and P. Trens, *J. Phys. Chem. C*, 2011, 115, 18683–18695.

38 S. Couck, E. Gobechiya, C. E. A Kirschhock, P. Serra-Crespo, J. Juan-Alcañiz, A. Martinez Joaristi, E. Stavitski, J. Gascon, F. Kapteijn, G. V Baron, and J. F. M. Denayer, *ChemSusChem*, 2012, 5, 740–750.

39 T. Devic, F. Salles, S. Bourrelly, B. Moulin, G. Maurin, P. Horcajada, C. Serre, A. Vimont, J.-C. Lavalley, H. Leclerc, G. Clet, M. Daturi, P. L. Llewellyn, Y. Filinchuk, and G. Férey, *J. Mater. Chem.*, 2012, 22, 10266.

40 S. Biswas, T. Rémy, S. Couck, D. Denysenko, G. Rampelberg, J. F. M. Denayer, D. Volkmer, C. Detavernier, and P. Van Der Voort, *Phys. Chem. Chem. Phys.*, 2013, 15, 3552.

41 E. J. Carrington, I. J. Vitórica-Yrezábal, and L. Brammer, *Acta Crystallogr. B.*, 2014, 70, 1–19.